FULLY DEVELOPED TURBULENT FLOW IN STRAIGHT RECTANGULAR DUCTS -

Secondary Flow, Its Cause and Effect On The Primary Flow

by

Lawrence C. Hoagland

B.M.E., General Motors Institute
(1954)
S.M., Massachusetts Institute of Technology
(1955)
M.E., Massachusetts Institute of Technology
(1956)

Submitted in Partial Fulfillment
of the Requirements for the
Degree of Doctor of Science

at the

Massachusetts Institute of Technology

September, 1960

Signature of Author.....
Department of Mechanical Engineering, September 2, 1960

Certified by .....
Thesis Supervisor

Accepted by.....
Chairman, Departmental Committee
on Graduate Students

Title: FULLY DEVELOPED TURBULENT FLOW IN STRAIGHT RECTANGULAR DUCTS - Secondary Flow, Its Cause and Effect on the Primary Flow

Author: Lawrence C. Hoagland

Submitted to the Department of Mechanical Engineering in partial fulfillment of the requirements for the Degree of Doctor of Science, M.I.T., September, 1960.

ABSTRACT

The problem of fully developed turbulent flow in rectangular ducts is investigated principally by obtaining experimental measurements of the primary and secondary velocity distributions in ducts with aspect ratios of 1:1, 2:1 and 3:1. Mean primary (axial) velocities are measured with both hot wire annemometer and pitot tube instrumentation. Secondary velocities are determined from observations of flow direction using a very sensitive hot wire system developed by the author.

Secondary flows are found to behave in the manner originally suggested by Prandtl. They are about the same magnitude in all three ducts. Maximum secondary velocities of approximately 1 to 1 1/2 percent of the axial centerline velocity occur near the wall in the corner region where the large wall shear stress gradient is observed.

The secondary flows, by convection of axial momentum, are seen to have a significant effect on the primary flow distribution, particularly by causing the wall shear stress to be nearly uniform around the duct periphery except for the corner region. An evaluation of the axial momentum terms from the experimental measurements shows the secondary convective terms to be important throughout much of the flow.

The behavior near the wall of the transverse turbulence intensity components ($\tilde{v}'$ and $\tilde{w}'$) in the presence of a transverse gradient of wall shear is shown to be a major cause of the secondary flow. Expressing these intensity components by a universal relation in the viscous wall region, it is shown that wall shear gradients produce secondary motion driving forces of significant magnitude.

Mixture length theories are shown to be inadequate and the need for measurements of turbulent stresses is discussed.

Thesis Supervisor: A. H. Shapiro
Title: Professor of Mechanical Engineering

ACKNOWLEDGMENTS

This work would not be complete without proper acknowledgment of the invaluable encouragement, advice and assistance I have received from many sources. Special thanks are due to the entire faculty and student body of the institute for establishing and maintaining the excellent academic and research environment in which this work was done. My experiences as a student, teacher, and researcher at M.I.T. have certainly been the highlight of my overall educational experience.

In particular, I would like to express my sincere gratitude to the following people:

Professor A.H.Shapiro who, as my thesis advisor, has so generously given his time and advice. His valuable guidance and careful thought have contributed much to this work and are sincerely appreciated.

To Professors W.M.Rohsenow and R.J.Nickerson, who as members of my thesis committee have contributed their valuable advice and criticism.

I am especially endebted to Mr. Gerald Gilbert who conducted the experimental work with the two rectangular ducts. His laborious efforts made an extremely important contribution to this work.

To Mr. Bernard Goodwin, a doctoral candidate in the Chemical Engineering department, for his many stimulating discussions of our mutual difficulties with hot wire measurements near solid boundaries.

To Mr. Howard Grant of Flow Corporation and Professor Kronauer of Harvard University for their patient advice on my hot wire problems.

To the Staff of the Mechanical Engineering Laboratory of M.I.T. for their help with equipment and instrumentation.

I am particularly grateful to my wife, Carol, for 10 years of patience and encouragement, and for her typing of the manuscript.

The constant encouragement of my parents in the pursuit of my graduate studies is hereby gratefully acknowledged.

This project was sponsored initially by the Mechanical Engineering Department under a Grant-in-Aid from the John B. Pierce Foundation of Connecticut, Inc and throughout most of the effort by the U.S. Army Ordnance Department through the M.I.T. Division of Sponsored Research.

I am also indebted to General Motors Corporation and the Fluor Foundation for providing the Fellowships that made possible my first two years of graduate study.

L. C. Hoagland
Sept. 1, 1960

TABLE OF CONTENTS

TABLE OF CONTENTS (CONT.)

LIST OF TABLES

LIST OF FIGURES

LIST OF FIGURES (CONT.)

LIST OF FIGURES (CONT.)

NOMENCLATURE

English Letter Symbols

A	flow cross sectional area
A	constant in King's Law
a	half width of duct - short dimension
B	constant in King's Law
b	half width of duct - long dimension
C_d	discharge coefficient of flow metering nozzles
d	diameter (flow nozzles, pitot tube, etc.)
f	fanning friction factor
f_n	denotes functional relationship
$F_1(y^*)$, $F_2(y^*)$	functions of similarity parameter y^*
g	gravitational acceleration
I	wire current (hot wire)
ℓ	mixture length
N_u	Nusselt number (hot wire)
p	pressure
Q	volume flow rate
R_e	Reynolds number
t	time
u	velocity component in x direction
v	velocity component in y direction
w	velocity component in z direction
$\bar{u}$, $\bar{v}$, $\bar{w}$	time average velocity components
u',v',w',	instantaneous deviation from time average velocities (fluctuating components)

$\tilde{u}'$, $\tilde{v}'$, $\tilde{w}'$ rms value of instantaneous fluctuating components

$\overline{u'^2}$, $\overline{v'^2}$, $\overline{w'^2}$ normal Reynolds stresses (when multiplied by density)

$\overline{u'v'}$, $\overline{u'w'}$, $\overline{v'w'}$ Reynolds shear stresses (when multiplied by density)

u^*	friction velocity = $\sqrt{\tau_o g/\rho}$
v^*	similarity parameter $\tilde{v}'/u^*$
w^*	similarity parameter $\tilde{w}'/u^*$
V	velocity
x	axial direction (Figure 1)
y,z	coordinates of cross section (Figure 1)
y^*	similarity parameter yu^*/ν

Greek Letter Symbols

δ	displacement correction for pitot tube in velocity gradient
ξ	vorticity component, page 6
η	vorticity component, page 6
ζ	vorticity component, page 6
κ	mixture length coefficient
μ	absolute viscosity
ν	kinematic viscosity
ρ	density
τ	shear stress
τ_o	local wall shear stress
$\bar{\tau}_o$	average wall shear stress
ψ	dimensionless stream function (defined by equation (10), page 33)
∇^2	Laplacian operator

NOMENCLATURE (CONT.)

Subscripts

$\mathfrak{C}$	denotes duct centerline (or center y=a, z=b)
b	denotes bulk velocity (mixed mean)
o	outside (diameter)
i	inside (diameter)

Other subscripts defined where used.

1.0 INTRODUCTION

Fully developed turbulent flow in straight rectangular ducts differs from ordinary turbulent pipe (circular) flow in two important respects; 1) it is three dimensional and hence much more complex in detail and 2) secondary currents have been found to exist, resulting in further complication of the flow.

This problem is of interest from both the engineering and the academic viewpoints. Although the engineer is usually concerned only with the gross characteristics of the flow such as mean pressure drop and heat transfer, certain important engineering problems demand a deeper insight into the mechanism of the flow.

The recent interest in the problem of heat transfer to fluids in turbulent flow through rectangular nuclear reactor coolant channels is a case in point. Experimental heat transfer studies by Levy et.al.(1)* in electrically heated rectangular ducts indicate average Nusselt numbers from 30 to 40 percent below the accepted values for uniform duct wall temperature. Analysis of laminar flow heat transfer in non-circular ducts with various thermal boundary conditions shows that the peripheral wall temperature distribution (which is, of course, related to the local flow conditions) has a strong affect on the Nusselt number, the uniform wall heat flux condition yielding much lower Nusselt numbers than uniform wall temperature. (Irvine (2)). The author believes that the key to the solution of this engineering problem is a better understanding of the detailed flow mechanism with particular emphasis on the flow distribution near the solid boundaries. Deissler (3) has recently attempted a solution to this problem by neglecting the secondary flow. His analytical results are not in agreement with the author's measurements. It is shown here that the secondary flow plays an important role in determining the overall flow distribution and hence must

* Numbers in parentheses refer to items in the Bibliography.

be considered in an attempt to explain the heat transfer results.

Another important engineering problem requiring a detailed understanding of the flow is that of sediment flow in rivers and canals. Civil engineers have long been interested in sediment transportation and deposition as influenced by secondary flows. Both the secondary flows in bends and straight sections are of interest. Although this application involves turbulent flow in open channels, the secondary flow phenomena in open and closed channels are much alike. Recently Delleur and McManus (4) have studied the open channel problem and measured the primary flow distribution. They observed secondary flows and attempted a simplified theoretical solution involving the secondary flows.

From the academic viewpoint the nature and cause of the secondary flows is still somewhat of a mystery. Although secondary flow in straight non-circular ducts was discovered long ago by Nikuradse and Prandtl (5-6-7), a complete understanding of its cause has never been achieved. Moreover, the author knows of no instance except the present work where quantitative measurements of these flows has been made. The lack of a complete understanding of this phenomenon so many years after its discovery is in itself a challenge for further study.

Nikuradse (5-6) measured fully developed turbulent axial velocity distributions in many non-circular ducts including a 3.5:1 rectangle and presented evidence for the existence of secondary flows. Moissis (8) and Maslen (9) show that these secondary flows do not appear in fully developed laminar duct flow but are confined to the turbulent case. Howarth (10) and Einstein and Li (11) attempt to explain the cause of these secondary flows. Deissler (3), neglecting the secondary flow, computes axial velocity distributions for square and triangular ducts. A detailed review of these efforts is best handled in Section 2.0 after an introduction to some analytical

considerations.

The primary objective of this study is to provide some detailed experimental measurements of both the primary and secondary flows in three rectangular duct configurations, and, using these measurements, to attempt an extension of the current understanding of this flow phenomenon. After reviewing some preliminary analytical considerations and the current status of the problem, the experimental measurements are described and interpreted. Finally some speculations are set forth concerning the cause of the secondary flow and its effect on the primary flow.

2.0 ANALYTICAL CONSIDERATIONS AND REVIEW OF CURRENT STATUS

An historical review of the problem is far more meaningful after a consideration of the fundamental equations governing the fluid motion.

2.1 Equations of Motion

Consider a straight duct of uniform rectangular cross section. Let x denote the axial direction while y and z denote the coordinates of the cross section. (Figure 1.) The velocities corresponding to these coordinate directions are u, v, and w respectively.

It is generally accepted that the Navier-Stokes momentum equations are valid for turbulent as well as laminar flows if the parameters are considered to consist of a mean and a fluctuating component. (e.g. $u = \bar{u} + u'$) The "Reynold's Equations" obtained by a substitution of mean and fluctuating components into the incompressible Navier-Stokes equations, and taking time averages are: (See for example Rouse (17) pp 267-271)

$$\frac{\partial \bar{u}}{\partial t} + \bar{u}\frac{\partial \bar{u}}{\partial x} + \bar{v}\frac{\partial \bar{u}}{\partial y} + \bar{w}\frac{\partial \bar{u}}{\partial z} = -\frac{1}{\rho}\frac{\partial \bar{p}}{\partial x} + \nu\nabla^2\bar{u} - \left[\frac{\partial}{\partial x}(\overline{u'^2}) + \frac{\partial}{\partial y}(\overline{u'v'}) + \frac{\partial}{\partial z}(\overline{u'w'})\right] \quad \cdots (1a)$$

$$\frac{\partial \bar{v}}{\partial t} + \bar{u}\frac{\partial \bar{v}}{\partial x} + \bar{v}\frac{\partial \bar{v}}{\partial y} + \bar{w}\frac{\partial \bar{v}}{\partial z} = -\frac{1}{\rho}\frac{\partial \bar{p}}{\partial y} + \nu\nabla^2\bar{v} - \left[\frac{\partial}{\partial x}(\overline{u'v'}) + \frac{\partial}{\partial y}(\overline{v'^2}) + \frac{\partial}{\partial z}(\overline{v'w'})\right] \quad \cdots (1b)$$

$$\frac{\partial \bar{w}}{\partial t} + \bar{u}\frac{\partial \bar{w}}{\partial x} + \bar{v}\frac{\partial \bar{w}}{\partial y} + \bar{w}\frac{\partial \bar{w}}{\partial z} = -\frac{1}{\rho}\frac{\partial \bar{p}}{\partial z} + \nu\nabla^2\bar{w} - \left[\frac{\partial}{\partial x}(\overline{u'w'}) + \frac{\partial}{\partial y}(\overline{v'w'}) + \frac{\partial}{\partial z}(\overline{w'^2})\right] \quad \cdots (1c)$$

The equation of continuity for steady incompressible flow may be written as

$$\frac{\partial \bar{u}}{\partial x} + \frac{\partial \bar{v}}{\partial y} + \frac{\partial \bar{w}}{\partial z} = 0 \qquad \cdots (2)$$

A continuity equation may also be written for the instantaneous fluctuating quantities as

$$\frac{\partial u'}{\partial x} + \frac{\partial v'}{\partial y} + \frac{\partial w'}{\partial z} = 0 \qquad \cdots \quad (3)$$

The problem under consideration here is that of a fully developed steady duct flow (mean values do not vary with time or x). Therefore, all of the derivatives with respect to time and axial distance (x) vanish yielding the following set of equations for fully developed steady flow

$$\bar{v}\frac{\partial \bar{u}}{\partial y} + \bar{w}\frac{\partial \bar{u}}{\partial z} = -\frac{1}{\rho}\frac{\partial \bar{p}}{\partial x} + \nu\nabla^2\bar{u} - \frac{\partial}{\partial y}(\overline{u'v'}) - \frac{\partial}{\partial z}(\overline{u'w'}) \qquad (4a)$$

$$\bar{v}\frac{\partial \bar{v}}{\partial y} + \bar{w}\frac{\partial \bar{v}}{\partial z} = -\frac{1}{\rho}\frac{\partial \bar{p}}{\partial y} + \nu\nabla^2\bar{v} - \frac{\partial}{\partial y}(\overline{v'^2}) - \frac{\partial}{\partial z}(\overline{v'w'}) \qquad (4b)$$

$$\bar{v}\frac{\partial \bar{w}}{\partial y} + \bar{w}\frac{\partial \bar{w}}{\partial z} = -\frac{1}{\rho}\frac{\partial \bar{p}}{\partial z} + \nu\nabla^2\bar{w} - \frac{\partial}{\partial y}(\overline{v'w'}) - \frac{\partial}{\partial z}(\overline{w'^2}) \qquad (4c)$$

$$\frac{\partial \bar{v}}{\partial y} + \frac{\partial \bar{w}}{\partial z} = 0 \qquad (4d)$$

The boundary conditions are $\bar{u} = \bar{v} = \bar{w} = \overline{u'v'} = \overline{u'w'} = \overline{v'w'} = \overline{v'^2} = \overline{w'^2} = 0$ at all solid boundaries. There are four independent equations involving nine unknown quantities ($\bar{u}$, $\bar{v}$, $\bar{w}$, $\bar{p}$, $\overline{u'v'}$, $\overline{u'w'}$, $\overline{v'^2}$, $\overline{w'^2}$, and $\overline{v'w'}$). Obviously these equations are not sufficient to solve for all of these unknown quantities. Missing are the necessary equations for relating the turbulent stresses ($\overline{u'v'}$, $\overline{u'w'}$, $\overline{v'w'}$, $\overline{v'^2}$ and $\overline{w'^2}$) to the other flow parameters. No entirely satisfactory theory has yet been produced to provide these relations.

Before reviewing the history of this problem it is enlightening to consider the equations of motion in a slightly different form. By combining successive pairs of the Reynold's momentum equations (1) in a manner so as to eliminate the pressure terms and then simplifying by the use of the continuity relation (2), the vorticity equations with Reynold's stresses are obtained (after considerable manipulation).

$$\frac{\partial \bar{\xi}}{\partial t} + \bar{u}\frac{\partial \bar{\xi}}{\partial x} + \bar{v}\frac{\partial \bar{\xi}}{\partial y} + \bar{w}\frac{\partial \bar{\xi}}{\partial z} = \bar{\xi}\frac{\partial \bar{u}}{\partial x} + \bar{\eta}\frac{\partial \bar{u}}{\partial y} + \bar{\zeta}\frac{\partial \bar{u}}{\partial z} + \nu\nabla^2\bar{\xi} + \cdots$$

$$+ \frac{\partial^2}{\partial x\partial z}(\overline{u'v'}) + \frac{\partial^2}{\partial y\partial z}(\overline{v'^2}) + \frac{\partial^2}{\partial z^2}(\overline{v'w'}) - \frac{\partial^2}{\partial x\partial y}(\overline{u'w'}) - \frac{\partial^2}{\partial y^2}(\overline{v'w'}) - \frac{\partial^2}{\partial y\partial z}(\overline{w'^2}) \tag{5a}$$

$$\frac{\partial \bar{\eta}}{\partial t} + \bar{u}\frac{\partial \bar{\eta}}{\partial x} + \bar{v}\frac{\partial \bar{\eta}}{\partial y} + \bar{w}\frac{\partial \bar{\eta}}{\partial z} = \bar{\xi}\frac{\partial \bar{v}}{\partial x} + \bar{\eta}\frac{\partial \bar{v}}{\partial y} + \bar{\zeta}\frac{\partial \bar{v}}{\partial z} + \nu\nabla^2\bar{\eta} + \cdots$$

$$+ \frac{\partial^2}{\partial x^2}(\overline{u'w'}) + \frac{\partial^2}{\partial x\partial y}(\overline{v'w'}) + \frac{\partial^2}{\partial x\partial z}(\overline{w'^2}) - \frac{\partial^2}{\partial x\partial z}(\overline{u'^2}) - \frac{\partial^2}{\partial y\partial z}(\overline{u'v'}) - \frac{\partial^2}{\partial z^2}(\overline{u'w'}) \tag{5b}$$

$$\frac{\partial \bar{\zeta}}{\partial t} + \bar{u}\frac{\partial \bar{\zeta}}{\partial x} + \bar{v}\frac{\partial \bar{\zeta}}{\partial y} + \bar{w}\frac{\partial \bar{\zeta}}{\partial z} = \bar{\xi}\frac{\partial \bar{w}}{\partial x} + \bar{\eta}\frac{\partial \bar{w}}{\partial y} + \bar{\zeta}\frac{\partial \bar{w}}{\partial z} + \nu\nabla^2\bar{\zeta} + \cdots$$

$$+ \frac{\partial^2}{\partial x\partial y}(\overline{u'^2}) + \frac{\partial^2}{\partial y^2}(\overline{u'v'}) + \frac{\partial^2}{\partial y\partial z}(\overline{u'w'}) - \frac{\partial^2}{\partial x^2}(\overline{u'v'}) - \frac{\partial^2}{\partial x\partial y}(\overline{v'^2}) - \frac{\partial^2}{\partial x\partial z}(\overline{v'w'}) \tag{5c}$$

where the vorticity components are defined by

$$\bar{\xi} = \frac{\partial \bar{w}}{\partial y} - \frac{\partial \bar{v}}{\partial z} \quad ; \quad \bar{\eta} = \frac{\partial \bar{u}}{\partial z} - \frac{\partial \bar{w}}{\partial x} \quad ; \quad \bar{\zeta} = \frac{\partial \bar{v}}{\partial x} - \frac{\partial \bar{u}}{\partial y}$$

a continuity equation for vorticity takes a form analogous to (2)

$$\frac{\partial \bar{\xi}}{\partial x} + \frac{\partial \bar{\eta}}{\partial y} + \frac{\partial \bar{\zeta}}{\partial z} = 0 \quad \text{also} \quad \frac{\partial \xi'}{\partial x} + \frac{\partial \eta'}{\partial y} + \frac{\partial \zeta'}{\partial z} = 0 \tag{6}$$

This is easily demonstrated by substitution of the vorticity definitions into (6).

Considerable simplification of equations (5) is attained by the restriction to a steady, fully developed flow. The vorticity equations then reduce to

$$\bar{v}\frac{\partial \bar{\xi}}{\partial y} + \bar{w}\frac{\partial \bar{\xi}}{\partial z} = \nu\nabla^2\bar{\xi} + \frac{\partial^2}{\partial y\partial z}(\overline{v'^2} - \overline{w'^2}) - \frac{\partial^2}{\partial y^2}(\overline{v'w'}) + \frac{\partial^2}{\partial z^2}(\overline{v'w'}) \tag{7a}$$

$$\bar{v}\frac{\partial \bar{\eta}}{\partial y} + \bar{w}\frac{\partial \bar{\eta}}{\partial z} = \bar{\eta}\frac{\partial \bar{v}}{\partial y} + \bar{\zeta}\frac{\partial \bar{v}}{\partial z} + \nu\nabla^2\bar{\eta} - \frac{\partial^2}{\partial y\partial z}(\overline{u'v'}) - \frac{\partial^2}{\partial z^2}(\overline{u'w'}) \tag{7b}$$

$$\bar{v}\frac{\partial \bar{\zeta}}{\partial y} + \bar{w}\frac{\partial \bar{\zeta}}{\partial z} = \bar{\eta}\frac{\partial \bar{w}}{\partial y} + \bar{\zeta}\frac{\partial \bar{w}}{\partial z} + \nu\nabla^2\bar{\zeta} + \frac{\partial^2}{\partial y^2}\left(\overline{u'v'}\right) + \frac{\partial^2}{\partial y\,\partial z}\left(\overline{u'w'}\right) \qquad (7c)$$

Equations (7b) and (7c) can be shown by appropriate manipulation to be identical. Therefore (7) represents only 2 independent equations.

From the axial momentum equation (7a) the cause of the secondary flows can be seen in broad, general terms. The vorticity component $\bar{\zeta}$ represents a mean rotation of a fluid element about an axis parallel to the duct axis. If there were no secondary flow $\bar{v}$, $\bar{w}$, and $\bar{\zeta}$ would be zero everywhere and the first three terms of equation (7a) would vanish. The three terms involving the turbulent stresses must, in general, be expected to have finite values. Although the shear stress $\overline{v'w'}$ may be zero in the absence of secondary motion, the intensities $\overline{v'^2}$ and $\overline{w'^2}$ will not be zero. Moreover, they will in general not be equal in the absence of symmetry. Also, from the lack of symmetry, it must be concluded that all three turbulent stress terms in equation (7a) will, in general, have finite values. Because these terms cannot be expected to cancel one another exactly, it must be concluded that they will cause a secondary motion such that the first three terms are non-zero. Although the preceeding argument by no means constitutes a proof of the existence or the cause of the secondary motion, it is interesting that such an argument can be made simply by observing the equations of motion.

2.2 Historical Review

Nikuradse (5) first measured axial velocity distribution for fully developed turbulent flow in straight ducts of rectangular and triangular cross section. He discovered that the "isovels" (contours of constant velocity) were unreasonably distorted, having bumps which protruded toward the corners. Prandtl (7) postulated that this isovel distortion was caused by transverse or secondary velocities bringing high momentum fluid from the center of the duct toward the corners and, to preserve continuity,

a flow of low momentum fluid from the corner region along the walls and back to the duct center. He reasoned that the secondary flows were due to large turbulent fluctuations along the isovel lines resulting in centrifugal forces causing flow toward the corner. Prandtl envisioned secondary flow streamlines similar to those shown in Figures 34, 37, and 40. Later Nikuradse (6) made similar measurements on other non-circular ducts and confirmed the secondary flow hypothesis by visual observation of a milky substance injected into the water flowing through his ducts. He also noted the nearly uniform distribution of wall shearing stress and on this basis proposed the hydraulic diameter concept with which he was able to correlate the friction factor data from all his non-circular geometries.

Howarth (10) used modified vorticity transfer theory and Goldstein's assumed form for the turbulent stress tensor (an extension of the mixture length concept to multidimensional flows) to show that secondary flows will occur whenever the mixture length is not constant along lines of constant $|\text{grad } u|$. Although this work is interesting, it can hardly be considered a rigorous explanation for the cause of secondary flow, considering its dependence on the correctness of mixture length theory.

More recently Einstein and Li (11) have presented an explanation for the cause of these secondary flows. They derive the time dependent vorticity equation with Reynold's stresses (Equation 5a), and eliminate all x derivatives by assuming fully developed flow. They then assume that at some instant there are no secondary flows and investigate the conditions under which this assumption will result in a time derivative of the vorticity $\partial\xi/\partial t$ indicating that the no secondary flow condition is unstable. They thereby obtain

$$\frac{\partial \xi}{\partial t} = \frac{\partial^2}{\partial y \partial z}\left(\overline{v'^2} - \overline{w'^2}\right) - \frac{\partial^2}{\partial y^2}\left(\overline{v'w'}\right) + \frac{\partial^2}{\partial z^2}\left(\overline{v'w'}\right) \qquad (8)$$

and proceed to explain that the turbulent stress terms do not vanish principally when the lines of constant velocity are not parallel to the boundary, such as the corner regions in non-circular ducts. These terms then lead to a time derivative of vorticity $\partial\xi/\partial t$ indicating that the assumption of no secondary flow $\xi = 0$ was incorrect. They also point out that for a laminar flow the turbulent stress terms vanish; hence no secondary flows exist. This is not a rigorous proof of the non-existence of secondary flows in the laminar case; it merely indicates that the trivial solution of no secondary flow satisfies the governing equations.

Townsend (12) considers the problem of the two dimensional turbulent boundary layer with edge effects. He shows that near a wall the inherent differences in the $\overline{v'^2}$ and $\overline{w'^2}$ intensity terms and a gradient in wall shear stress combine to cause a cross-flow in the boundary layer. (See equation 7a). He implies that this phenomenon is also the cause of secondary flows in straight non-circular ducts. Delleur and McManus (4) agree with Townsend's idea and say that "boundary-shear turbulence was indicated to be the self-exciting generators of secondary motion" in their open channel experiments. The author has attempted to clarify and extend this idea as the true cause of the secondary flow (Section 6).

Moissis (8) provides an excellent review of the literature on secondary flows and presents a rigorous proof that secondary flows cannot exist in a fully developed laminar duct flow regardless of the cross-sectional shape. This is accomplished by certain manipulation of the Navier-Stokes equations forming various divergence terms and then using the Green's theorem to show from the boundary conditions of zero velocity that $v = w = 0$ throughout the entire flow. Maslen (9) published a similar proof shortly thereafter.

Recently Deissler and Taylor (3) computed axial velocity distributions for fully developed flow in square and equilateral triangular ducts by

neglecting the influence of secondary flows. They assume that $\bar{v} = \bar{w} = 0$ and that turbulent shear stresses $\overline{u'v'}$ and $\overline{u'w'}$ exist only on surfaces across which a finite gradient of mean velocity appears. They devised a clever method involving the "Law of the Wall" correlations and an "isovel" coordinate system for determining the wall shear stress from the axial pressure gradient. The assumption of negligible secondary flow magnitudes provides considerable simplification of the equations of motion. The y and z momentum equations (4b) and (4c) are eliminated entirely (i.e. of no concern) and the axial momentum equation (4a) is simplified by eliminating the non-linear convective terms.

Extensive comparisons are made herein between Deissler's analytical results and the author's measurements. It is shown that the secondary velocities are not negligible but rather make appreciable contributions to the convective terms in the axial momentum equation. At first it may appear that Deissler's results represent the flow distribution that would be obtained if the secondary flows were of negligible magnitude. This is not necessarily the case. It is important to examine his assumption regarding the turbulent shear stresses. He assumes that " $\overline{u'v'}$ type" turbulent shear stresses appear only on surfaces normal to which there is a finite gradient of $\bar{u}$. This assumption is in accordance with the classical concept from mixture length theory that a velocity fluctuation v' moving through a y gradient of $\bar{u}$ momentum produces a correlation between v' and u' and hence a turbulent shear stress $\overline{u'v'}$. While this reasoning appears physically sound, the converse is not necessarily true, i.e. that a correlation is not produced if no gradient of $\bar{u}$ exists in the direction of v'.

Unfortunately, in the simpler shear flows certain conditions exist which may, at first glance, tend to support this converse idea. Consider the fully developed turbulent flow in a circular pipe. Let u denote the

axial velocity v the radial and w the tangential. It is well known that the $\overline{u'v'}$ stress varies linearly with radius due to the equivalence of the pressure and shear stress forces (except very near the wall). Also well known is the fact that the $\overline{u'w'}$ stresses are everywhere zero. There is no gradient of $\bar{u}$ velocity in the direction of w', however, the $\overline{u'w'}$ stresses must be zero for reasons of symmetry not because the velocity gradient is zero. A similar argument applies to the $\overline{v'w'}$ stresses. Both $\overline{u'v'}$ and the velocity gradient $\partial u/\partial y$ are zero at the pipe axis but here too it is symmetry that demands $\overline{u'v'} = 0$. Another simple shear flow is the two dimension channel (flow between flat parallel plates). Here again the $\overline{u'w'}$ stress is zero everywhere for reasons of symmetry rather than the absence of a $\bar{u}$ gradient in the direction of w'. (w' being the velocity parallel to the boundary and normal to the flow, $\bar{u}$.) A similar argument applies to the two dimensional boundary layer. The author knows of no case of a turbulent flow where measurements indicate a zero turbulent shear stress that cannot be reasoned to be zero from symmetry arguments.

To visualize the possibility of a turbulent shear stress arising in the absence of a gradient of mean velocity, consider the case of a w' velocity component acting through an instantaneous gradient of u (in the w' direction). Physical considerations of momentum transfer suggest that an instantaneous correlation between w' and u' would exist. If the flow were homogeneous, the random nature of the turbulence suggests that on the average the correlation would be zero and no average shear stress would result. However, if the flow is not homogeneous and if the geometry of the flow is asymmetrical so that there exists a "preferred direction" for the fluctuating velocities, it is conceivable that an average correlation could exist. Furthermore, it is conceivable, but perhaps not too probable, that such a correlation could be of the same order of magnitude as that

caused by a mean velocity gradient.

Although the above arguments do not in any way prove that a turbulent shear stress must exist on surfaces normal to the isovels, they do raise a question about the validity of Deissler's assumption. This question can only be answered by some careful measurements of these stresses. Despite the fact that Deissler's solution does not necessarily represent the flow distribution that would be obtained if the secondary flows were negligible, it is compared with the present measurements with the implication that the discrepancy represents the effect of the secondary flow (see section 7).

Having considered the formulation of the problem and the enormous difficulties to be encountered in attempting a theoretical solution, it was decided that the best contribution would be some careful measurements of the flow field including, if possible, measurements of the secondary flows.

3.0 EXPERIMENTAL PROGRAM

The major objective of the experimental program was to obtain detailed measurements of the entire fully developed flow distribution including both the primary and the secondary flows in ducts having square and rectangular cross sections. At the outset it was not certain whether it would be possible to obtain quantitative measurements of the secondary flow. However, it was believed that such an attempt would, in any event, be informative because any failure to observe secondary flows would at least provide an indication of their relative magnitude. In addition it was hoped that visual observations of the flow by smoke injection might provide further visual evidence of secondary flow at least within the viscous sublayer. Finally, good measurements of the peripheral wall shear stress distribution were desired due to the apparent importance of wall shear distribution on the heat transfer behavior under certain thermal boundary conditions.

This section contains a description of the experimental apparatus, the instrumentation and some of the experimental measurements.

3.1 Apparatus

A schematic diagram of the experimental apparatus is shown in Figure 1. Air is drawn through a long straight duct by a blower located at the downstream end. A flow straightening section is attached to the entrance to remove any extraneous disturbances and to supply a homogeneous flow to the duct. A long length of duct is used to achieve a fully developed flow, the test section being located at the downstream end. Following the duct is a shallow angle diffuser and plenum. A blower draws air from the plenum through a flow metering nozzle and discharges to the atmosphere. Only a brief description of the apparatus is given here. For a more detailed account see Appendix 3.1.

3.1.1 Duct

A 5 inch square duct was selected as a compromise between a large cross section to minimize probe interference and a large velocity to facilitate measurements. This size resulted in a viscous sublayer thickness of about 0.030 - .040 inches at a Reynolds number of 15,000 (u_b = 6 ft/sec) making it possible to obtain hot wire measurements in the viscous layer. Furthermore, at the maximum flow capacity of the system (Re = 80,000) pitot tube velocity measurements were possible. Rectangular cross sections were then obtained by inserting partitions in the square duct.

A duct length of 32 feet (L/D_h = 75) was employed to insure fully developed flow. Measurements of velocity profiles and pressure gradient confirmed this. The duct was constructed in four sections; the entrance portion consisting of two 10 feet long wooden sections (3/4 inch plywood) and the test section consisting of two 6 foot long sections fabricated from 1/2 inch plexiglass. Figure 1 illustrates the method of construction. Duct dimensions were maintained with $\pm$ .005 inches and alignment of the joint between plexiglass sections was within .002 inches.

The rectangular ducts were formed by inserting a plexiglass partition in the square duct. The partition was sealed and held in position by long strips of rubber "O" seal as shown in Figure 1. The dimensions of the rectangular sections were 2.5x5 inches and 1.66x5 inches providing aspect ratios of 2:1 and 3:1 respectively.

The test section was located approximately one foot from the downstream end. Velocity probes were located at any desired point in the cross section by means of a two coordinate traversing system. (Figure 2.) The probes were inserted vertically through a moveable section in the top wall of the test duct. Horizontal and vertical traversing screws controlled the position of the probe to within $\pm$ .001 inches. Provision was made for probe rotation about its axis and observation of angular position from a protractor.

Probe location with respect to the duct wall was determined by electrical contact.

3.1.2 Auxiliary Equipment

The inlet flow straightener consisted of a large tube bundle followed by a pair of screens. It was connected to the duct entrance by a smooth nozzle providing a transition from an 11 inch diameter circle to the 5 inch square duct. It was found necessary also to insert a small tube bundle in the entrance of the duct in order to achieve symmetrical flow.

The diffuser following the test section had an included angle of 7.2 degrees and opened into a plenum chamber 10 x 10 x 18 inches long. Two screens were placed inside the plenum. Air discharged from the plenum through a 4 inch diameter smooth nozzle which was used to monitor the flow.

Air flow was provided by a blower driven by a 115-230 volt D.C. motor. A rheostat provided a continuous flow range and very fine control over the flow. A 12 inch length of flexible rubber hose connected the blower inlet to the plenum and provided vibration isolation between blower and duct.

3.2 Instrumentation

The major instrumentation was that required for the measurement of the primary and secondary velocities. Measurement of the flow direction was considered to be the best way to determine the secondary velocities. Secondary flows were believed so small that the difference between the primary velocity component and the total velocity vector was less than the instrument error. Thus no special effort was considered necessary for precise alignment of velocity probes with the axial direction.

Two methods were considered and employed for velocity measurements; 1) the hot wire annemometer and 2) the pitot tube. The pitot tube generally provides much more accurate velocity measurements but its use for this application was considered to involve two major drawbacks; 1) at velocities

below about 10 ft/second the velocity pressure is too small to be measured accurately by available means (.022 in H_2O) and 2) it is difficult to obtain pitot tube readings close to a solid boundary due to the size of the pitot tube and the presence of a steep velocity gradient. It was therefore decided to use a pitot tube for velocity measurements at the higher Reynolds numbers and a hot wire for the measurements at the lower Reynolds numbers where the velocities were below 10 ft/sec and where it was desired to obtain measurements in the viscous sub-layer.

Only the hot wire was employed for flow direction measurements, principally due to the necessity for avoiding velocity gradient errors. All known flow direction instruments employing pressure sensing elements have a velocity gradient error that would have been equal to or greater than the flow angles measured.

3.2.1 Hot Wire Instrumentation

Two different hot wire probes were employed for the various measurements. The original probe contained two 0.0005 inch diameter tungsten wires approximately 0.080 inches long in a "V" array. The construction features of this probe are illustrated in Figure 3. The original intention was to use one of the wires for measuring velocity and the other for sensing flow direction by aligning the wire parallel to the flow. A sharp peak in wire temperature was expected to occur when the wire passed through the wake from the forward supporting needle. Even though this scheme for measuring flow direction did not prove satisfactory, this probe was used for the velocity measurements in the square duct. In addition to the features already mentioned the probe stem was bent in a gooseneck fashion so that the needles supporting the wires were swept back about 60 degrees from the normal to the flow. This was done in an attempt to minimize the effect of probe stem interference on the flow in the vicinity of the wires. In addition the wire array was

arranged so that the plane of the gooseneck made an angle of 45 degrees with the flow direction. This was an attempt to minimize interference caused by close proximity of the probe stem to the vertical wall.

After considerable development it was discovered that flow direction could best be measured by using a standard probe with long straight needles. Such a probe was obtained with a 0.0003 inch diameter tungsten wire approximately 0.100 inches long. The supporting needles were .025 inches diameter by 1 inch long. The probe stem, like that of the gooseneck probe, was 0.134 inch diameter. Both probes were manufactured by Flow Corporation of Arlington, Mass. (Figure 3).

3.2.1.1 System for Mean Velocity Measurements

A simple bridge circuit with the wire operating at constant mean temperature was employed for the steady velocity measurements. Specifically, a Flow Corporation Model HWB system was used. The instrument reading error limited the accuracy to about $\pm$ 3 percent.

A special apparatus was constructed for hot wire calibration. This was done both to provide a reliable standard against which to calibrate the probes and for convenience in the experimental program. The probes were calibrated immediately before and after each test run to insure against calibration shift. The apparatus consisted of a blower discharging through a long tube with a nozzle at the end (Figure 4). The hot wires were calibrated in the jet formed by this nozzle. Velocities were determined by flow measurement with calibrated nozzles. For details of the calibration apparatus and procedure refer to Appendix 3.2.

The hot wire calibration data were best correlated by a relation presented recently by Collis (21) wherein the square of the wire current I^2 is proportional to $V^{.45}$. Figure 5 shows a typical calibration according to this relation. (Further discussion is given in Appendix 3.2)

3.2.1.2 System for Flow Direction Measurements

As previously mentioned the original concept of measuring flow direction with the hot wire proved unsatisfactory. This method involved rotating the hot wire until its axis was parallel to the flow and observing the peak in wire temperature as the wire entered the wake from the foreward support needle. Only the final method and instrumentation is described here. A more complete account of the development difficulties is presented in Appendix 3.3.

A standard single wire probe with long straight needles was used for flow direction measurement (Figure 3). The probe was inserted through the duct wall with the probe stem normal to the duct axis. It was then rotated until the wire axis was oriented about 10 to 20 degrees from the flow direction. The wheatstone bridge circuit, of which the wire constituted one leg, was then brought into balance and the angular position of the probe was noted from the protractor disc. The probe was then rotated until the wire assumed approximately the same position on the opposite side of the flow direction, and the bridge was brought back into balance by rotation of the probe to the proper position. This angle was then recorded and the bisector of the two angles was taken as the direction of the flow. It was found that the same flow angle was obtained regardless of the angle that the wire made with the flow direction when balancing the bridge. This indicated that the sensitivity of the hot wire to flow angle was perfectly symmetrical. As a result it was only necessary to make two angle observations to obtain the flow direction at a single point.

Obviously this method of measuring flow direction indicated only the component in the plane normal to the probe stem axis. Thus to determine the complete three-dimensional flow direction it was necessary to measure components in two mutually perpendicular planes.

The bridge circuit used for flow direction measurements is illustrated in Figure 6. A very sensitive spotlight galvanometer was used to sense bridge unbalance. The maximum sensitivity provided by this circuit was so good that it had to be reduced somewhat due to the magnitude of the flow direction fluctuations caused by the turbulence. At the higher Reynolds numbers the flow direction could be read within about 1/8 degree. At the low Reynolds numbers the accuracy was somewhat poorer due to the larger turbulent fluctuations. The accuracy indicated here represents primarily the accuracy of reading the protractor. A more detailed description of this circuit is given in Appendix 3.3.

3.2.2 Pitot Tube and Pressure Instrumentation

A pitot tube was used to measure primary velocity distribution in the square duct only at a Reynolds number of 75,000. The tip of the tube was made from stainless steel hyperdermic tubing .028 inches outer diameter by .016 inches inner diameter. The circular cross-section was retained at the tip and the nose was filed square with the axis. The stem had a diameter of .058 inches and was bent at a 45 degree angle from the vertical about 2 1/2 inches above the tip axis. The tip extended upstream about 1 3/8 inches from the stem.

Static taps were placed in the two side walls (one in each wall) located in the same cross-sectional plane as the pitot tip and approximately midway between corners. In addition three more static taps were placed in the top wall of the plexiglass section 18 inches apart for purposes of measuring the axial static pressure gradient.

Besides the pitot tube used to measure velocity distribution, a somewhat larger one (.058 in.O.D. by .042 in.I.D.) was used as a "Preston Tube" for measuring wall shear stress distribution. The tip of this probe extended 4 inches upstream from the stem. The calibration and use of this

probe for measurements of wall shear stress is discussed in Section 3.3.1.

The pressure measurements from these instruments were obtained on a Prandtl type micromanometer using red petroleum oil with a specific gravity of 0.830. These pressure readings were believed accurate to within about .001 inches of water. The resultant accuracy of the pitot tube velocity readings is estimated to be 1 percent.

3.2.3 Other Instrumentation

System flow rate was measured with smooth nozzles conforming approximately to the ASME standards for the long radius - low ratio nozzle. As stated earlier a 4 inch diameter nozzle was installed in the downstream plenum for this purpose. This nozzle was used for flow measurement and monitoring at the higher Reynolds numbers. There is some reason to question the accuracy of this measurement at the highest speeds (see discussion in Appendix 3.4). This may be due to flow separation in the diffuser or plenum. At the lower speeds, flow measurement was accomplished with a 1.800 inch diameter nozzle placed at the end of a short length of hose attached to the blower discharge opening. Flow readings with this nozzle appeared satisfactory.

The pressure drop across these flow nozzles was measured on a 3 inch Ellison inclined draft gage with an accuracy of 0.01 inch of water.

3.3 Measurements

Using the apparatus and instrumentation described above measurements of the following quantities were obtained:

1) Primary (axial) velocity distribution

2) Secondary velocity distribution

3) Wall shear stress distribution

4) Friction factor and flow development

5) Secondary flow visualization with smoke

6) Qualitative turbulence observations

All of these quantities were measured in the 5 inch square duct whereas only the primary and secondary velocity distributions were measured in the rectangular ducts. The primary and secondary velocity measurements constitute the major effort of this work. Consequently an entire section is devoted to their description (Section 4). Only the other measurements are discussed here.

3.3.1 Wall Shear Stress Distribution

A special effort was made to measure wall shear stress distribution in the square cross-section only. Careful hot wire velocity readings were made in the viscous sub-layer at Reynolds numbers of 14,600 and 22,300 (Tables 1 and 2, Appendix 3.4). It was hoped that a linear velocity distribution would be obtained so that the wall shear stress could be determined. Unfortunately the results were not good. Further discussion is given in Section 4.1.1.

The Preston tube was used to measure wall shear stress distribution at a Reynolds number of 78,500. The tube was calibrated in a 7/8 inch diameter circular tube with fully developed turbulent flow. Wall shear stress was determined by measuring the axial pressure drop and equating the pressure force to the wall shear force. The calibration is shown in Figure 10 along with Preston's calibration for his tubes. A discrepancy is noted between the calibration obtained here and that of Preston. The tubes used by Preston had a diameter ratio $d_i/d_o = 0.6$ whereas for the present tube $d_i/d_o = 0.78$.

The pitot tube used in this study for velocity measurements had a diameter ratio of 0.6. It was also calibrated as a Preston tube and the results are shown on Figure 10 to be essentially in agreement with Preston's.

The wall shear stress results obtained here with the larger Preston tube agree well with those from the calibrated pitot tube and are believed

to be more accurate due mainly to the increased accuracy of measuring the higher pressure involved. It is interesting to note from Figure 10 that the line representing the pressure at the geometric center of the Preston tube obtained by applying the conventional "law of the wall" closely parallels the calibration of the large Preston tube.

Figure 27 shows the distribution of wall shear stress obtained from the Preston tube. It is surprisingly flat over most of the duct periphery and drops sharply to zero at the corner. Although the hot wire velocity data in the viscous sublayer could not be interpreted in a satisfactory way, they nevertheless provide a qualitative check with the Preston tube measurements.

3.3.2 Friction Factor and Flow Development

The friction factor for fully developed flow in the square duct was measured by means of four static pressure taps equally spaced along the plexiglass section. The average velocity was determined by measurements of centerline velocity and of the velocity head at the throat of the square inlet nozzle. The two measurements were in good agreement. A Reynolds number range of 20,000 to 75,000 was covered. The measured friction factors ranged from 4 1/2 to 5 1/2 percent lower than the circular tube correlation represented by

$$f = 0.046\ Re^{-.2} \qquad (9)$$

Other friction factor measurements made by the author in a 1 inch square duct were in almost perfect agreement with this circular pipe correlation. This smaller duct had a much rougher surface than the 5 inch plexiglass duct which undoubtedly accounts for the difference in friction factor.

Flow development was checked by removing the two 10 foot wooden sections and operating the duct with a length of only about 11 feet. The velocity profiles measured at the test section were identical within

experimental error to those measured with the full length of duct.

3.3.3 Secondary Flow Visualization With Smoke

The secondary flows were observed directly by injecting smoke into the flow through a small hyperdermic. The plexiglass section was inverted placing the test section at the upstream end and joining it to the wooden entrance section. A very low speed turbulent flow (Re $\approx$ 9,000) was established so that the smoke would not be diffused too rapidly by the turbulence. Cigarette smoke was injected axially into the flow through a hyperdermic tube at various points in the cross-section. Weak secondary flows were actually observed. The bottom of the duct was covered with black art paper having lines drawn on it parallel to the duct axis to aid in detecting the cross flow. Figure 12 shows a sequence of photographs taken of the smoke trace at various positions in the duct. The slight deviations from axial flow clearly indicate secondary flows. The secondary flows at this low Reynolds number appear to be stronger than at the higher Reynolds numbers as indicated by the angle measurements. Although these visual observations cannot be used to obtain quantitative data, it is interesting to be able to "see" these secondary flows.

3.3.4 Qualitative Turbulence Observations

No quantitative measurements of turbulence quantities were made during this study. However, qualitative observations of the axial turbulence intensity $\tilde{u}'$ were made by observing the hot wire signal on the oscilloscope. The signal was first amplified with the constant current circuit within the Flow Corporation HWB system. After passing through a filter to remove the frequencies above about 10,000 cps, the signal was fed into a DuMont Model 304 oscilloscope.

The observations of primary velocity intensity were in complete accord with results from pipe flow reported by Laufer (24). The maximum intensity

was observed to occur near the outer edge of the viscous sublayer. From this point the intensity decreased continuously as the probe was moved toward the duct center. A rather large intensity was observed within the viscous sublayer right up to the wall. The most remarkable difference between the oscilloscope traces within the sublayer and without was the obvious absence of high frequency fluctuations in the viscous layer (no sharp peaks were seen in the oscilloscope trace).

4.0 DATA PRESENTATION AND INTERPRETATION

The fully developed turbulent flow in straight rectangular ducts is best described by stating that the streamlines representing the mean flow are very nearly parallel to the duct axis but actually follow somewhat distorted helical paths wherein a fluid particle beginning near the duct center moves gradually toward one of the corners, and upon approaching closely to the corner, turns and moves slowly out along one wall and finally returns to the center region. The streamlines are so nearly axial that the mean velocity vector at any point is essentially equal in magnitude to the axial component (with negligible error).

It is, therefore, convenient to regard the mean flow as consisting of a primary or purely axial flow with a secondary circulatory motion superimposed to yield the actual true flow. The streamlines representing the primary flow are simply straight lines parallel to the axis. The streamlines representing the secondary flow are a series of closed loops in the cross-sectional plane describing the circulatory motion into and out of the corner regions (Figure 34). The continuity equation specialized for fully developed flow lends itself to the definition of a stream function representing the secondary flow alone. The measurements of the primary and secondary flows in the three different rectangular ducts are presented and interpreted separately below. Measurements from the square duct were obtained by the author. Those from the rectangular ducts were obtained by G. B. Gilbert with the same apparatus and instrumentation and presented in his Masters thesis (20).

4.1 Primary Velocity Distributions

Measurements of primary velocity distributions were obtained from the 5 inch square duct with both the gooseneck hot wire probe and the pitot tube. The hot wire was used for measurements at Reynolds numbers of 14,600;

22,300; 34,300; 43,800; 57,000; and 66,000 while pitot tube measurements were obtained at a Reynolds number of 75,500 only. These velocity data are presented in Tables 1 through 7 of Appendix 3.4. Although measurements from only one quadrant are shown, spot checks of points in the other quadrants indicated symmetrical flow. Pitot tube data were corrected near the walls for the effects of turbulence intensity and velocity gradient error. The details of these corrections are given in Appendix 4.1. No corrections were made to the hot wire data for reasons explained later in the discussion of viscous sublayer data. Figures 13 through 19 contain the velocity profiles obtained from this data. Integration of these profiles provides a measure of the average or bulk velocity which is compared with the flow measurement in Tables 1 through 7.

Primary velocity measurements were obtained from the two rectangular duct sections using the standard hot wire probe with long straight needles. From the 2.5 by 5 inch duct primary velocity profiles were measured at Reynolds numbers of 24,400 and 88,000 (Figures 20 and 21). Measurements in the 1.66 by 5 inch duct were made at a Reynolds number of 60,000 only (Figure 22). In the rectangular sections the velocity profiles were measured both with the probe extending through the short side and through the long side. Because the readings obtained with the probe stem near the vertical wall (steep velocity gradient along wire axis) are not believed to be accurate, the profiles shown are constructed from a weighted average of these readings.

4.1.1 Square Duct

Consider first the measurements from the square duct. The velocities obtained with the pitot tube show some rather weak evidence of secondary flow by virtue of the profiles at $z/a = 0.1$ and 0.2 where the velocity is slightly larger near the corner than at the centerline. (Figure 19.) No such evidence was noticed in the hot wire profiles, although the hot wire did not appear

accurate enough to detect these small differences. It is interesting to note that in the central portion of the flow (about 75 percent of the area) the normalized velocity distribution is identical within the accuracy of the measurements for all Reynolds numbers observed. Near the wall, as expected, the velocity profiles vary due to the dependence of wall shear stress on Reynolds number.

Figures 23 through 26 show the velocity profiles near the wall for the pitot tube data and three lowest hot wire Reynolds numbers with the distance scale expanded. The pitot tube data (Figure 23) are corrected for turbulence intensity and velocity gradient errors as indicated in Appendix 4.1. The conventional generalized velocity distribution or "law of the wall" correlation as fit to the first four data points is shown by the solid lines. The fit to these points is very good. At greater distances from the wall the data fall below the "law of the wall" curve. This is easily explained as the effect of the secondary flows since they tend to convect low momentum fluid out from the wall region along most of these profiles. The straight dashed lines emanating from the origin represent the velocity gradients at the wall corresponding to the "law of the wall" fit to the velocity data. Pressure drop measurements from the square duct indicated friction factors from 4 1/2 to 5 1/2 percent below the circular pipe correlation represented by the simple emperical equation

$$f = .046/ Re^{.2} \qquad (9)$$

The friction factor obtained from the wall velocity gradients shown in Figure 23 agrees with these pressure drop measurements within 2 percent.

The hot wire data near the wall is not nearly so good as the pitot tube data. The original intention was to obtain hot wire velocity data in the viscous sublayer at the low Reynolds numbers as a means of determining the wall shear stress distribution. Figures 24, 25 and 26 show the data

near the wall for Reynolds numbers of 14,600; 22,300; and 34,300. The data within the viscous sublayer appear to define linear profiles, but they indicate a finite velocity at the wall. This effect appears more pronounced at the lower Reynolds numbers. Moreover, the velocity gradients indicated by these points give friction factors from 10 to 20 percent below those from pressure drop measurements. Observation of the hot wire under a microscope revealed that at the point of contact of the probe with the wall the filament was about .003 to .005 inches from the wall. Even this displacement of the profiles .005 inches to the right is not sufficient to eliminate the discrepancy.

In an attempt to explain these results the author made several independent checks of the hot wire calibration as explained in Appendix 3.2. They merely substantiated the original calibration. No corrections were made to the hot wire readings. A discussion in Appendix 4.1 indicates that the wall cooling effect is negligible and the generally accepted correction for turbulence intensity, although small, shifts the data in the wrong direction. The author believes the discrepancy may be caused by either of two phenomena; 1) probe interference or 2) intensity error. It is well known that when a probe is inserted in a shear flow the varying stagnation pressure along the stem causes a secondary flow which tends to convect high velocity fluid toward a lower velocity region. This phenomenon, producing a secondary flow along the needles, could cause the hot wire to read high, particularly near the wall. Nickerson (18) found in order to obtain good hot wire velocity data in a boundary layer, it was necessary to "sweep back" the hot wire probe so that the needles made an angle with the flow of about 20 degrees or less. The gooseneck probe used for the above measurements made about a 30 degree angle with the flow.

Secondly the author believes that the presence of large turbulence

intensities near the wall should cause an increase in heat transfer over the steady state value corresponding to the mean velocity, thereby causing the hot wire to read high. He has been unable to find any confirmation of this viewpoint.

The distribution of wall shear stress may be obtained from the pitot tube profiles (Figure 23). To confirm this distribution direct shear stress measurements were made at approximately the same Reynolds number with a calibrated Preston tube as explained in Section 3.3.1. Figure 27 illustrates the resulting shear distribution. Hot wire measurements at the lower Reynolds numbers give approximately the same shear distribution. It is interesting to note that the shear stress is very nearly uniform over about 75 percent of the duct wall and decreases sharply to zero at the corners. The wall shear distribution obtained from Deissler's calculations is also shown on Figure 27 for comparison. With his assumption of no secondary flow he obtains a shear distribution not nearly as flat as that indicated by measurements.

Finally it is interesting to observe a map of constant velocity contours (isovels). Figure 28 shows such a map constructed from the pitot tube measurements. Also included are the results of Deissler's calculations (dashed lines). The measurements show isovels which are nearly parallel to the duct walls except in the regions very near the corner and near the axis. In contrast Deissler's results for no secondary flow indicate much more rounded isovel lines. Further discussion is given in Section 7.2.

4.1.2 Rectangular Ducts

The primary velocity measurements from the rectangular ducts are not considered as accurate as those from the square duct, principally due to the use of the long needle probe with the needles protruding normal to the flow. The velocity profiles obtained from the two rectangular cross sections

(Figures 20 to 22) show definite peaks near the corner regions indicating the presence of secondary flows (except at Re = 24,400 in the 2.5x5 inch duct). This evidence of secondary flow was much more pronounced here than with the square cross section. The corresponding isovel contour maps (Figures 29 through 31) also provide evidence of secondary flows by the displacement of isovels toward the corners. The isovel map for the duct with a 3:1 aspect ratio (Figure 31) is very similar to the results of Nikuradse (6) for an aspect ratio of 3.5:1.

4.2 Secondary Velocity Distributions

In the square duct secondary flow angles were measured in the horizontal or x-z plane only. The assumption of symmetry across the diagonal emanating from the corner makes it unnecessary to take angle measurements in the x-y plane. As a check on the symmetry of the flow, angle measurements were made in all four quadrants at a total of about 220 points of the cross section. Flow angle distributions, measured at several Reynolds numbers during the course of instrumentation development, were very nearly identical.

Only near the walls did the results depend on Reynolds number, higher angles being observed at the lower Reynolds numbers. Data for Reynolds numbers of 15,000; 34,000; and 60,000 are tabulated in Appendix 3.4 (Tables 8, 9 and 10).

For the rectangular ducts it was necessary to measure flow angles in both the x-z and y-z planes. This was accomplished by making two duct assemblies for each of the rectangular geometries, one with the partition mounted vertically and one with it mounted horizontally. For the 2.5x5 inch rectangular configuration, direction data were obtained at Reynolds numbers of 88,000 and 24,400 (Tables 11 and 12, Appendix 3.4). Measurements in the 1.66 x 5 inch duct were made only at a Reynolds number of 60,000 (Table 13). Traverses covering both of the lower quadrants indicated

symmetrical flow within the instrument accuracy. Only the averaged data representing a single quadrant are tabulated.

Because the secondary flow angles were usually less than 1 degree compared with an instrument accuracy of $\pm$ 1/8 degree, these data are admittedly somewhat crude. It is particularly important, then, to bear in mind certain restrictions imposed on the secondary flow distribution by continuity, boundary and symmetry conditions when analyzing and interpreting these data. These conditions may be stated as follows: (considering only the quadrant near the origin - Figure 1)

1) Continuity (equation 4d) requires that $\frac{\partial \bar{v}}{\partial y} = -\frac{\partial \bar{w}}{\partial z}$ at each point in the flow
2) $\bar{v} = \bar{w} = 0$ along $y = 0$ and $z = 0$
3) Along boundary $y = 0$, $\partial\bar{w}/\partial z = 0$, hence from continuity $\partial\bar{v}/\partial y = 0$
4) Similarly along the boundary $z = 0$, $\partial\bar{v}/\partial y = 0$, and from continuity $\partial\bar{w}/\partial z = 0$.
5) Along the axis of symmetry $y = a$, $\bar{v} = 0$ and $\partial\bar{w}/\partial y = 0$. However, $\partial\bar{v}/\partial y \neq 0$ (See Appendix 4.2 for proof).
6) Similarly along the axis of symmetry $z = b$, $\bar{w} = 0$ and $\partial\bar{v}/\partial z = 0$ but $\partial\bar{w}/\partial z \neq 0$.
7) For the square duct only, symmetry across the diagonal requires that $\partial\bar{v}/\partial y = \partial\bar{w}/\partial z$ at all points along the diagonal. Considering continuity, this condition is satisfied only when $\partial\bar{v}/\partial y = 0$ & $\frac{\partial \bar{w}}{\partial z} = 0$.

Consider first the measurements from the square duct. Data from the various runs were averaged to obtain the "best interpretation" of the secondary flow. Because, in certain portions of the upper quadrants only the hot wire needles and filament protruded into the flow, these data were weighted most heavily in the averaging. This was particularly important

near the vertical walls. Figure 32 shows the secondary velocity profiles so obtained. The secondary velocity components are normalized with the axial centerline velocity, thereby making the profiles nearly correct for all Reynolds numbers within the range observed. Although the profiles are plotted as $\bar{v}$ vs y they also may be interpreted as plots of $\bar{w}$ vs z.

Included in Figure 32 are the data points representing the averaged measurements and the solid lines representing the "best interpretation" of the data by observing the boundary and symmetry conditions mentioned above. Besides meeting these conditions, care was taken to insure that the "continuity integral" was satisfied. (Considering a control volume bounded by the walls y=0, z=0 and by the centerline z=b across which no secondary flow passes, the integral of v along the line y=y must be equal to zero.) The resulting curves fit the data points remarkably well. Only certain data very near the wall must be ignored to satisfy these restrictions.

Before imposing all of the above conditions on the interpretation of the data, smooth curves were drawn directly through the data points. From these curves the divergence $\left(\partial\bar{v}/\partial y + \partial\bar{w}/\partial z \right)$ was evaluated at several points as an indication of the data quality. Of course, continuity requires that the divergence be everywhere equal to zero. Figure 33 illustrates the divergence values so obtained. They are normalized by multiplying by a/U_{ℓ}. The resulting numbers represent physically the inverse length of the stream tube (x/a) over which all of the fluid entering the stream tube at x will leak out. A zero divergence indicates an infinite stream tube length and thus no leakage. In the central portion of the flow the divergence is everywhere zero within the accuracy of evaluating slopes from the resulting curves. Near the boundaries the divergence is non zero, reaching a maximum value of .04. As indicated in the discussion (Appendix 3.3) of the measuring technique development, the flow angle readings near the

wall are not believed to be particularly accurate. Thus the finite divergence values near the wall are not surprising. However, the precision to which the data satisfy continuity in the bulk of the flow indicates that the probe errors were satisfactorily eliminated and the final measurements were a true representation of the secondary flow.

The secondary flow streamlines, constructed from the adjusted profiles of Figure 32, are shown in Figure 34. The flow is seen to behave in the manner originally postulated by Prandtl. The stream function ψ was defined by

$$\bar{v}/u_\ell = \frac{\partial \psi}{\partial (z/a)} \quad ; \quad \bar{w}/u_\ell = -\frac{\partial \psi}{\partial (y/a)} \tag{10}$$

By integrating along lines of constant y, the stream function was evaluated at various points throughout the flow to enable construction of the streamline map, e.g.

$$d\psi = \partial\psi/\partial y \, dy + \partial\psi/\partial z \, dz$$

for constant y

$$d\psi = \bar{v}/u_\ell \, d(z/a) \quad ; \quad \psi = \int_0^{z/a} \bar{v}/u_\ell \, d(z/a) \tag{11}$$

This dimensionless stream function, when multiplied by the centerline axial velocity u_ℓ and the duct half width "a" represents the volume rate of secondary circulation (per unit axial length) between the streamline labeled zero and the streamline in question. The velocity along any streamline is inversely proportional to the normal distance from the neighboring streamline. In this manner the secondary flow streamline map serves to define completely the secondary flow. It is convenient, however, to also show a map with contours of constant secondary velocity (Figure 35). Maximum velocities about 1 1/2 percent of the axial centerline velocity occur along

the walls near the corner. Along the diagonal they reach 1 percent. Near the center of the duct the secondary velocities are very small.

The distribution of axial vorticity $\bar{\xi} = \partial\bar{w}/\partial y - \partial\bar{v}/\partial z$ is also of interest. Figure 36 shows the vorticity map constructed from the measured slopes of the secondary flow profiles from Figure 32. The vorticity is also normalized by multiplying by a/u_{ξ} . It is interesting how the region of greatest vorticity occurs near the walls in the corner region where the wall shear gradient is large. This is discussed further in Section 6. Although it is not clearly shown in Figure 36, the vorticity changes sign in the region very close to the wall and assumes a large value at the wall due to the finite gradient of the secondary velocity component parallel to the wall.

The previous discussion has been confined to the experimental results from the square duct. Similar analysis was made by Gilbert (20) of the measurements from the two rectangular sections. Figures 37, 38, and 39 contain respectively the streamline map, secondary velocity map, and the vorticity map for the 2.5 x 5 inch duct. These results are representative of both Reynolds numbers tested. Figures 40, 41, and 42 contain analogous results for the 1.66 x 5 inch duct.

It is interesting to compare the secondary flow measurements from the three different configurations. The maximum secondary velocities are observed in all three ducts to be about 1 1/2 percent of the centerline velocity. These maximum velocities occur near the walls in the vicinity of the corner. Relatively large velocities also appear along the diagonal feeding the flow toward the corner. Thus the duct aspect ratio does not appear to influence the magnitude of the secondary velocities.

The streamline maps (Figures 34, 37, and 40) show two eddies occupying each quadrant in all three cases. The eddies appear to be divided in all three ducts by the bisector of the corner angle. Thus in the rectangular

cross sections there is a large eddy near the long side and a smaller eddy near the short side. The physical size of the eddies are perhaps not so significant as the flow rates within them. It was shown earlier that the stream function ψ indicated on the streamline maps is a measure of the volume flow rate between the streamline under consideration and the zero streamline. Referring to the streamline maps it is seen that the larger eddy always carries a larger volume flow. In particular the 2:1 rectangle shows a small eddy with about 45 percent as much volume flow as the large eddy, whereas in the 3:1 rectangle the small eddy carries only about 20 percent of the volume flow of the large eddy. All three ducts have a large eddy with approximately equal volume flow.

The secondary flow near the center of the duct appears to diminish as the aspect ratio is increased, indicating that the flow is generally confined to the corner region.

5.0 EVALUATION OF TERMS IN EQUATIONS OF MOTION

The experimental measurements described in the previous sections constitute a relatively complete determination of the mean flow distribution. It is particularly interesting now to evaluate from these measurements the various terms in the equations of motion. This will provide further insight into the mechanism of the flow and will serve as a basis for making assumptions for further analytical work.

5.1 Axial Momentum Equation

The equation of motion governing the primary velocity distribution is appropriately referred to as the axial momentum equation (4a).

$$\rho\left(\bar{v}\frac{\partial\bar{u}}{\partial y}+\bar{w}\frac{\partial\bar{u}}{\partial z}\right)=-\frac{\partial\bar{p}}{\partial x}+\mu\nabla^2\bar{u}-\rho\left[\frac{\partial}{\partial y}(\overline{u'v'})+\frac{\partial}{\partial z}(\overline{u'w'})\right] \quad (4a)$$

In the absence of a secondary flow this equation (with relations for the turbulent stresses) is sufficient for determining the axial velocity distribution (Deissler's problem). When secondary velocities are present this equation becomes coupled to the other two momentum equations (4b) and (4c) through the non-linear convective terms, and the mathematical problem becomes very difficult indeed.

First consider the physical significance of the various terms appearing in equation (4a). The pressure term $\partial\bar{p}/\partial x$ represents the net pressure force acting in the axial direction on an elemental control volume. The viscous term $\mu\nabla^2\bar{u}$ describes the sum of the axial forces acting on the element due to viscous stresses, both shear and normal. The turbulent stress terms $\rho\left[\partial/\partial y(\overline{u'v'})+\partial/\partial z(\overline{u'w'})\right]$ denote the effective net axial shear force on the element resulting from turbulent fluctuations. Finally the convective terms $\rho\bar{v}\,\partial\bar{u}/\partial y+\rho\bar{w}\,\partial\bar{u}/\partial z$ represent the net rate of convection of axial momentum out of the control volume.

The convective terms, pressure term, and the viscous terms are readily evaluated from the measurements. The turbulent stress term can only be computed from the others through equation (4a). The viscous and convective terms vary from point to point throughout the cross section, the pressure term being uniform. Figure 43 shows the distribution of the viscous, convective and turbulent stress terms for the square duct at a Reynolds number of 34,300. They are normalized by dividing by the constant pressure term. The viscous stress term is seen to dominate near the wall. At the wall the convective term and turbulent stress term are both zero so the viscous term must exactly balance the pressure gradient. Moving away from the wall, the viscous term rises sharply to a peak value which is off the scale of Figure 43 and then decreases rapidly to zero. Because the required second derivatives of u are very difficult to obtain, (especially near the wall) the viscous term is only approximate. Its behavior is similar for all of the profiles shown.

The convective terms are observed to be of approximately the same order of magnitude as the pressure gradient. Near the axis of the duct they are negligible. In certain regions, particularly near the corner, these terms are larger than the pressure gradient. Hence, it is obvious that the secondary flow terms cannot be discarded from the axial momentum equation if the velocity distribution is to be predicted accurately.

The turbulent shear stress terms are seen to be important over the entire flow, except of course in the viscous sublayer which is hardly evident from the curves. They are very large and nearly equal (but opposite in sign) to the viscous stress terms in the region near the wall, indicating that both the turbulence generation and viscous dissipation are large there. This observation corresponds with results from the circular pipe. Near the centerline the turbulent stress terms are essentially equal

to the pressure gradient, as in the case of the circular pipe and two dimensional channel. Throughout the remainder of the flow, however, (particularly near the corners) the turbulent stress terms are large in order to offset the large convective terms. An attempt was made to compare the turbulent stress terms as computed above with those predicted from the various mixture length theories. The results were not good. This effort is discussed further in Section 7.

Originally it was hoped that the distributions of the turbulent shear stresses $\overline{u'v'}$ and $\overline{u'w'}$ could be evaluated from the present experimental measurements of the mean flow. From initial observation of the vorticity equations (7b) and (7c) it appears as though they constitute a set of two equations in the two unknown stresses $\overline{u'v'}$ and $\overline{u'w'}$. However, as already stated in Section 2, these two equations are not independent and can be shown by appropriate manipulation to be identical. The axial momentum equation (4a) constitutes a much simpler relation involving these same two unknown stresses.

In conclusion, the secondary flow convective terms are shown to make significant contributions to the axial momentum equation particularly near the corners. Their exclusion from any analysis cannot be justified. This result is not really surprising, since the original discovery of these secondary flows resulted from their effect on the axial velocity distribution.

5.2 Axial Vorticity Equation

The y and z vorticity equations (7b) and (7c) were discussed above in connection with the turbulent shear stresses $\overline{u'v'}$ and $\overline{u'w'}$. Observation of equation (7a) involving the axial vorticity component ξ_x reveals two unknown turbulent stresses ($\overline{v'^2} - \overline{w'^2}$) and $\overline{v'w'}$.

$$\rho\left(\bar{v}\frac{\partial\bar{\xi}}{\partial y}+\bar{w}\frac{\partial\bar{\xi}}{\partial z}\right)=\mu\nabla^2\bar{\xi}+\rho\left[\frac{\partial^2}{\partial y\partial z}\left(\overline{v'^2}-\overline{w'^2}\right)-\frac{\partial^2}{\partial y^2}\left(\overline{v'w'}\right)+\frac{\partial^2}{\partial y^2}\left(\overline{v'w'}\right)\right]\quad\cdots(7a)$$

The normal stress term can be evaluated near the walls by making use of the wall similarity concept applied to the intensity components $\overline{v'^2}$ and $\overline{w'^2}$. A detailed discussion of wall similarity for intensities is presented in Section 6. Although wall similarity only applies very near the wall, it was believed that this term would become negligible away from the wall. Then in principle, with $\overline{v'w'}$ as the only unknown, equation (7a) with appropriate boundary conditions is sufficient for evaluating the distribution of the turbulent shear stress $\overline{v'w'}$ from the mean flow measurements.

Before proceeding to describe the attempted computation of the $\overline{v'w'}$ distribution, it is interesting to consider the physical interpretation of the various terms appearing in the axial vorticity equation (7a). The two terms on the left hand side represent the substantial time derivative of the axial vorticity or, alternately, the net convection of vorticity out of an elemental control volume due to the secondary velocities. The terms on the right hand side may all be interpreted as torques acting on a fluid element. The viscous term $\mu\nabla^2\bar{\xi}$ denotes the net torque exerted by the viscous stresses, both normal and shear. The term involving intensities $\overline{v'^2}$ and $\overline{w'^2}$ may be interpreted as the net torque exerted by the normal turbulent fluctuations which act like pressure forces. Finally the second y derivative and the second z derivative of $\overline{v'w'}$ signify the net torques exerted by the turbulent shear stresses $\overline{v'w'}$ on the y and z faces respectively of an elemental control volume.

The various terms of equation (7a) were computed from the mean flow measurements at several points throughout the duct cross section

(square duct at Re = 34,300). Unfortunately, the inability to make an accurate evaluation of the viscous terms has prevented a solution for the shear stress distribution $\overline{v'w'}$. The viscous terms involve formation of third derivatives of the relatively crude secondary velocity measurements. Slopes may be obtained with fair accuracy but it is questionable whether the determinations of the second and particularly the third derivatives are even of the correct order of magnitude.

In view of the difficulties encountered the results are described only briefly. The viscous terms were found to be very much larger near the wall than any of the other terms throughout the entire flow. As a result, an integration of the turbulent stress terms $-\frac{\partial^2}{\partial y^2}(\overline{v'w'}) + \frac{\partial^2}{\partial z^2}(\overline{v'w'})$ out from the wall would have resulted in an integral whose value over the entire flow was determined by the viscous terms near the wall. This observation made the solution for $\overline{v'w'}$ appear hopeless.

As stated earlier the computed value of the intensity term $\frac{\partial^2}{\partial y \partial z}(\overline{v'^2}-\overline{w'^2})$ was expected to become negligible away from the wall. Although this term decreases rapidly with increasing distance from the wall (after reaching a peak value of course) so do the other terms of equation (7a) so that the intensity term does not appear to be everywhere negligible in comparison.

In the central region away from the walls there appeared to be a tendency for the convective terms to offset one another approximately. The viscous dissipation terms, while being so large near the wall, were generally small throughout the remainder of the flow. Hence, this crude evaluation of terms in the vorticity equation indicates that the axial vorticity is generated and dissipated principally near the wall and is mostly convected about throughout the remainder of the flow. It was not obvious, however, that either the viscous terms or the turbulent stresses

could be neglected in the central region. The author believes that actual measurements of the turbulent stresses will be necessary to obtain a better understanding of the distribution of these various terms.

6.0 SOME SPECULATIONS CONCERNING THE CAUSE OF SECONDARY FLOWS

It has been well established by previous investigators that the secondary flows are in some way caused by the turbulence phenomenon. (See Section 2 for a detailed review.) Moissis (8) and Maslen (9) prove that secondary flows cannot exist in the laminar case. Originally Prandtl (7) and later Howarth (10) and Einstein (11) indicate that the asymmetric nature of the turbulent stresses provides the cause of the secondary flow.

Recently Townsend (12) shows that the difference between the turbulent fluctuation intensities $\overline{v'^2}$ and $\overline{w'^2}$ near a solid boundary leads to cross flows in turbulent boundary layers which are not quite two-dimensional. He demonstrates that a transverse gradient of wall shear stress results in a driving force for a secondary flow and suggests that this phenomenon is the cause of secondary flows in straight non circular ducts. Delleur (4) adopts Townsend's idea and suggests that "boundary-shear turbulence" is the "self-exciting generator" of the secondary motion.

The objective of this section is to clarify this concept of boundary-shear turbulence as the cause of secondary flow and to discuss the evidence from the experimental measurements in support of this idea.

6.1 Wall Similiarity Applied To Turbulence Intensities

Wall similiarity or the generally accepted "Law of the Wall" has long been used successfully to describe the mean velocity distribution in turbulent flow near a solid boundary. The relation is generally expressed by

$$\bar{u}/u^* = fn\left(y/\nu\, u^*\right) \tag{12}$$

where $u^* = \sqrt{\tau_0 g/\rho}$

Recently it has been suggested by many sources that this same concept may apply to the fluctuating components $\overline{u'^2}$, $\overline{v'^2}$ and $\overline{w'^2}$ as well as the

mean velocity. However, the available experimental data on turbulence intensities near a boundary are indeed few.

The most complete data known to the author are the measurements of Laufer (24) in a 10 inch diameter circular pipe. He measured intensities near the wall at two Reynolds numbers (50,000 and 500,000) and presented the data in the form $\tilde{u}'/u^*$ versus $y^* = y/\nu u^*$. These data are shown in Figure 44. As expected the intensity component normal to the wall ($\tilde{v}'$) is the smallest and approaches zero at the wall with zero slope. The axial intensity component ($\tilde{u}'$) is the greatest while the transverse component ($\tilde{w}'$) assumes intermediate values. The $\tilde{u}'$ and $\tilde{v}'$ data for the two Reynolds numbers agree remarkably well in the region near the wall ($y^* < 20$). The $\tilde{v}'$ data are actually in agreement over the entire y^* range shown. However, the $\tilde{w}'$ data appear to differ for the two Reynolds numbers. Unfortunately, Laufer was unable to obtain $\tilde{w}'$ and $\tilde{v}'$ data very near the wall at the higher Reynolds number due to the required size and arrangement of the "X" wire probe. Thus the validity of wall similarity applied to $\tilde{w}'$ very near the wall is not confirmed.

The author has found very little additional data to help confirm this wall similarity concept. Klebanoff (14) made measurements in an artificially thickened turbulent boundary layer and obtained the intensity data shown by the triangles in Figure 44. These data generally confirm those of Laufer. Ruetenik (15) measured equilibrium turbulent flow in a slightly divergent channel and reported intensity results in general agreement with the above. Only a few of his data points fall on the scale of Figure 44. Although a more precise determination of the relationships for $\tilde{u}'$, $\tilde{v}'$ and $\tilde{w}'$ near the wall must await further experimental measurements, the solid curves passed through the data shown on Figure 44 are used here to demonstrate the consequences of such a wall similarity relation.

Some general features of these intensity data are noteworthy. Like the mean axial velocity $\bar{u}$, the intensity component $\tilde{u}'$ has a finite slope at the wall and varies linearly with distance from the wall out to about $y^* = 8$. As a result it is seen that the intensity normalized with the local mean velocity ($\tilde{u}'/\bar{u}$) reaches a maximum constant value in the region near the wall (e.g. see Hinze (13). This sort of behavior was seen qualitatively by the oscilloscope observations of the present study. In contrast, both of the transverse intensities ($\tilde{v}'/\bar{u}$ and $\tilde{w}'/\bar{u}$) appear to approach zero at the wall.

6.2 Secondary Flow Driving Force

Using the concept of a wall similarity relation for the intensity components $\tilde{v}'$ and $\tilde{w}'$ as discussed above it will now be shown that a secondary flow driving force of significant magnitude results whenever a transverse gradient of wall shear stress exists.

Consider again the axial vorticity equation specialized for fully developed flow

$$\bar{v}\frac{\partial \bar{\xi}}{\partial y} + \bar{w}\frac{\partial \bar{\xi}}{\partial z} = \nu \nabla^2 \bar{\xi} + \frac{\partial^2}{\partial y \partial z}\left(\overline{v'^2} - \overline{w'^2}\right) - \frac{\partial^2}{\partial y^2}\left(\overline{v'w'}\right) + \frac{\partial^2}{\partial z^2}\left(\overline{v'w'}\right) \cdots (7a)$$

It has already been stated that the turbulent stress terms represent torques exerted on a fluid element by the turbulent fluctuations. The term involving the intensities $\frac{\partial^2}{\partial y \partial z}\left(\overline{v'^2} - \overline{w'^2}\right)$ can be evaluated from the similarity relations of Figure 44. Let y represent the normal distance from the wall and z the coordinate distance measured along it. In regions where the wall shear stress τ_o is invariant with z it is obvious that this turbulent stress term vanishes. However, when $\partial \tau_o / \partial z$ is finite the intensity term has a value. This is best seen by expressing the quantity $\frac{\partial^2}{\partial y \partial z}\left(\overline{v'^2} - \overline{w'^2}\right)$ in terms of the similarity variables of Figure 44.

First consider only the $\overline{v'^2}$ term.

$$\frac{\partial^2}{\partial y \partial z}\left(\overline{v'^2}\right) = \frac{\partial^2}{\partial y \partial z}\left(u^{*2} v^{*2}\right)$$

$$\text{WHERE} \quad v^* = \tilde{v}'/u^*$$

Taking the y derivative

$$\frac{\partial^2}{\partial y \partial z}\left(\overline{v'^2}\right) = \frac{\partial}{\partial z}\left[u^{*2} \frac{\partial v^{*2}}{\partial y^*} \frac{\partial y^*}{\partial y} + v^{*2} \cancel{\frac{\partial u^{*2}}{\partial y}}^{0}\right] = \frac{\partial}{\partial z}\left[\frac{u^{*3}}{\nu} \frac{\partial v^{*2}}{\partial y^*}\right]$$

Now taking the z derivative

$$\frac{\partial^2}{\partial y \partial z}\left(\overline{v'^2}\right) = \frac{1}{2} \frac{u^*}{\nu} \frac{\partial}{\partial z}\left(u^{*2}\right)\left[y^* \frac{\partial^2 v^{*2}}{\partial y^{*2}} + 3 \frac{\partial v^{*2}}{\partial y^*}\right]$$

After expanding the v^{*2} terms and simplifying the term becomes

$$\frac{\partial^2}{\partial y \partial z}\left(\overline{v'^2}\right) = \frac{u^*}{\nu} \frac{\partial}{\partial z}\left(u^{*2}\right)\left[y^* v^* \frac{\partial^2 v^*}{\partial y^{*2}} + y^*\left(\frac{\partial v^*}{\partial y^*}\right)^2 + 3 v^* \frac{\partial v^*}{\partial y^*}\right] \cdots (13)$$

A similar expression applies for the $\overline{w'^2}$ term by replacing w^* for v^* in equation (13). Remember that $u^{*2} = \tau_0 g/\rho$ so that the entire quantity in brackets is multiplied by the transverse wall shear stress gradient. When this gradient is zero the entire term vanishes as stated earlier. In addition to a transverse shear gradient $\partial/\partial z\,(u^{*2})$, it is necessary for either $\partial v^*/\partial y^*$ or $\partial^2 v^*/\partial y^{*2}$ to be non zero and different from the analogous w^* terms to produce a secondary flow driving torque. Referring to Figure 44 it is seen that these terms are non zero principally in the range $0 < y^* < 30$. Although the slope $\partial v^*/\partial y^*$ is not yet zero at $y^* = 30$, the w^* and v^* terms combine so that the stress term $\partial^2/\partial y \partial z\left(\overline{v'^2} - \overline{w'^2}\right)$ is very nearly zero beyond $y^* = 30$.

Having shown that the behavior of the $\tilde{v}'$ and $\tilde{w}'$ turbulent fluctuations in a wall shear gradient produces a driving torque for a secondary flow, it

is now important to investigate the magnitude of this driving force to see if it is large enough to explain the observed secondary flows. In the region very close to the wall certain terms of the axial vorticity equation (7a) are negligible. In particular, at the boundary y = 0, $\bar{v} = \partial\bar{v}/\partial y = 0$. Hence $\bar{v}$ is very small in the region under consideration and the convection term $\bar{v}\,\partial\bar{\xi}/\partial y$ is negligible. Although both $\bar{w}$ and $\partial\bar{w}/\partial y$ are probably significant, the z derivative $\partial\bar{\xi}/\partial z$ is small making the other convective term $\bar{w}\,\partial\bar{\xi}/\partial z$ negligible. Of the viscous terms, the z derivative $\partial^2\bar{\xi}/\partial z^2$ may be neglected in comparison with $\partial^2\bar{\xi}/\partial y^2$. The turbulent shear stress terms involving $\overline{v'w'}$ are neglected in order to determine the effect of the intensity term under discussion. With these simplifications the vorticity equation becomes*

$$\nu \frac{\partial^2}{\partial y^2}\left(\frac{\partial \bar{w}}{\partial y}\right) = \frac{\partial^2}{\partial y\,\partial z}\left(\overline{w'^2} - \overline{v'^2}\right) \tag{14}$$

Triple integration over y yields an expression for the secondary velocity $\bar{w}$ as a function of y. To solve for numerical values it is necessary to apply boundary conditions for $\bar{w}$ and its derivatives at the wall. It seems quite reasonable to set these derivatives equal to zero (as though there were no secondary flow) and investigate the resulting distribution of $\bar{w}$. Calculations for the square duct at Re = 66,000** and z = .5 inches gave a $\bar{w}/u_\ell$ profile which rose to a value of 0.014 at about 0.075 inches from the wall. (It should be noted that $\partial\tau_0/\partial z$ is quite moderate at z = .5 inches. Figure 27) Measurements indicated a peak value of $\bar{w}/u_\ell$ = .016 at .050 inches from the wall. Both measured and calculated flows were in the same direction. The fact that the calculated driving force was large enough to cause the computed $\bar{w}$ profile to rise to

---

* Numerical evaluation from the experimental data provided further justification for neglecting these terms.

** Similar results are obtained for other Reynolds numbers.

the peak measured value so close to the wall (in spite of having forced the gradient and curvature to be zero at the wall) indicates that this intensity phenomenon may well constitute the major cause of the secondary flow. Details of this calculation are given in Appendix 6.1.

In the preceeding discussion the shear stress terms involving $\overline{v'w'}$ were assumed zero for the purpose of estimating the effect of the intensity term. Most likely these shear stress terms are not zero.* Whether they act as an additional driving force or merely serve to alter the flow is unknown. Thus, without knowing more about the shear stress terms it can only be stated that the behavior of the transverse intensity components in a transverse shear gradient at least makes a contribution to the cause of the secondary flow. For the sake of brevity this effect is hereinafter referred to as "boundary-shear turbulence" after Delleur (4).

One further observation is at least interesting although by no means rigorous. Adopting the concept from mixture length theory that a gradient of mean velocity is required to produce a correlation and hence a turbulent shear stress, one concludes that the shear stresses $\overline{v'w'}$ would be zero in the absence of a secondary flow. Then the neglect of the $\overline{v'w'}$ terms in equation (14) is justified and it may be stated that the intensity term constitutes the cause of secondary flow and the $\overline{v'w'}$ shear term merely the result.

6.3 Experimental Evidence

The secondary velocity measurements reveal some noteworthy facts lending general support to the idea that boundary-shear turbulence causes the secondary flow.

1) The greatest secondary velocities are observed to occur along the walls near the corner region where the wall shear stress gradient

* The evaluation of these terms from the measurements of the mean flow (discussed in Section 5) revealed significant values. The accuracy of this evaluation, however, was poor.

is large. (Figures 35, 38, and 41.)

2) The greatest vorticity also is observed to occur in this region. (Figures 36, 39, and 42.)

3) The maximum secondary velocities were observed to be nearly equal in all three duct configurations. Although Preston tube measurements of wall shear stress were not obtained from the rectangular ducts, the transverse shear gradient near the corners appeared to be approximately equal for all three ducts (at corresponding Reynolds numbers). This observation suggests that the degree of asymmetry of the cross section does not seem to have an important influence on the secondary flow magnitudes.

4) Finally, in all three duct configurations, the secondary flow angles were observed to be independent of Reynolds number throughout the bulk of the cross-section but appeared to be Reynolds number dependent very near the walls. Larger flow angles were observed near the walls (particularly near the corners) at the lower Reynolds numbers. This effect was most striking at a Reynolds number of 9000 where the secondary flow was actually observed with smoke traces near the wall (Figure 12). The preceeding analysis for the $\bar{w}$ profile near the wall indicated, at the lower Reynolds numbers, slightly lower flow angles at any given distance y from the wall. However, the fact that the driving force due to boundary-shear turbulence extends further into the flow at the lower Reynolds numbers ($y^* = 30$ corresponds to a larger y) suggests that it should have a greater effect and produce larger flow angles near the wall.

Although the foregoing observations and speculations are indeed interesting, it will be necessary to learn more about the behavior of the turbulent shear stresses (particularly $\overline{v'w'}$) before the true cause of secondary flow can be ascertained. The author believes that this can only be done by obtaining good measurements of these stresses.

7.0 EFFECT OF SECONDARY FLOW ON PRIMARY FLOW DISTRIBUTION

The existence of secondary flow is straight noncircular ducts was first discovered as a result of its effects in altering the primary flow distribution. Moreover, it has already been shown in Section 5 from the experimental measurements presented here, that the secondary flow convective terms in the axial momentum equation are of significant magnitude and thus should have a pronounced effect on the primary flow distribution. Yet, with our present restricted knowledge of the turbulent stress tensor it is impossible to determine precisely the effect of the secondary flow on the primary flow distribution. At best this effect can only be estimated by the use of approximate turbulence theories. First, the present experimental results are compared with the analytical results of Deissler (3) which presumably represents an approximation to the flow without secondary currents. Secondly using mixture length theory, a comparison is made between velocity profiles determined by neglecting the secondary flows and those determined by using the measured secondary flows.

7.1 Comparison Of Measurements With Deissler's Solution

The calculation by Deissler and Taylor (3) of the turbulent velocity distribution in a square duct assuming no secondary flow is discussed in detail in Section 2. It is recalled that the major objection to their solution, aside from the neglect of the secondary flow, is the assumption that no turbulent shear stress exists on surfaces normal to the constant velocity lines. This assumption is in harmony with mixture length concepts but cannot be justified rigorously. Nevertheless the present measurements are compared with Deissler's results with the implication that the discrepancy represents the effect of the secondary flow.

Figure 28 shows the map of constant velocity lines for the square duct. The solid lines represent the present measurements (Re = 75,500) while the dashed lines represent Deissler's solution. The most striking difference

is the presence of velocities in the corner region significantly higher than predicted by Deissler, while the velocities along the axes of symmetry are noticably lower. These differences are easily explained by the secondary flow which convects high velocity fluid from the central portion of the duct toward the corners and low velocity fluid from the central wall region out toward the duct center. The contour lines obtained by Deissler are well rounded throughout the entire flow whereas the contours obtained from measurements are very nearly parallel to the walls except for the region near the diagonal emanating from the corner and in the region close to the axis. The experimental contour lines are well approximated by a series of concentric squares with small fillets in the corners.*

The distribution of wall shear stress is particularly important in the solution of the heat transfer problem with variable wall temperature. A comparison of the measured wall shear stress distribution with the calculated results of Deissler is shown in Figure 27. Experimental measurements indicate that the wall shear stress is very nearly uniform over about 75 percent of the wall surface with a sharp drop to zero stress in the corner region. The maximum wall shear stress is actually observed about midway between the corner and the center of the wall. In contrast Deissler's solution gives a shear stress distribution which increases continuously from the corner to the centerpoint. The ratio of the peak to mean shear stress is 0.95 from the measurements whereas Deissler's solution gives a

* The velocity contour map of Figure 28 was constructed from the pitot tube measurements. The exact shape of the contour lines and particularly their tendency to bulge toward the corner was extremely difficult to determine. It should be pointed out that the hot wire measurements indicated contour lines exactly parallel to the walls with no bulging toward the corner. Although a very slight tendency toward bulging in the corner region was detected with the hot wire, it was not recorded since its magnitude was of the order of the instrument reading error. Early measurements from the author's research program made by Kihara(16) in a 1 3/4 inch square duct also indicated bulging velocity contours although the consistency was poor. For these reasons a slight bulging is shown in the contours of Figure 28.

value of 0.80. It is interesting to note that the secondary flows, believed to be caused by a transverse wall shear stress gradient, have the effect of acting to wipe out a wall shear gradient.

Based on this comparison, it is concluded that the secondary flows definitely have a pronounced effect on the primary velocity distribution, not only by altering the velocity at certain points in the flow, but also by changing the character of the wall shear stress distribution. The author believes that it will be necessary to account for the effect of secondary flows in any future work on the heat transfer problem if meaningful results are to be obtained.

7.2 Prediction Of Axial Velocity Profiles With Measured Secondary Flows

Using mixture length theory it has been possible to make a reasonably good prediction of the axial velocity profiles by accounting for the momentum convection due to secondary flows. Preceeding discussions (7.1), (5.1) have demonstrated the importance of the secondary flow convection terms in the axial momentum equation. In Section (5.1) it was also pointed out that the turbulent shear stress terms computed from mixture length theory, although of the correct order-of-magnitude, were not in good agreement with those evaluated from the measured mean flow properties. In spite of this lack of general agreement at each point of the flow field, mixture length theory was used in conjunction with the measured secondary flows to predict the primary velocity distribution.

The vonKármán mixture length concept was employed for relating the turbulent stresses to the mean velocity distribution. It is expressed by

$$\overline{u'v'} = \ell^2 \left(\frac{\partial \bar{u}}{\partial y}\right)^2 \tag{15}$$

where

$$\ell = \kappa \frac{\partial \bar{u}/\partial y}{\partial^2 \bar{u}/\partial y^2}$$

The axial momentum equation (4a) is rearranged and integrated over y to produce the following relation (see Appendix 7.1 for a detailed derivation).

$$\frac{\partial \bar{u}}{\partial y} = \left[\frac{\frac{\tau_o g}{\rho} - 2\frac{\bar{\tau}_o g}{\rho}\left(\frac{y}{y_o}\right) + \int_o^y \bar{v}\frac{\partial \bar{u}}{\partial y}dy + \int_o^y \bar{w}\frac{\partial \bar{u}}{\partial z}dy - \int_o^y \frac{\partial}{\partial z}\left[\ell_z^2\left(\frac{\partial u}{\partial z}\right)^2\right]dy}{\ell_y^2} \right]^{1/2} \qquad (16)$$

where $\ell_y = K\dfrac{\partial u/\partial y}{\partial^2 u/\partial y^2}$; $\ell_z = K\dfrac{\partial u/\partial z}{\partial^2 u/\partial z^2}$ $\qquad K = 0.36$

Here the viscous stresses have been neglected for use in the turbulent region. A different relation is used in the viscous region. The velocity profile ($\bar{u}$ vs y) is obtained by a stepwise numerical calculation beginning at the wall and marching outward, evaluating the derivative $\partial\bar{u}/\partial y$ at each point along the profile and integrating to obtain $\bar{u}$. The right hand side is evaluated from measured values of $\bar{v}$, $\bar{w}$ and $\partial\bar{u}/\partial z$. Using an iterative procedure, $\partial u/\partial z$ could actually be computed by this method. According to equation (16) employing Kármán's mixture length the calculation of $\partial\bar{u}/\partial y$ at each point involves iteration because $\partial u/\partial y$ and $\partial^2 u/\partial y^2$ appearing in the mixture length are unknown. To avoid tedious iteration Prandtl's mixture length ($l_y = .4y$) was used as a first approximation and actually coincided with Kármán's mixture length over much of the flow. Better final results were obtained with Kármán's expression. A more detailed description of the solution procedure is given in Appendix 7.1.

Two velocity profiles were computed and compared with experimental measurements; 1) a profile along the centerline or axis of symmetry and 2) a profile along z = 1.0 inches, both in the 5 inch square duct. The results are shown in Figure 45. The general agreement between measured

and calculated profiles is seen to be remarkably good. However, as stated earlier, the mixture length theory apparently does not predict the proper turbulent stress distribution as evidenced by the comparison of turbulent stress terms in the momentum equation. Further indication of this discrepancy is seen from Figure 45 by the fact that the slopes of the calculated and measured profiles are not in agreement everywhere. The integrated result, however, compares well.

The method employed here for calculating the velocity profiles is essentially equivalent to Deissler's method when the secondary flows are neglected. Thus, the fact that the calculated and measured profiles were in essential agreement further substantiates the belief that the discrepancy between Deissler's results and the present measurements (Figure 28) represents the effect of the secondary flow.

8.0 CONCLUSIONS AND RECOMMENDATIONS

The problem of fully developed turbulent flow in straight rectangular ducts was investigated primarily by obtaining experimental measurements of the primary and secondary velocity distributions in rectangular ducts with aspect ratios of 1:1, 2:1 and 3:1. The secondary flows were found to have a significant effect on the primary velocity distribution. Specifically, the following conclusions are drawn:

1) Primary velocity distributions (normalized with the centerline velocity) were found to be independent of Reynolds number except in the region close to the wall and to show indications of secondary flow effects.

2) Secondary flows were found to behave in the general manner originally indicated by Prandtl and to exhibit maximum secondary velocities of about 1 to 1 1/2 percent of the axial centerline velocity in all three duct configurations. The maximum secondary velocities occurred close to the walls near the corner region where large transverse wall shear stress gradients exist. Large velocities were also observed along the diagonal feeding flow to the corner region. Secondary flow angles were independent of Reynolds number except very near the walls where larger angles were observed at the lower Reynolds numbers.

3) The secondary flows were found to have a pronounced effect on the primary flow distribution increasing the velocities near the corner and decreasing them along the central portions of the walls. They appear to cause a nearly uniform wall shear stress distribution except very near the corners where large shear gradients were observed. The secondary flow convective terms make important contributions to the axial momentum equation and therefore should

not be neglected in any attempt at a theoretical solution of the flow problem.

4) Secondary flows are believed to be caused principally by the action near the walls of the transverse turbulence intensity components $\tilde{v}'$ and $\tilde{w}'$ in the presence of a transverse wall shear stress gradient. This effect is termed "boundary-shear turbulence". Expressing $\tilde{v}'$ and $\tilde{w}'$ by a universal relationship in the viscous wall region, it has been shown that a secondary flow driving force of significant magnitude exists in the corner regions where the transverse wall shear gradient is large.

In view of the enormous difficulty of the theoretical problem and of the necessity for a better understanding of the turbulent stress tensor in formulating the problem, it is strongly recommended that measurements be made of the turbulent stresses in order to provide further insight into this specific problem and to the general problem of three dimensional turbulent shear flow.

APPENDIX 3.1 DESCRIPTION OF APPARATUS

Figure 1 contains a schematic diagram of the apparatus. Photographs of the test section and instrumentation are shown in Figure 2. The following description is somewhat more detailed than that given in Section 3.

Air is drawn through a long straight duct by means of a blower located at the downstream end. A flow straightening section is located at the entrance to remove extraneous disturbances. A long length of duct is used to achieve a fully developed flow, the test section being located at the downstream end. The flow leaves the duct through a shallow angle diffuser and plenum. A blower draws air from the plenum through a flow metering nozzle and discharges to the atmosphere.

Duct

It was desired to obtain flow measurements at turbulent Reynolds numbers in the approximate range from 10,000 to 100,000. The lower figure represents the approximate minimum Reynolds number for which turbulent flow is assured. The lower Reynolds numbers provide a relatively thick viscous sublayer and enable measurements to be obtained within this sublayer. The larger Reynolds number represents the desired range of the apparatus for detecting any significant Reynolds number effects. In designing this apparatus it was considered desirable to be capable also of operating in laminar flow so as to check the laminar flow velocity profile against the theoretical one thereby providing a check on the construction and alignment of the apparatus. A duct with a relatively large cross section was desired in an effort to 1) minimize the flow interference due to the insertion of flow measuring instruments and 2) to provide a relatively thick viscous sublayer

so that measurements might be obtained within this layer. The major factors which impose a limitation on the size of the duct are; 1) the minimum velocity which can be measured accurately with available instrumentation (as related to the desired Reynolds number range) and 2) the length of duct required to obtain fully developed flow (approximately 50 diameters of length). After a careful study of all of the factors involved a 5 inch square cross-section was chosen for the basic duct. With this duct size the viscous sublayer thickness is estimated to be about .040 inches at Re = 10,000 and .005 inches at Re = 100,000. The average axial velocity is 4 ft/sec at Re = 10,000 and 40 ft/sec at Re = 100,000.

The length of the duct from the entrance to the test section was made equal to 75 hydraulic diameters, or 31 feet. Eckert and Irvine (19) measured entrance length in a 3:1 rectangular duct and found that a length equal to about 50 hydraulic diameters was required for flow development with a smooth duct entrance. The author made some preliminary measurements in a 1 3/4 inch square duct and found the entrance length to be about 40 hydraulic diameters. Both of these observations were based on the development of the axial pressure gradient. Indeed a later check of the 5 inch square duct with two of the duct sections removed ($L/D_h = 22$) indicated a velocity distribution identical within experimental error to that obtained with the full duct length.

The duct was constructed in four sections; the entrance consisting of two - 10 ft long sections fabricated from 3/4 inch plywood with the interior surfaces shellacked and rubbed to a smooth finish, and the test section consisting of two 6 ft long sections fabricated from 1/2 inch plexiglass sheet. A great deal of care was taken to insure square corners and proper alignment of the joints between sections. The duct

dimensions were maintained within .005 inches of the nominal 5 inch dimension and joint alignment between plexiglass sections was maintained within .002 inches.

The rectangular cross-sections were formed by inserting a plexiglass partition in the 5 inch square duct. The two edges of the partition were slotted and fitted with a long rubber "O" seal strip to act both as a seal and as a spring against which to clamp the partition firmly in place. (See Figure 1.) The partition was positioned by means of spacers placed between it and the opposite wall of the square duct. For further details on the construction of the rectangular section see Gilbert (20).

Test Section

The test section was located approximately one foot from the downstream end of the duct. Provisions were made for probe traversing in two directions so that the probe sensing element could be placed at any position within the duct cross-section. The test section and traversing device is shown in Figure 2. The horizontal traversing was accomplished by fitting the top wall (roof) of the duct with a sliding plate (A) whose motion is perpendicular to the duct axis. The motion of the plate is controlled by a horizontal traversing screw (B) employing an adjustable split nut to eliminate backlash. The position of the horizontal traversing plate is indicated by a pointer and scale (C) and a graduated micrometer drum (D) to within .001 inches.

Vertical probe traversing was accomplished by inserting the probe through a hole in the sliding plate and controlling its vertical position with the vertical traversing screw (E). The screw was equipped with a spring loaded split nut and indicated vertical position within .001 inch. The probe was secured to the vertical traversing screw in

the following way. A protractor disc (F) was clamped firmly around the probe stem by means of a split collar. The probe stem was inserted through a hole in the travelling block (G) of the vertical screw and the protractor disc was allowed to come to rest on the top surface of the block. A spring yoke (H) was used to press the protractor disc firmly against the bearing surface of the travelling block so as to maintain the vertical location of the probe with respect to the traversing screw. This arrangement permitted the probe and protractor disc to be rotated freely (for flow direction measurement) while maintaining precise vertical and horizontal positioning.

Split lucite bushings provided electrical isolation of the probe stem from the sliding plate and the vertical travelling block in order to permit wall location by measurement of electrical continuity. Also to permit wall location by electrical means, a band of electrical conducting paint was applied to the interior surfaces of the test section.

Inlet

The inlet flow straightening section consisted of a 12 inch diameter cardboard cylinder about 22 inches long. The upstream portion was filled with cardboard mailing tubes 1 inch in diameter by about 12 inches long. The tube bundle was followed by a fibreglas filter disc to remove dust particles and two screens made from ordinary 14 mesh aluminum window screen. The screens were separated by an axial distance of about 5 inches. The 12 inch cylindrical flow straightener was attached to the duct entrance via a smooth, well rounded nozzle or transition piece in an attempt to produce a uniform, parallel flow at the entrance to the duct. During preliminary running a slight asymmetry was present in the velocity distribution. A tube bundle composed of 1/2 inch diameter thin wall plastic tubes 7 inches long was placed in

the entrance of the test duct and provided symmetrical flow.

Exit Diffuser

The test section was followed by a 7.2 degree included angle diffuser with a square cross-section (the diffuser was fitted with a partition for the rectangular duct configurations). The diffuser was 34 inches long and discharged into a plenum chamber 10 x 10 x 18 inches long. Two screens were placed inside the plenum normal to the flow. The air discharged from the rear of the plenum through a 4 inch diameter smooth circular nozzle. Pressure taps were provided for measuring pressure drop across the nozzle in order to meter the system air flow. The main function of this nozzle was to provide an instrument for monitoring the flow so as to maintain it constant during a run. Surrounding the nozzle was a length of 5 inch diameter steel pipe. A 12 inch long section of flexible rubber hose connected this pipe to the blower inlet. The flexible hose coupling provided vibration isolation between the test duct and the blower system.

Blower And Controls

Air flow was provided by a centrifugal blower driven by 115-230 volt D.C. motor. The motor was controled by a rheostat, thereby providing a continuous speed range from zero to maximum speed. This system provided fine control so that the pressure drop across the flow metering nozzle could be maintained constant within about 1 percent throughout the course of a test run. By placing restrictions in the blower discharge the system was capable of steady flow operation over a speed range from laminar flow to a Reynolds number of about 90,000.

APPENDIX 3.2 CALIBRATION OF HOT WIRE FOR MEAN VELOCITY MEASUREMENTS

The hot wire must be calibrated for steady velocity measurements against some reliable standard if accurate velocity measurements are desired. Moreover this calibration should be checked periodically to insure against calibration shift as the wire ages or becomes dirty. For convenience in this investigation a reliable calibration apparatus was constructed for use adjacent to the test duct so that calibration checks could be made immediately before and after each run.

Apparatus

The apparatus is shown in Figure 4. It consists of a small high head-low flow blower drawing air from the ambient and discharging it through a long tube with a 1/2 inch (.512 diameter) nozzle at the end. The hot wire is placed in the jet formed by this nozzle for calibration. The velocity in the jet is determined by measuring the flow through the pipe with a smooth nozzle placed in the pipe about midway between the blower discharge and the jet nozzle.

The flow metering nozzle is secured between a pair of flanges connecting two sections of brass tubing. The section between the blower discharge and the flow nozzle has a .521 inch inside diameter and a length of about 29 inches. The section between the flow nozzle and the jet nozzle has a 1.040 inch inside diameter and is about 18 inches long. Smooth nozzles conforming approximately to the ASME standards for the long radius-low ratio nozzle are used. The three flow metering nozzles have throat diameters of 0.063 inches, 0.127 inches, and 0.250 inches respectively. Static taps in the tubing on either side of the flange connection provide a means of measuring nozzle pressure drop. An inclined draft gage with a range of 3 inches of water is used for this measurement.

The flow through the metering nozzle may be expressed in terms of the pressure drop by (subscripts refer to the stations indicated in Figure 4)

$$Q = C_{d_2} V_2 A_2 = C_{d_2} A_2 \sqrt{\frac{2g(p_1 - p_2)}{\rho\left[1 - (d_2/d_1)^4\right]}} \qquad \text{(A-1)}$$

The flow through the jet nozzle may be expressed in terms of the velocity V_3 in the core of the jet (outside the boundary layer) as

$$Q = C_{d_3} V_3 A_3 \qquad \text{(A-2)}$$

Combining these two relationships and solving for the jet velocity V_3 in terms of the pressure drop across the metering nozzle

$$V_3 = \frac{C_{d_2}}{C_{d_3}} \left(\frac{d_2}{d_3}\right)^2 \sqrt{\frac{2g(p_1 - p_2)}{\rho\left[1 - (d_2/d_1)^4\right]}} \qquad \text{(A-3)}$$

To evaluate the jet velocity, V_3, in terms of the nozzle pressure drop it is necessary to know the discharge coefficients for the metering nozzle and the jet nozzle.

Nozzle Calibration

The nozzles were at first assumed to behave according to the ASME standard discharge coefficient curve (Reference 22). Although the ASME standard curve only accounts for Reynolds numbers of 10,000 and up, Rivas and Shapiro (23) have applied boundary layer theory and computed discharge coefficients for the ASME long radius-low ratio geometry. Their results for their L'/D parameter equal to 1.0 are in good agreement with the ASME standards at a Reynolds number of 10,000 and thereby provide a good extrapolation for the ASME standards.

Using these discharge coefficient relationships it was found possible to express the ratio of the discharge coefficients C_{d_2}/C_{d_3} as

a constant for each of the three metering nozzles over its range of operation (.05 to 3.0 inches of water). These ratios were found to be constant over this range within approximately $\pm$ 1 percent. They are:

Nozzle Size	Cd_2/Cd_3
0.063 in.	1.2
0.127 in.	1.06
0.250 in.	1.025

Early attempts to fit the hot wire calibration data to King's law ($I^2 = A + B\sqrt{V}$) were not very successful. Figure 7 shows the data plotted as I^2 vs $\sqrt{V}$. When a straight line was fit to this data the calibration data fell below this line at velocities below 4 ft/second. Since much of the desired test data, particularly data in the viscous sublayer, came within the range of 1 to 4 ft/second it was felt necessary to ascertain the proper wire calibration.

One of the steps taken to assure a more reliable calibration was to make a direct calibration of the small flow metering nozzles. A small gasometer was constructed from a standard 55 gallon oil drum. The drum was filled with water. A valve was provided in the bottom of the drum for draining the water. The top was fitted with a line to admit air to fill the space above the water level. This air was admitted through the brass tube and nozzle assembly used in the calibration apparatus. The water was drained in steady flow from the bottom of the drum into a pail where it was timed and weighed to determine the volume flow rate. Simultaneously air was admitted to the space above the water level in steady flow through the flow metering nozzle. The pressure drop across the nozzle was recorded. In this manner a direct calibration of the discharge coefficients was obtained. Corrections were made for the pressure inside the drum, and for changes in air temperature and humidity upon entering the drum. These corrections were small. The

discharge coefficients from this calibration checked within $\pm$ 1 percent of the curves mentioned previously. These results are shown in Figure 8.

Pitot Tube Check

At the higher velocities (above 10 ft/sec) it was possible to check the calibration apparatus directly against a pitot tube placed in the discharge jet. This type of check verified the discharge coefficients for the 0.127 inch and 0.250 inch nozzles. Because this method could not be used to check the low velocity calibration another means was sought.

Smoke Trace Calibration

Some method for providing a direct calibration of the hot wire at low velocities was desired. This was accomplished by establishing a laminar flow of air through a 7/8 inch inside diameter by 12 ft long lucite tube, mounted vertically. A smoke trace was injected along the axis of the lucite tube through a small hyperdermic near the entrance. The velocity along the centerline was measured by noting the time required for the smoke trace to traverse a fixed distance. The hot wire was then placed on the axis of the tube in the exit plane and calibrated against this velocity. Care was taken to insure fully developed laminar flow at the smoke injection station. The results of this direct low speed calibration were in good agreement with the calibration apparatus (Figure 7).

Correlation Of Calibration Data

After completing the aforementioned efforts to improve the quality of the hot wire calibration, the data were still not in accord with the widely accepted King's law. A search for an explanation revealed a publication by Collis (21) where he presents some recent steady state heat transfer correlations for hot wires. Below the critical Reynolds number of 44, above which vortex shedding occurs, Collis finds his data are best correlated by the following relation.

$$Nu \left(\frac{T_m}{T_a}\right)^{-0.17} = 0.24 + 0.56\, Re^{0.45} \qquad \text{(A-4)}$$

For a given wire temperature the Nusselt number is proportional to I^2, hence this relationship can be expressed by

$$I^2 = A + BV^{.45} \qquad \text{(A-5)}$$

Although the difference between this relation and King's law is slight, the calibration data obtained during this investigation fit Collis' relationship much better than King's law. A plot of I^2 vs $V^{.45}$ is shown in Figure 5. Accordingly the hot wire data analysis for the present study was based on a correlation to Collis' equation.

The accuracy of the hot wire for steady velocity measurements was considered to be limited principally by the reading error of the HWB system. Accordingly the uncertainty in hot wire velocity measurements is estimated to be about 5 percent at 2 ft/sec and about 2 1/2 percent at 20 ft/sec.

Effect Of Turbulence Intensity

The flow in which the hot wire was calibrated was sometimes laminar and sometimes turbulent depending on the velocity. When the flow was turbulent the intensity was very low (at the center of the jet). Thus the wire was always calibrated in a low intensity flow and was then used to measure a relatively high intensity flow (near the duct walls). The author believes that a large intensity such as that occurring near the outer edge of the viscous sublayer ($\tilde{u}'/\tilde{u} \approx 0.30$) may have a considerable effect on the heat transfer from the wire. He knows of no information on such an effect and so has had to ignore it in reducing hot wire data. This possible error is discussed further in section 4.1.1 dealing with the reduction of velocity data near the duct walls.

APPENDIX 3.3 DEVELOPMENT OF FLOW DIRECTION MEASURING TECHNIQUE

The deviation from axial flow due to secondary flows was expected to be extremely small. All pressure sensitive flow direction instruments known to the author involve the use of two independent pressure openings separated by a finite distance. These instruments are all vulnerable to a velocity gradient error much too large for measuring the secondary flows. It was felt that an instrument involving only one sensing element, and therefore not subject to a velocity gradient error, would need to be used for this task.

The hot wire annemometer offers various means for using a single sensing element to measure flow direction. To measure the secondary flows close to the duct walls it was necessary to choose a method which would allow the sensing wire to be operated parallel to the duct wall. The first method attempted was to use one of the two wires in the "V" array of the gooseneck probe described in Section 3.2.1 and Figure 3. The wire was connected into one leg of the bridge circuit which is described in more detail on the following pages. An indication of flow direction was attempted by rotating the probe until the axis of the direction sensing wire was aligned with the flow. A sharp peak in wire temperature was expected to occur (constant current being maintained across the bridge) as the wire became aligned with the flow. The resultant variation of wire temperature (or galvanometer reading) with angular position did not contain a sharp peak but was rather flat and noticeably asymmetrical. This behavior was believed to be caused by the asymmetric configuration of the wire supporting needles.

The second attempt involved using both wires of the "V" array oriented so that the flow bisected the angle between the wires. This method proved unsatisfactory due to 1) excessive velocity or current

sensitivity and 2) velocity gradient error. A more complete description of the attempt to develop the "V" array system is contained in the latter part of this appendix. First, the final system used for the measurements is described.

Single Wire Instrument

The instrument finally used for the flow direction measurements was a standard single wire probe with long straight needles. A 0.0003 inch diameter tungsten wire approximately 0.10 inch long was mounted on needles of 0.025 inch diameter by 1 inch long. The probe stem diameter was 0.134 inches. The probe was inserted through the duct wall with the probe stem normal to the duct axis. It was rotated until the wire axis was oriented about 10 to 20 degrees from the flow direction. The bridge circuit, of which the wire constituted one leg, was then brought into balance and the angular position of the probe was noted from the protractor disc. The probe was then rotated back until the wire was oriented in approximately the same position on the opposite side of the flow direction, and the bridge was brought back into balance by rotation of the probe to the proper position (Figure 3). This angle was then read and the bisector of the two angles was taken as the direction of the flow. The same flow angle was obtained regardless of the angle that the wire made with the flow direction when balancing the bridge. This indicated that the sensitivity of the hot wire to flow angle was perfectly symmetrical. As a result it was only necessary to make two angle observations to obtain the flow direction at a single point.

The bridge circuit used with the single wire is shown in Figure 6. The hot wire constituted one leg of the bridge. Its resistance was about 5-7 ohms. An adjustable resistor was placed in the opposite leg. The two legs on the opposite side of the galvanometer connections contained

identical one ohm precision wire wound resistors. Power was supplied with a 1 1/2 volt dry cell battery through a 5 ohm adjustable resistor used to select the proper wire current. A milliammeter was provided for measuring the bridge current. The total bridge current was usually maintained at about 200 ma.

A very sensitive spotlight galvanometer (Rubicon - model 3400H - sensitivity 2.8 μV /mm) was used to indicate bridge unbalance. A 12 ohm external critical damping resistance placed in series with the galvanometer prevented oscillation of the galvanometer works. Additional adjustable resistors were provided in the galvanometer circuit for sensitivity adjustment. The maximum sensitivity of this system was actually too great. When the maximum sensitivity was used flow angle fluctuations due to the turbulence caused the galvanometer spot to fluctuate excessively so that it was extremely difficult to determine the null point. Therefore, the sensitivity was reduced to a tolerable level by either decreasing the wire current or adding resistance to the galvanometer circuit.

By utilizing the single wire system as described above both of the disadvantages of the "V" wire method are avoided. First, because the wire is exposed to the same velocity field in both of the bridge balance positions, the velocity gradient error is avoided. Care must be taken, however, to insure that the wire rotates about its center as the probe is rotated. Secondly, with a single hot wire in the bridge circuit the current dependent solder joint resistances become inconsequential (see following description of "V" array system). Freedom from these two sources of error was absolutely essential for the successful measurement of the secondary velocities.

Preliminary testing of this system was conducted with a standard

Flow Corporation single wire probe exactly like the long needle probe described above except that the needles were only about 1/4 inch long. A slight error in angle indication due to wall interference was expected as the probe stem was brought into close proximity to the vertical wall. This effect was considered to be caused by a preferential diversion of the flow streamlines around the side of the probe stem facing away from the vertical wall. The ratio of the distance (X) between the wall and the probe stem axis to the probe stem diameter (D) was believed to be the significant parameter governing this angle error.

Measurements of flow angle in the 5 inch square duct were obtained with this standard probe for several traverses at different horizontal levels. The traverses began at the duct centerline and continued toward one of the vertical walls. The probe was then removed and a sheath made from rubber hose was placed around the probe stem to increase its diameter. The flow angle traverses were then repeated. Angle readings were taken in this manner with the bare probe stem (0.134 inch diameter), and with rubber sheaths of 1/4 and 3/8 inch diameter. A definite wall interference effect was observed. The readings in the central portion of the duct, however, were in agreement. The results of these observations were interpreted in the following way. First the readings obtained with the bare probe stem were assumed to be correct over the entire traverse. The angle error was then computed from the readings obtained with the two sheaths and plotted as a function of X/D. Using this plot a correction was made to the readings from the bare probe. This process was then repeated until convergence. The final results are shown in Figure 9 as a plot of angle error versus the distance parameter X/D. It is seen that the wall proximity error extends out to about X/D = 5.

It was desired to avoid, if possible, angle errors due to wall proximity. The use of a probe with long needles was expected to reduce this error by allowing the needles to act as the major flow blockage near the wire as the probe stem did in the aforementioned experiments. Angle measurements were desired as close as 0.10 inches from the vertical wall. With a needle diameter of 0.025 inches making X/D = 4 the angle error at this position should indeed be small (according to the results of Figure 9). However, one question still remained; how long must the needles be in order to avoid probe stem interference at the hot wire filament? To answer this question the 3/8 inch rubber sheath was placed over the stem of the standard probe with the lower end of the sheath at various distances from the wire. Angle measurements were made close to the wall. It was necessary to maintain the sheath about 2 inches above the wire to avoid interference from the sheath. Because the probe stem and needle diameters were much less than the sheath and stem diameters used in this test, it was felt that needles approximately 1 inch long would be satisfactory. A greater needle length would have made it very difficult to center the wire on the probe stem axis. This was considered to be very important to eliminate velocity gradient error.

Besides the method indicated above for measurement of flow direction, attempts were made to observe the peaking of the galvanometer reading as the wire was aligned with the direction of flow. Turbulent fluctuations and the finite width of the peaking band made this method for indicating flow direction inferior to the one used.

Although the "V" array direction probe was not used for the present measurements, the development experiences and difficulties encountered by the author in attempting to use this instrument are recounted in the following section for the benefit of those interested in it.

"V" Array Flow Direction Probe

The "V" array probe consisted of the two wire gooseneck probe described in Section 3.2.1 and discussed earlier in this appendix. This probe used both wires of the "V" array oriented so that the flow bisected the angle between the wires. A bridge circuit was constructed with the two wires in opposite legs of the bridge and with two identical precision resistors in the other two legs. Because the two wires would never have exactly the same resistance, additional small adjustable resistors were placed in series with each wire in their respective legs. These resistors provided a means for balancing the bridge.

Consider the bridge in balance when the flow bisects the two wires. Since each wire is sensitive to the component of velocity normal to it, a rotation of the array in either direction would increase the velocity component on one wire while decreasing that on the other. This would result in a decrease in the temperature and resistance of the former wire and an increase in the resistance of the latter wire, thereby upsetting the balance of the bridge.

There is one additional complication necessary to make this scheme work properly. Means must be provided to insure that the two wires are always operated at the same temperature (when aligned symmetrically about the flow direction). The calibration or bridge balance must also be made at this same temperature. The reason is as follows: The two wires will never have exactly the same resistance. If the original calibration or bridge balance is made at one temperature (T_1) the two wires will have resistances R_1 and R_2. The two adjustable resistors (R_3 and R_4) in series with R_1 and R_2 will be adjusted so that $R_1 + R_3 = R_2 + R_4$. Now suppose the array is operated at a second temperature T_2. When the probe is oriented so that the flow vector bisects the wires (wire

temperatures equal) the wire resistances will be $R_1 \cdot {}^{T2}/_{T1}$ and $R_2 \cdot {}^{T2}/_{T1}$. Since the resistances R_3 and R_4 will not change with wire temperature changes, the resistances of the two bridge legs will be $R_1 \cdot {}^{T2}/_{T1} + R_3$ and $R_2 \cdot {}^{T2}/_{T1} + R_4$. They will not be equal unless either $R_1 = R_2$ or $T_1 = T_2$. Hence the bridge will not be in balance. If the probe is rotated to balance the bridge an error in flow direction indication will result. This difficulty can be avoided, however, by providing a standard preset resistance as a temporary substitute for one of the hot wire legs. By switching this standard resistance in place of one hot wire leg when the probe is in the null position and adjusting the bridge current until the bridge is nulled, the wire temperature may be maintained constant as the probe is used at various velocities. This method was employed by the author in the checking of the "V" wire probe operation.

Testing of the "V" wire system revealed two major drawbacks, either of which would preclude its use for measuring secondary flows. First the instrument was found to be velocity or wire current sensitive, even when operated at constant temperature by the means discussed above. When the probe was placed on the duct centerline or in the calibration jet and balanced in various velocity flows (all at the same wire temperature) the angle indication was found to vary as much as 1 or 2 degrees over a factor of 2 difference in velocity. This magnitude of velocity sensitivity was clearly intolerable for the measurement of secondary flows. This effect is believed to be caused by current sensitive contact resistances at the solder joints between the wires and needles.

The second undesirable effect is the velocity gradient error inherent in the "V" array construction. When the probe is placed in a transverse velocity gradient one wire sees a larger average velocity over its length than the other. Because one wire is cooled more effectively than the

other, the probe must be rotated slightly toward the low velocity side of the true flow direction in order to cause the bridge to balance. Experimentation with the "V" array probe indicated rather large flow angles (about 5 degrees) when the probe was brought into the steep velocity gradient near the vertical wall. Subsequent calculation of the velocity gradient error based on the probe geometry and the known velocity distribution indicated that the error was 3 to 5 degrees at 0.10 inches from the vertical wall and about 1/2 to 1 degree close to the duct centerline. This magnitude of velocity gradient error was clearly too great to be tolerated. Normally a correction might be applied to observed readings based on a calculated velocity gradient error but it was felt that such a correction should be only a small fraction of the total reading due to the uncertainty of the correction.

An "X" array probe was considered as a possible way to avoid the velocity gradient error but this type of probe would still require the same bridge circuit as the "V" array with the attendent difficulties with velocity sensitivity. At this point the standard straight needle single wire probe was considered the best instrument for precise measurement of flow direction.

APPENDIX 3.4 MEASUREMENTS AND DATA

The measurements of primary and secondary velocities in the three rectangular duct configurations constitute the major portion of this work. These experimental measurements are tabulated on the following pages. Hot wire velocity readings were reduced with the aid of calibration curves similar to the one shown in Figure 5. No corrections were applied to obtain the tabulated values. Pitot tube velocity readings were reduced in the usual manner and corrections were applied for turbulence intensity and velocity gradient error as indicated in Appendix 4.1.

Flow measurements were made with the monitoring flow nozzle and compared with the integrated velocity distributions (bulk velocity - U_b). These comparisons are indicated on Tables 1 - 7. Most of the flow measurements agreed well with the measured velocity distributions. However, the nozzle flow readings were 10-15 percent high at the higher Reynolds numbers (57,000 and 66,000). At these high flows the hot wire velocities checked within 5 percent with pitot tube measurements of centerline velocity. It is believed that flow separation may have occurred in the diffuser at these flows thereby causing asymmetric flow in the plenum resulting in high nozzle pressure drop. (At the time these measurements were taken, a wide angle diffuser was employed.)

Flow direction readings for the square duct are tabulated as received from the test apparatus and do not contain any corrections. Readings are shown for all quadrants. Flow angle tabulations for the rectangular ducts represent averages of readings from the two lower quadrants. The flow was found to be very nearly symmetrical. The numbers tabulated represent the flow angle in degrees. Positive angles indicate a flow toward the duct center while negative angles indicate flow toward the walls.

TABLE 1

AXIAL VELOCITY DISTRIBUTION IN FIVE INCH SQUARE DUCT - BASED ON HOT WIRE MEASUREMENTS

Re = 14.600

u_b/u_c = 0.79

Measured Flow = $1.004 \int_0^{2a} \int_0^{2a} \rho u \, dy \, dz$

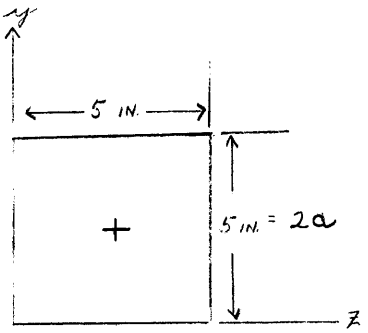

Velocities in Feet Per Second

y(in)*	z=0.10"	z=0.25"	z=0.50"	z=1.0"	z=1.5"	z=2.0"	z=2.5"
0.010	0.80	0.90	1.02	1.115	1.115	1.115	1.115
0.020	1.06	1.36	1.47	1.53	1.585	1.585	1.585
0.025	1.20	1.64	1.70	1.83	1.90	1.90	1.90
0.030	1.31	1.83	1.96	2.11	2.11	2.11	2.11
0.035	1.47	2.11	2.25	2.33	2.39	2.33	2.39
0.040	1.53	2.25	2.39	2.55	2.61	2.55	2.61
0.045	1.64	2.43	2.55	2.78	2.78	2.78	2.78
0.050	1.70	2.61	2.71	2.96	2.96	2.96	2.96
0.060	1.90	3.03	3.03	3.21	3.21	3.21	3.21
0.070	2.11	3.12	3.37	3.47	3.47	3.47	3.47
0.080	2.25	3.29	3.55	3.72	3.72	3.72	3.72
0.100	2.39	3.55	3.85	3.95	3.95	3.95	4.06
0.250	3.47	4.59	4.82	5.20	5.20	5.20	5.20
0.500	3.55	4.82	5.54	5.76	5.67	5.67	5.76
1.000	3.95	4.94	5.67	6.47	6.33	6.47	6.62
1.500	3.95	4.94	5.67	6.47	6.62	7.05	7.05
2.000	3.95	4.94	5.67	6.47	6.75	7.18	7.33
2.500	3.95	4.94	5.67	6.47	6.89	7.33	7.50

* y denotes distance of probe from point of contact with wall and does not necessarily represent distance of sensing element from wall. (See discussion on page 28.)

TABLE 2

AXIAL VELOCITY DISTRIBUTION IN FIVE INCH SQUARE DUCT - BASED ON HOT WIRE MEASUREMENTS

Re = 22.300

u_b/u_ℓ = 0.81

Measured Flow = $0.965 \int_0^{2a}\int_0^{2a} \rho u \, dy \, dz$

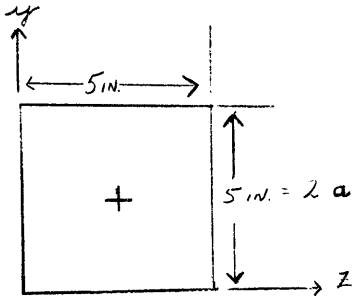

Velocities in Feet Per Second

y(in)*	z=0.10"	z=0.25"	z=0.50"	z=1.0"	z=1.5"	z=2.0"	z=2.5"
0.010	1.50	1.67	1.92	2.08	2.23	2.23	2.23
0.015	1.75	2.16	2.32	2.57	2.66	2.66	2.66
0.020	2.16	2.74	2.91	3.16	3.16	3.16	3.16
0.025	2.49	3.08	3.34	3.62	3.70	3.62	3.70
0.030	2.91	3.52	3.80	4.11	4.11	4.11	4.11
0.035	3.25	4.01	4.11	4.55	4.55	4.46	4.55
0.040	3.62	4.34	4.46	4.80	4.80	4.80	4.80
0.045	3.80	4.68	4.68	5.00	5.00	5.00	5.00
0.050	4.01	4.91	4.91	5.25	5.25	5.25	5.25
0.060	4.22	5.15	5.25	5.65	5.65	5.65	5.65
0.070	4.46	5.53	5.65	6.06	6.06	6.06	6.06
0.080	4.80	5.93	5.93	6.36	6.50	6.36	6.50
0.100	5.25	6.36	6.36	6.78	6.93	6.93	6.93
0.250	5.93	7.37	7.52	8.00	8.00	7.84	8.00
0.500	6.22	7.68	8.46	8.78	8.78	8.78	8.60
1.000	6.56	7.82	8.60	9.60	9.78	9.60	9.60
1.500	6.56	7.82	8.60	9.60	10.32	10.32	10.60
2.000	6.56	7.82	8.60	9.60	10.60	10.68	10.85
2.500	6.56	7.82	8.60	9.60	10.60	10.88	11.10

* y denotes distance of probe from point of contact with wall and does not necessarily represent distance of sensing element from wall. (See discussion on page 28.)

TABLE 3

AXIAL VELOCITY DISTRIBUTION IN FIVE INCH SQUARE

DUCT - BASED ON HOT WIRE MEASUREMENTS

Re = 34,300

$u_b/u_\ell = 0.81$

Measured Flow = $0.965 \int_0^{2a} \int_0^{2a} \rho u \, dy \, dz$

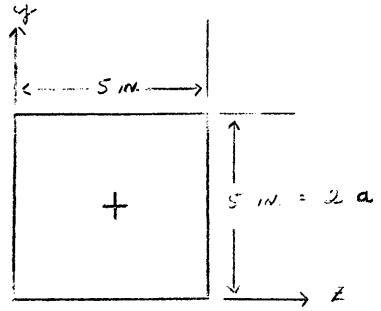

Velocities in Feet Per Second

y(in)*	z=0.10"	z=0.25"	z=0.50"	z=1.0"	z=1.5"	z=2.0"	z=2.5"
0.005	2.01	2.11	2.23	2.61	2.61	2.75	2.75
0.010	2.61	2.88	3.30	3.79	3.79	3.86	3.86
0.015	3.86	4.10	4.26	4.80	4.80	4.90	4.90
0.020	4.77	4.88	5.25	5.88	5.88	5.88	5.88
0.025	5.45	5.88	6.20	6.60	6.60	6.38	6.38
0.030	5.95	6.20	6.60	7.05	7.05	6.93	6.93
0.040	6.80	7.05	7.40	8.10	8.10	8.10	8.10
0.050	7.50	8.10	8.38	8.83	8.83	8.83	8.83
0.070	8.38	8.60	9.20	9.52	9.52	9.52	9.52
0.100	8.95	9.52	10.00	10.45	10.45	10.45	10.45
0.250	9.70	10.82	11.60	12.00	12.00	12.00	12.00
0.500	10.00	11.80	13.00	13.45	13.45	13.45	13.45
1.000	10.45	12.00	13.45	15.15	15.00	15.15	15.15
1.500	10.45	12.00	13.45	15.15	16.20	16.40	16.40
2.000	10.45	12.00	13.45	15.15	16.40	16.60	17.00
2.500	10.45	12.00	13.45	15.15	16.40	17.00	17.20

* y denotes distance of probe from point of contact with wall and does not necessarily represent distance of sensing element from wall. (See discussion on page 28.)

TABLE 4

AXIAL VELOCITY DISTRIBUTION IN FIVE INCH SQUARE

DUCT - BASED ON HOT WIRE MEASUREMENTS

Re = 43,800

u_b/u_ℓ = 0.81

Measured Flow = $1.013 \int_0^{2a} \int_0^{2a} \rho u \, dy \, dz$

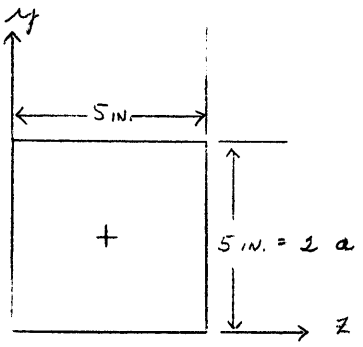

Velocities in Feet Per Second

y(in)*	z=0.10"	z=0.25"	z=0.50"	z=1.0"	z=1.5"	z=2.0"	z=2.5"
0.010	5.21	5.96	6.10	6.41	6.23	6.58	6.15
0.020	7.51	7.80	8.73	9.21	9.05	9.16	8.50
0.030	9.20	9.35	10.15	9.70	9.45	10.60	10.25
0.050	10.4	10.9	11.70	12.22	11.90	12.00	11.75
0.100	12.0	12.45	13.35	14.00	13.60	13.40	13.80
0.250	12.6	13.90	15.10	16.05	15.60	15.25	15.90
0.500	13.2	14.85	17.05	18.00	17.40	16.80	17.35
1.000	13.8	15.90	17.30	19.55	19.40	19.15	19.35
1.500	13.8	15.90	17.30	19.55	19.85	20.55	20.80
2.000	13.8	15.90	17.30	19.30	20.40	21.20	21.65
2.500	13.8	15.90	17.30	19.30	20.80	21.65	22.10

* y denotes distance of probe from point of contact with wall and does not necessarily represent distance of sensing element from wall. (See discussion on page 28.)

TABLE 5

AXIAL VELOCITY DISTRIBUTION IN FIVE INCH SQUARE DUCT - BASED ON HOT WIRE MEASUREMENTS

Re = 57,000

u_b/u_ℓ = .805

Measured Flow = $1.145 \int_0^{2a}\int_0^{2a} \rho u \, dy \, dz$

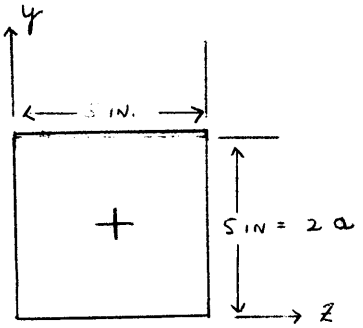

Velocities in Feet Per Second

y(in)*	z=0.10"	z=0.25"	z=0.50"	z=1.0"	z=1.5"	z=2.0"	z=2.5"
0.010	8.1	8.85	9.75	11.2	11.2	11.2	11.2
0.020	11.2	11.4	11.8	13.5	13.6	13.6	13.6
0.030	12.65	12.85	13.3	14.8	14.8	14.8	14.8
0.050	13.9	14.15	14.8	16.4	16.4	16.4	16.4
0.100	15.5	15.75	16.4	17.9	17.9	17.9	17.9
0.250	16.7	18.18	18.7	20.0	20.0	20.0	20.0
0.500	17.4	19.5	20.81	22.0	22.0	22.0	22.0
1.000	17.9	20.0	21.7	24.1	24.4	24.4	24.7
1.500	17.9	20.0	21.7	24.4	25.3	26.4	26.7
2.000	17.9	20.0	21.7	24.4	26.0	27.4	27.8
2.500	17.9	20.0	21.7	24.4	26.4	27.8	28.5

* y denotes distance of probe from point of contact with wall and does not necessarily represent distance of sensing element from wall. (See discussion on page 28 .)

TABLE 6

AXIAL VELOCITY DISTRIBUTION IN FIVE INCH SQUARE

DUCT - BASED ON HOT WIRE MEASUREMENTS

Re = 66,000

u_b/u_ℓ = 0.81

Measured Flow = $1.085 \int_0^{2a}\int_0^{2a} \rho u \, dy \, dz$

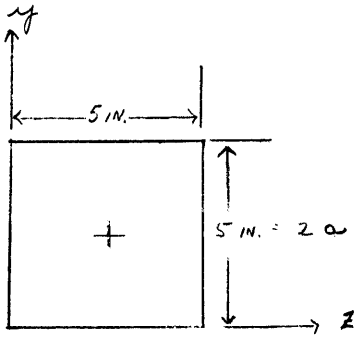

Velocities In Feet Per Second

y(in)*	z=0.10"	z=0.25"	z=0.50"	z=1.0"	z=1.5"	z=2.0"	z=2.5"
0.010	9.25	9.8	11.35	21.1	12.1	12.1	12.1
0.020	12.40	12.90	14.00	14.8	14.8	14.8	14.8
0.030	14.00	14.69	15.82	16.4	16.4	16.4	16.4
0.050	15.80	16.40	17.62	18.5	18.5	18.5	18.5
0.100	16.70	18.30	19.70	20.7	20.7	20.7	20.7
0.250	17.90	20.70	21.60	23.0	23.0	23.0	23.0
0.500	19.70	22.65	24.60	25.7	25.7	25.7	25.7
1.000	20.40	23.05	25.60	28.0	28.0	28.0	28.6
1.500	20.40	23.05	25.60	28.3	29.2	29.7	30.8
2.000	20.40	23.05	25.60	28.3	29.7	31.0	32.2
2.500	20.40	23.05	25.60	28.3	30.2	31.7	32.8

* y denotes distance of probe from point of contact with wall and does not necessarily represent distance of sensing element from wall. (See discussion on page 28.)

TABLE 7

AXIAL VELOCITY DISTRIBUTION IN FIVE INCH SQUARE DUCT - BASED ON PITOT TUBE MEASUREMENTS

Re = 75,500

u_b/u_ℓ = .814

Measured Flow = $1.09\int_0^{2a}\int_0^{2a} \rho u\,dy\,dz$

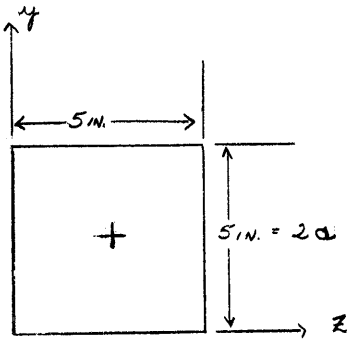

Velocities In Feet Per Second*

y(in)**	z=0.10"	z=0.25"	z=0.5"	z=1.0"	z=1.5"	z=2.0"	z=2.5"
0.019	12.20	12.75	14.00	14.75	15.15	14.80	14.70
0.025	14.00	14.83	15.80	17.00	17.00	17.00	16.60
0.035	16.25	16.90	17.95	19.05	19.35	19.05	19.05
0.045	17.45	18.38	19.40	20.35	20.70	20.30	20.20
0.055	18.10	18.80	20.10	21.20	21.50	21.20	21.10
0.105	19.80	21.40	22.65	23.80	24.00	23.40	23.40
0.255	21.70	24.90	26.40	27.40	27.40	26.80	26.80
0.505	23.10	26.60	29.30	30.40	30.40	29.60	29.40
1.000	23.80	27.00	30.20	32.90	33.20	32.60	32.60
1.500	23.70	27.00	29.80	32.90	34.40	34.60	35.00
2.000	23.60	26.60	29.60	32.80	35.00	36.00	36.60
2.500	32.60	26.80	29.60	32.80	35.10	36.60	37.40
τ_o - lb/ft² ***	0.00384	0.00409	0.00452	0.00493	0.00505	0.00493	0.00485

* Velocities are corrected for high turbulence intensities near wall.

** This distance includes the effective probe displacement for the velocity gradient error.

*** Calculated from universal velocity distribution fit to data near wall.

TABLE 8

FLOW DIRECTION DATA FROM 5 INCH SQUARE DUCT -

OBTAINED WITH STANDARD FLOW CORPORATION HOT WIRE PROBE

Re $\approx$ 15,000

(Data are not corrected for wall interference)

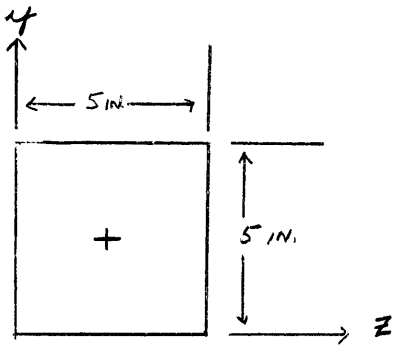

Tabulated Numbers Represent Angle In Degrees Between X Axis And Velocity Vector Projection Onto XZ Plane - Positive Angles Denote Flow Toward Duct Center, Negative Angles Denote Flow Toward Duct Walls

z IN → / y IN ↓	.10	.25	.50	1.0	1.5	2.0	2.5	3.0	3.5	4.0	4.5	4.75	4.90
0.010	+			+1 1/4						+1 1/4			
0.030	+8	+2	+2 1/2	+1 1/4	+1	+3/4	0	+3/4	+1	+1 1/4	+2 1/4	+1 3/4	+6
0.050	+6 1/2	+2	+2	+1 1/2	+1	+3/4	0	+3/4	+1	+1 1/2	+2	+1 7/8	+4 1/4
0.100	+2 1/2	+1/2	+1	+1 1/4	+1 1/8	+1/2	0	+1/2	+1	+1 1/4	+1	+1/2	+1 1/2
0.250	+2 1/2	-3/8	-1/4	+1/2	+3/4	+1/2	0	+1/2	+3/4	+1/2	-1/4	-1/2	0
0.50	+2	+1/2	-3/8	0	0	+1/8	0	+1/8	0	-1/4	-1/2	-3/8	+3/4
1.0	+1 3/4	+3/8	+1/8	-3/8	-3/8	-1/8	0	-1/4	-3/8	-5/8	-3/8	+1/4	+1/4
1.5	-	+1/4	+1/4	0	-1/4	-1/4	0	-1/4	-1/4	-1/4	0	+1/8	-
2.0	+2	+5/8	+5/8	+3/8	0	0	0	0	0	+3/8	+3/8	+1/2	-
2.5	+2 1/2	+3/4	+3/4	+1/2	+1/4	0	0	0	+1/4	+1/2	+3/4	+3/4	+2

TABLE 9

FLOW DIRECTION DATA FROM 5 INCH SQUARE DUCT

- OBTAINED WITH STANDARD FLOW CORPORATION HOT WIRE PROBE

Re ≈ 34,000

(Data are not corrected for wall interference)

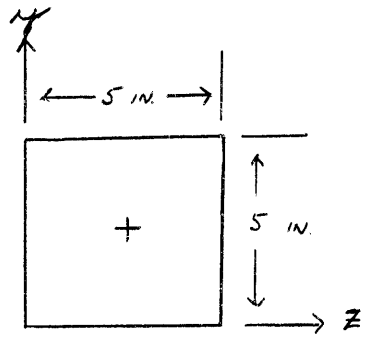

Tabulated Numbers Represent Angle In Degrees Between X Axis And Velocity Vector Projection Onto XZ Plane - Positive Angles Denote Flow Toward Duct Center, Negative Angles Denote Flow Toward Duct Walls

Z IN → / Y IN ↓	1.0	.25	.50	1.0	1.5	2.0	2.5	3.0	3.5	4.0	4.5	4.75	4.90
0.050	+5	+2	+1 3/4	+1 1/2	+1	+1/2	0	+3/8	+1	+1 1/2	+1 3/4	+1 3/4	+3
0.100	+3	+1/2	+1	+1 1/4	+1	+1/2	0	+1/2	+1 1/8	+1 1/4	+1	+1/2	+1 1/2
0.250	+2 1/2	-1/8	-1/8	+1/2	+3/4	+1/2	0	+3/8	+3/4	+1/2	-1/4	-3/8	+2
0.5	+2	+1/4	-1/4	-1/8	0	+1/8	0	+1/8	0	-1/4	-1/2	-1/8	+1
1.0	+2	+1/4	-1/4	-1/2	-3/8	-1/4	0	-1/4	-3/8	-1/2	-1/4	+1/4	+1 1/4
1.5	+1 1/2	+1/2	0	-1/4	-1/4	-1/4	0	-1/4	-1/4	-1/4	0	+1/2	+1
2.0	+1 3/4	+3/4	+1/2	+3/8	0	0	0	0	0	+3/8	+1/2	+5/8	+1
2.5	+2	+3/4	+3/4	+1/2	+1/4	0	0	0	+1/4	+1/2	+5/8	+3/4	+1 1/2
3.0													
3.5	+1	+3/8	+1/8	-1/8	-1/4	-1/4	0	-1/4	-1/4	-1/4	0	+1/4	+1/2
4.0	+1 3/4	+1/4	-1/4	-1/2	-3/8	-1/4	0	-1/4	-3/8	-1/2	-1/4	+1/4	+1
4.5	0	-1/8	-1/2	-1/4	0	0	0	+1/8	0	-1/4	-1/2	-1/4	0
4.75	-1/4	-3/4	-3/8	+1/2	+3/4	+1/2	0	+1/2	+3/4	+1/2	-1/8	-5/8	-3/8
4.90	-1	0	+1	+1 1/4	+1 1/4	+1/2	0	+1/2	+1 1/4	+1 1/4	+1	0	-1
4.95	-1/4	+1 3/8	+1 1/2	+1 1/2	+1 1/8	+3/4	0	+3/4	+1 1/4	+1 1/2	+1 3/4	+1 3/8	-1/4

TABLE 10

FLOW DIRECTION DATA FROM 5 INCH SQUARE DUCT

- OBTAINED WITH LONG NEEDLE PROBE

Re ≈ 60,000

(Data are not corrected for wall interference)

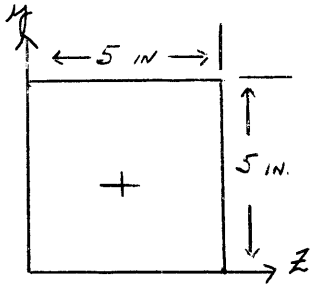

Tabulated Numbers Represent Angle In Degrees Between X Axis And Velocity Vector Projection Onto XZ Plane - Positive Angles Denote Flow Toward Duct Center, Negative Angles Denote Flow Toward Duct Walls

z" → / y" ↓	.10	.25	.5	1.0	1.5	2.0	2.5	3.0	3.5	4.0	4.5	4.75	4.90
0.010	+2 3/8	+1 3/4	+1 3/4	+1 1/2	+1 1/4	+ 3/4	0	+3/4	+1	+1 1/2	+1 3/4	+1 3/4	+2 1/2
0.030	+1 3/8	+1 3/4	+1 3/4	+1 1/2	+1 1/4	+ 3/4	0	+ 3/4	+1	+1 1/2	+1 3/4	+1 3/4	+1 1/2
0.050	+ 1/8	+1 3/8	+1 3/4	+1 1/2	+1 1/4	+3/4	0	+ 3/4	+1	+1 1/2	+1 3/4	+1 1/2	+ 1/4
0.100	- 1/2	+ 1/8	+1	+1 1/4	+1 1/4	+ 1/2	0	+ 1/2	+1	+1 1/4	+1	0	- 1/2
0.250	+ 1/4	- 1/4	- 1/4	+ 1/2	+ 3/4	+1/2	0	+ 1/2	+ 3/4	+ 1/2	- 1/4	- 5/8	+ 1/4
0.500	+ 1/4	- 1/4	- 1/2	- 1/4	+ 1/8	+ 1/8	0	+ 1/8	0	- 1/4	- 5/8	- 3/8	+ 1/4
1.000	+ 3/8	+ 1/4	- 1/4	- 1/2	- 3/8	- 1/4	0	- 1/4	- 3/8	- 1/2	- 1/4	+ 1/4	+ 1/4
1.500	+ 3/8	+ 1/4	+ 1/4	- 1/8	- 1/4	- 1/4	0	- 1/4	- 1/4	- 1/4	0	+ 1/8	+ 3/8
2.000	+ 1/2	+ 1/2	+ 1/2	+ 3/8	0	0	0	0	0	+ 3/8	+ 1/2	+ 1/2	+ 1/2
2.500	+ 1/2	+ 5/8	+ 3/4	+ 5/8	+ 1/4	0	0	0	+ 1/4	+ 1/2	+ 5/8	+ 1/4	+ 3/8
3.000	+ 1/2	+ 1/2	+ 1/2	+ 3/8	0	0	0	0	0	+ 3/8	+ 1/2	+ 1/2	+ 1/4
3.500	+ 1/2	+ 1/4	0	- 1/4	- 1/4	- 1/4	0	- 1/4	- 1/4	- 1/4	0	+ 1/8	+ 1/4
4.000	+ 3/8	+ 1/4	- 1/4	- 1/2	- 3/8	- 1/4	0	- 1/4	- 3/8	- 1/2	- 1/4	+ 1/4	+ 1/4
4.500	+ 1/4	- 1/4	- 1/2	- 1/4	+ 1/8	+ 1/8	0	+ 1/4	0	- 1/4	- 1/2	- 3/8	0
4.750	- 1/4	- 1/2	- 1/4	+ 1/2	+ 3/4	+ 1/2	0	+ 1/2	+ 3/4	+ 1/2	- 1/4	- 5/8	- 1/4
4.900	-1	0	+ 1	+ 1 1/4	+ 1 1/4	+ 1/2	0	+ 1/2	+ 1	+ 1 1/4	+1	0	- 3/4
4.950	- 1/4	+ 1 1/4	+ 1 1/2	+ 1 1/2	+ 1 1/8	+ 3/4	0	+ 3/4	+ 1 1/8	+ 1 1/2	+ 1 3/4	+ 1 1/2	- 1/8

TABLE II

DATA TABULATION OF VELOCITY VECTOR DIRECTIONS

(X AXIS AS REFERENCE)

2.5 x 5 inch Duct

Re ≈ 88,000 U_{ℓ} = 60.2 fps

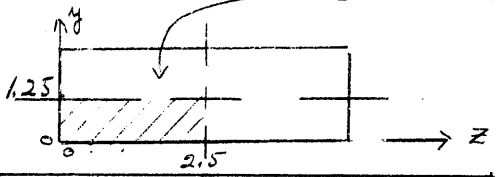

Data For ZX Plane

+ Toward
- Away From
} Centerline

Tabulated Numbers Are Angles In Degrees

inches ↓z y→	1.25	1.125	1.0	.875	.75	.625	.5	.375	.25	.1
.10	+ 15/16	+ 7/8	+ 3/4	+ 7/8	+ 11/16	+ 5/8	+ 1/2	+ 7/16	+ 1/4	+ 1/8
.175	+ 7/8	+ 13/16	+ 3/4	+ 5/8	+ 7/16	+ 5/8	+ 1/2	+ 1/16	- 5/16	0
.25	+ 3/4	+ 3/4	+ 11/16	+ 9/16	+ 1/4	+ 1/4	- 1/16	- 3/8	- 3/8	+ 1/8
.375	+ 5/8	+ 3/4	+ 5/8	+ 7/16	+ 1/8	- 1/16	- 3/8	- 3/8	- 3/8	+ 9/16
.50	+ 1/2	+ 7/16	+ 1/2	+ 3/16	- 1/16	- 3/16	- 3/8	- 3/8	- 3/16	+ 11/16
.75	+ 1/8	+ 1/8	+ 1/8	0	- 1/4	- 7/16	- 3/8	- 1/8	+ 1/4	+ 1 1/16
1.0	- 1/16	- 1/8	- 1/8	- 3/16	- 3/8	- 3/8	- 1/16	+ 1/8	+ 3/8	+ 1 1/8
1.25	- 1/8	- 1/8	- 3/16	- 1/4	- 3/8	- 1/4	+ 1/16	+ 1/4	+ 1/2	+ 1
1.50	- 1/4	- 1/4	- 5/16	- 1/4	- 1/4	- 1/8	+ 1/8	- 5/16	+ 1/2	+ 3/4
2.0	- 1/8	- 1/8	- 1/8	- 1/8	0	0	+ 1/8	+ 1/8	+ 1/8	+ 1/4
2.5	0	0	0	0	0	0	0	0	0	0

Data For YX Plane

(Same information above applies)

inches ↓z y→	1.25	1.125	1.0	.875	.75	.625	.5	.375	.25	.1
.10	0	+ 1/4	+ 1/2	+ 7/8	+ 7/8	+ 1	+ 7/8	+ 1/2	+ 3/8	+ 1/2
.175	0	+ 3/16	+ 3/8	+ 5/8	+ 5/8	+ 1/2	+ 1/4	+ 1/16	- 1/8	+ 5/8
.25	0	+ 1/8	+ 1/8	+ 1/4	+ 1/4	0	- 1/8	- 3/8	- 3/8	+ 3/4
.375	0	- 1/8	- 1/8	0	- 1/8	- 1/4	- 3/8	- 3/8	- 1/8	+ 3/4
.5	0	- 1/8	- 1/4	- 3/8	- 1/2	- 3/8	- 3/8	- 3/8	0	+ 3/4
.75	0	- 1/8	- 1/4	- 3/8	- 1/2	- 3/8	- 1/4	- 1/8	+ 1/4	+ 7/8
1.0	0	- 1/8	- 1/4	- 1/4	- 1/4	- 1/4	- 1/8	+ 1/8	+ 3/8	+ 3/4
1.25	0	0	0	0	+ 1/8	+ 1/4	+ 1/4	+ 3/8	+ 1/2	+ 7/8
1.50	0	+ 1/16	+ 1/8	+ 1/8	+ 3/8	+ 3/8	+ 3/8	+ 7/16	+ 1/2	+ 7/8
2.0	0	—	+ 1/8	—	+ 1/8	—	+ 1/4	—	+ 1/4	+ 3/4
2.5	0	—	+ 1/8	—	+ 1/8	—	+ 1/8	—	+ 1/4	+ 3/4

TABLE 12

DATA TABULATION OF VELOCITY VECTOR DIRECTIONS

(X AXIS AS REFERENCE)

Data for Quadrant Shown

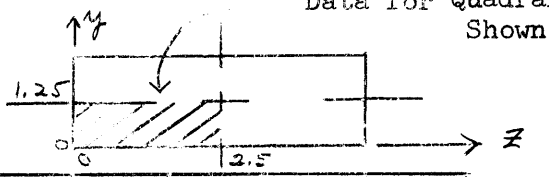

2.5 x 5 inch Duct

Re ≈ 24,400 U_c = 17.9 fps

Data For ZX Plane

+ Toward } Centerline
- Away From }

Tabulated Numbers Are Angles In Degrees

inches ↓z → x	1.25	1.125	1.0	.875	.75	.625	.50	.375	.25	.10
.1	+7/8	+15/16	+5/8	+7/8	+13/16	+5/8	+11/16	+15/16	+3/4	-1/4
.175	+1/2	+3/4	+9/16	+11/16	+1/2	+3/8	+5/16	+3/16	-1/16	-3/16
.25	+11/16	+5/8	+5/8	+5/8	+1/4	+1/16	-1/8	+1/16	-1/4	+1/8
.375	+1/2	+1/2	-7/16	+3/16	+3/16	0	-1/8	-3/16	-3/16	+9/16
.50	+1/2	+3/8	-1/8	+1/16	+1/16	-1/8	-3/8	-3/16	-1/16	+15/16
.75	+1/16	-1/16	+1/16	-1/16	-7/16	-5/16	-1/4	-1/16	3/16	+1
1.0	-3/16	-1/4	-5/16	-5/16	-5/16	-1/4	-1/8	+1/8	+5/8	+1 1/4
1.35	-3/8	-3/8	-7/16	-3/8	-1/4	-3/16	0	+5/16	+9/16	+15/16
1.50	-5/16	-5/16	-1/4	-5/16	-1/4	-1/4	+1/8	+1/4	+1/2	+15/16
2.00	-1/4	-1/8	-1/4	-1/8	-1/16	-1/8	+1/8	+3/16	+1/4	+1/4
2.50	0	0	0	0	0	0	0	0	0	0

Data For YX Plane

(Same information above applies)

inches ↓z → y	1.25	1.125	1.0	.875	.75	.625	.50	.375	.25	.10
.10	0	0	+1/2	+5/8	-5/8	+1	+3/4	+3/8	+1/4	+3/4
.175	0	—	+1/8	—	+3/8	—	+1/8	-1/8	-3/8	+7/8
.25	0	+1/8	+1/8	+1/8	+1/8	-1/8	-1/4	-1/2	-3/8	+1 3/4
.375	0	—	-3/8	—	-1/2	—	-5/8	—	-1/8	+1 1/2
.5	0	-1/8	-1/8	-3/8	-1/2	-5/8	-1/2	-3/8	-1/4	+1 3/8
.75	0	-1/8	-3/8	-1/2	-1/4	-3/8	-3/8	-1/4	+1/8	+1
1.0	0	0	-1/8	-1/8	+1/8	-1/8	0	+1/4	+1/4	+1 1/2
1.35	0	-1/8	0	0	+1/4	+1/4	+3/8	+1/4	+1/2	+1 1/2
1.50	0	—	+1/8	—	+1/4	—	+3/8	—	+1/2	+1 1/2
2.0	0	—	+1/8	—	+1/4	—	+3/8	—	+1/2	+1 1/2
2.5	0	—	+1/8	—	+1/8	—	+1/8	—	+1/4	+1 1/2

TABLE 13

DATA TABULATION OF VELOCITY VECTOR DIRECTIONS

(X AXIS AS REFERENCE)

1.66 x 5 inch Duct

Re ≈ 60,000

U_{ℓ} = 51.8 fps

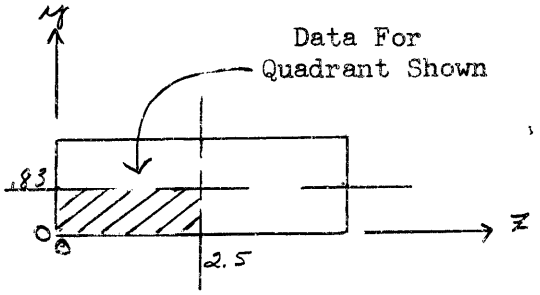

Data For ZX Plane

+ Toward
- Away From
} Centerline

inches — Tabulated Numbers Are Angles In Degrees

Z → / Y ↓	2.5	2.0	1.5	1.25	1.0	.75	.625	.50	.375	.25	.175	.10	.05
.83	0	-1/8	-1/4	-3/8	-3/8	-3/16	+1/16	+1/4	+9/16	+3/4	+3/4	+1	—
.70	0	-1/8	-3/16	-3/8	-7/16	-5/16	0	+3/16	+9/16	+11/16	+11/16	+7/8	—
.60	0	0	-3/16	-1/4	-3/8	-3/8	-5/16	0	+3/16	+3/8	+9/16	+7/8	—
.50	0	0	-1/16	-1/4	-5/16	-7/16	-3/8	-5/16	-1/16	+1/4	+7/16	+9/16	—
.40	0	0	-1/16	0	-3/16	-1/4	-5/16	-3/8	-3/8	-1/16	+1/4	+5/8	—
.30	0	0	+1/16	+1/8	+1/4	-1/16	-1/16	-7/16	-1/2	-1/4	0	+1/2	—
.20	0	+1/8	+1/8	+1/4	+5/16	+5/16	+5/16	+5/16	-3/16	-5/16	-3/16	+3/8	—
.10	0	+1/8	0	+7/16	+3/4	+1 1/8	+1 1/8	+5/16	+9/16	+1/4	-1/16	-1/16	—
.05	0	+1/8	+1/16	+3/8	+7/8	+1 1/4	+1 1/4	+1 1/4	+1 1/8	+7/8	+11/16	+1/4	—

Data For YX Plane

(Same information above applies)

inches

Z → / Y ↓	2.5	2.0	1.5	1.25	1.0	.75	.625	.50	.375	.25	.175	.10	.05
.83	0	0	0	0	0	0	0	0	0	0	0	0	0
.70	0	0	0	0	0	0	-1/4	-5/16	-3/16	0	+1/8	-5/16	+1/4
.60	0	0	+1/16	+1/8	+1/8	-1/8	-5/16	-7/16	-5/16	-1/8	+1/8	-1/8	+3/4
.50	+1/8	+1/16	+3/16	+1/4	+1/4	-1/8	-1/4	-7/16	-3/8	-1/4	+1/16	+1/2	+1 1/16
.40	+1/8	+1/16	+1/4	+5/16	+1/4	-1/8	-1/16	-7/16	-1/2	-5/16	-3/16	+9/16	+1 3/16
.30	+1/8	+1/8	+3/16	+5/16	+5/16	+1/8	-1/16	-5/16	-7/16	-7/16	-5/16	+5/16	+1 1/16
.20	+1/4	+1/8	+1/4	+5/16	+7/16	+1/4	+3/16	-1/16	-1/8	-3/16	-3/8	-1/4	+1 1/16
.10	+7/16	+5/16	+1/2	+9/16	+9/16	+5/8	+7/16	+7/16	+7/16	+1/2	+7/16	+1/4	+1/4
.05	—	—	—	—	—	—	—	—	—	—	—	—	—

APPENDIX 4.1 CORRECTIONS APPLIED TO DATA

Corrections for various types of errors were investigated for both the pitot tube and hot wire. Pitot tube data near the duct walls were corrected for turbulence intensity and velocity gradient errors. No corrections were made to the hot wire data primarily because the resulting velocity profiles near the wall appeared incorrect. Nevertheless the various sources of error and corresponding corrections are discussed below.

Pitot Tube

When a pitot tube is used in a transverse velocity gradient it does not sense the stagnation pressure of the streamline coincident with the tube axis. Rather, it senses a slightly higher pressure, indicating a displacement δ of the "effective tube center" toward the higher velocity region. Young and Maas (26) studied this problem and presented the following emperical relation for the effective displacement δ:

$$\delta/d_o = 0.131 + 0.083\, d_i/d_o \qquad \text{(A-6)}$$

Applying this relation to the pitot tube used for the present velocity measurements the effective displacement is 0.005 inches away from the wall. This correction is indicated in the data of Table 7.

Turbulence intensity causes a pitot tube to read high. According to Goldstein (28) the pitot tube senses the sum of the velocity heads corresponding to the correct mean velocity and the rms intensity, i.e.

$$\Delta p_{\text{indicated}} = \frac{\rho}{2g}\left(\bar{u}^2 + \tilde{u}'^2\right) \qquad \text{(A-7)}$$

The effect of the intensity term $(\tilde{u}'^2)$ is generally negligible except in the region very close to the walls where $\tilde{u}' \approx .30\ \bar{u}$. Here the use of Equation (A-7) results in a correction of 4 percent, giving velocities lower than otherwise computed.

In order to apply this correction it is necessary to know the intensity at various positions throughout the flow. No quantitative intensity measurements were made during this study. The intensity corrections were made by assuming that intensities are correlated by the wall similarity relation shown in Figure 44. Only in the region very close to the wall are the intensities large enough to yield a significant correction. The maximum correction applied to the pitot tube data (Table 7) was about 3 1/2 percent.

Hot Wire

Two sources of error for hot wire mean velocity measurements were considered; 1) wall cooling and 2) turbulence intensity. Neither was found to require a significant correction to the present data.

When a hot wire is brought in close proximity to a solid boundary, direct cooling occurs by heat conduction through the fluid to the wall. At large distances from the wall this conduction effect is negligible. However, at distances of 20 wire diameters or less this excess cooling by direct conduction causes significant changes in the hot wire readings. During the present experiments a wall cooling effect was observed in still air at distances up to 0.030 inches from the wall. Velocity measurements were desired as close as 0.005 to 0.010 inches from the wall. It was therefore necessary to investigate this effect.

Richardson (27) reports results of an analytical and experimental study of this wall cooling phenomenon. According to his results, the velocities and distances employed herein are large enough to avoid completely the wall cooling error. The author's measurements of the wall cooling effect in still air agreed very well with those of Richardson, thereby providing greater confidence in the use of his results. Also, in a personal communication with the author, Prof. Kronauer of Harvard

University, who has been working on this hot wire conduction phenomenon, indicated that there should be no wall cooling error in the present measurements.

The effect of turbulence intensity on hot wire readings is felt by the author to be somewhat uncertain. It appears to be generally accepted that turbulent fluctuations cause the hot wire to read low. The author, however, believes that the reverse may be true.

Consider first the generally accepted correction for intensity. It is assumed that the heat transfer behavior of the hot wire at any instant during turbulent flow is given by the steady state relation expressed by King's law, i.e.

$$I^2 = A + B\sqrt{V} \qquad \text{(A-8)}$$

Here, A and B are constants only when the wire is operated at constant temperature. A plot according to equation (A-8) of wire current I (ordinate) versus velocity V results in a curve that is concave downward. Imagine an oscillation of V about some mean value $\overline{V}$. Because of the curvature of I vs V, the rms value of I will not correspond with the rms value of V through equation (A-8). Rather, the downward curvature will cause the rms value of I to correspond to a velocity somewhat lower than the true average $\overline{V}$. Thus, if the rms wire current is observed as a measure of the average velocity, the resultant velocity measurement will be low.

The magnitude of this effect can be determined by forming the average wire current from equation (A-8). Thus

$$I^2_{ave} = \frac{1}{t}\int_0^t (A + B\sqrt{V})\,dt = A + B\frac{1}{t}\int_0^t \sqrt{V}\,dt \qquad \text{(A-9)}$$

The velocity V to which the hot wire is sensitive is the instantaneous velocity normal to the wire.

$$V_{eff} = \sqrt{(\bar{u}+u')^2 + v'^2}$$

whence

$$\sqrt{V_{eff}} = \sqrt[4]{(\bar{u}+u')^2+v'^2} = \sqrt{\bar{u}}\sqrt[4]{\left(1+\frac{u'}{\bar{u}}\right)^2+\left(\frac{v'}{\bar{u}}\right)^2} \qquad \text{(A-10)}$$

Upon expanding and forming the time average the following result is obtained

$$\bar{V}_{eff} = \int_0^t \sqrt{V_{eff}}\, dt = \sqrt{\bar{u}}\left[1 - \frac{1}{8}\left(\frac{\tilde{u}'}{\bar{u}}\right)^2 + \frac{1}{4}\left(\frac{\tilde{v}'}{\bar{u}}\right)^2 + \cdots\right]$$

Here $\bar{u}$ is the correct average velocity whereas $\bar{V}_{eff}$ is the velocity determined from the instrument reading. The correct mean velocity is then expressed in terms of the measured velocity as

$$\bar{V}_{meas} = \bar{u}_{Correct}\left[1 - \frac{1}{4}\left(\frac{\tilde{u}'}{\bar{u}}\right)^2 + \frac{1}{2}\left(\frac{\tilde{v}'}{\bar{u}}\right)^2 + \cdots\right] \qquad \text{(A-11)}$$

The intensities are large enough to be important mainly near a solid boundary. There the $\tilde{v}'$ intensity component is small compared with the $\tilde{u}'$ intensity component and can therefore be neglected in equation (A-11). Thus equation (A-11) indicates that the effect of intensities is to cause the indicated mean velocity to be lower than the true mean velocity. The correction near the wall where $\tilde{u}'/\bar{u} \approx 0.3$ is only 2 1/2 percent. This result (equation A-11) is identical to that given by Hinze (13), page 97.

In the discussion of the hot wire measurements made within the viscous sublayer (Section 4.1.1) it is pointed out that velocities near the wall appear to be high. The above intensity correction, although small, is in the wrong direction to explain these data. This fact led the author to look more deeply into the question of intensity error.

In the development of equation (A-11) for the intensity correction two major assumptions were made; 1) the instantaneous heat transfer

behavior is described by King's law - equation (A-8) and 2) the wire is operated at constant temperature so that A and B are constants. For the mean velocity measurements obtained here, the wire was not actually operated at constant instantaneous temperature but rather only at a constant mean temperature. Assuming thermal inertia of the wire to be negligible, the author made an elaborate analysis of the behavior of the actual circuit to determine the response of the galvanometer voltage to changes in instantaneous velocity. The galvanometer voltage was found to vary nearly linearly with $\sqrt{V}$ thereby indicating that the above analysis for intensity effect in the constant temperature case is also valid for the actual circuit used here.

The other major assumption is that the instantaneous heat transfer behavior is expressed by King's law. The author doubts whether this assumption is valid. In most cases of oscillating flows the average heat transfer coefficient is increased by the oscillations above that value corresponding to a steady flow at the average velocity. It is believed that large turbulent fluctuations should produce a similar effect. Such an effect would cause the hot wire to read high. A correction lowering the velocities near the wall would in the present case improve the appearance of the hot wire data taken in the viscous sublayer (see Section 4.1.1). Without some evidence of the existence of this intensity effect it has only been possible to speculate about it as a means of explaining the present data.

The wall cooling error was shown to be negligible. The generally accepted intensity correction was small but in the wrong direction to explain the measurements. Because of the uncertainty of the intensity correction as discussed above no corrections were made to the hot wire velocity data.

APPENDIX 4.2 DISCUSSION OF BOUNDARY AND SYMMETRY CONDITIONS

The secondary velocity data were analyzed and interpreted with the aid of certain boundary and symmetry conditions that must be satisfied by the actual flow. These conditions are discussed briefly in Section 4.2, page 31. Most of them are self evident, however, some require further explanation which is given below. In Section 2 it was stated that the transverse turbulent shear stresses $\overline{u'w'}$ and $\overline{v'w'}$ in a circular pipe must be zero for reasons of symmetry, not due to the zero gradient of mean velocity. These symmetry arguments are discussed here. Finally, although it was not possible to solve for the turbulent stresses in the rectangular ducts from the mean flow measurements, it was necessary to determine the boundary and symmetry conditions for the $\overline{u'v'}$, $\overline{u'w'}$ and $\overline{v'w'}$ stresses in attempting such a solution. These are also discussed below.

Secondary Velocities

The boundary and symmetry conditions that must be satisfied by the secondary velocity field are presented and discussed individually below. These results are presented in Section 4.2. Consider only the quadrant containing the origin (Figure 1).

1) The continuity relation for the mean flow specialized for fully developed flow with $\partial\bar{u}/\partial x = 0$ (equation 4d) requires that

$$\frac{\partial \bar{v}}{\partial y} = - \frac{\partial \bar{w}}{\partial z}$$

at each point in the flow.

2) The velocities are zero at all solid boundaries

$$\bar{v} = \bar{w} = 0 \quad \text{along} \quad y = 0 \quad \text{and} \quad z = 0$$

3) Because of condition 2), $\partial\bar{w}/\partial z = 0$ along $y = 0$; hence from continuity $\partial\bar{v}/\partial y = 0$ along $y = 0$.

4) Similarly $\partial\bar{v}/\partial y = 0$ along $z = 0$; hence from continuity $\partial\bar{w}/\partial z = 0$ along $z = 0$

5) Along the axis of symmetry $y = a$, $v = 0$ from symmetry considerations. (The only way an observer on either side of $y = a$ would see the same flow conditions at $y = a$ is when $v = 0$. However, w need not be zero here.) Also along $y = a$ it can be shown that $\partial\bar{w}/\partial y = 0$. This requires a little explanation. Consider an elemental fluid control volume on the axis $y = a$ (sketch). The shear stress τ_{yz} acting on a z face must be zero for reasons of symmetry. The forces acting on the element must look the same to an observer on either side of $y = a$. This is possible only when the shear stresses $\tau_{yz} = 0$. The viscous shear stress τ_{yz} may be expressed as

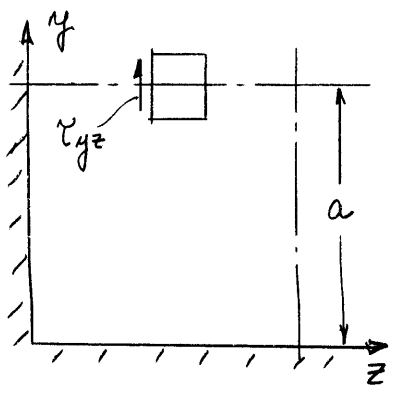

$$\tau_{yz\ vis.} = \mu\left(\frac{\partial\bar{v}}{\partial z} + \frac{\partial\bar{w}}{\partial y}\right)$$

It was reasoned above that $v = 0$ along $y = a$. Therefore, $\partial\bar{v}/\partial z = 0$ along $y = a$ and in order for the shear stress to vanish $\partial\bar{w}/\partial y$ must also be zero. q.e.d.

Although it may seem that the derivative $\partial\bar{w}/\partial y$ should also be zero from symmetry considerations, this is not true. The gradient $\partial\bar{v}/\partial y$ must merely be discontinuous across $y = a$ so that the slope $\partial\bar{w}/\partial y$ on either side appears the same to an observer. Consider the continuity relation $\partial\bar{v}/\partial y + \partial\bar{w}/\partial z = 0$. If a gradient in w exists along $y = a$, a corresponding gradient of v must exist to satisfy continuity. A gradient $\partial w/\partial z$ is expected if w is to be non zero along $y = a$ because $w = 0$ both at $z = 0$ and at $z = b$.

6) By reasoning similar to 5) above it is seen that $\bar{w} = 0$ and $\partial\bar{v}/\partial z = 0$ along the axis of symmetry $z = b$.

7) In the square duct the flow must also be symmetrical about the diagonal emanating from the corner. This additional symmetry condition provides another relation that may be used to advantage in data interpretation. Along the diagonal, symmetry demands that $\bar{v} = \bar{w}$ and that $\partial\bar{v}/\partial y = \partial\bar{w}/\partial z$ and $\partial\bar{v}/\partial z = \partial\bar{w}/\partial y$ etc. Considering the continuity condition $\partial\bar{v}/\partial y = -\partial\bar{w}/\partial z$ and the symmetry condition $\partial\bar{v}/\partial y = \partial\bar{w}/\partial z$ it is seen that both conditions are satisfied only when $\partial\bar{v}/\partial y = \partial\bar{w}/\partial z = 0$ along the diagonal.

Turbulent Stresses In Circular Pipe

Section 2.2 discusses the question of whether a turbulent shear stress $\overline{u'v'}$ can exist in the absence of a gradient of mean velocity $\bar{u}$ or $\bar{v}$. In this discussion reference is made to the fact that the $\overline{u'w'}$ and $\overline{v'w'}$ stresses in a circular pipe must be zero from symmetry considerations rather than the absence of mean velocity gradients. The following paragraphs present these symmetry arguments.

Consider an axisymmetric flow in a circular pipe and let x, y, and z denote the axial, radial and tangential directions respectively. Thus, u, v, and w are the axial, radial and tangential velocities.

First, imagine an elemental fluid control volume as shown to the right. The $\overline{v'w'}$ shear stress acts in the tangential direction (also radial) on an x z plane. In order to satisfy axial symmetry the forces on the fluid element must appear the same to an observer on either side of a radial line through the element. This is true only if the $\overline{v'w'}$ shear stress is zero.

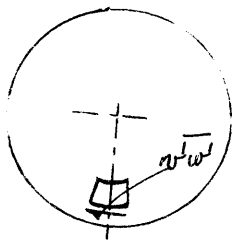

Next consider the $\overline{u'w'}$ shear stress acting on the xy plane. (See sketch at right.) The forces acting on the elemental control volume must be symmetrical about the duct axis. Therefore, if a $\overline{u'w'}$ stress acts on the one face as shown, an equal stress $\overline{u'w'}$ (same direction) must act on the other xy face in order to satisfy symmetry. Considering Newton's third law an adjacent element would need to have an equal and opposite shear stress $\overline{u'w'}$ acting in the -x direction. Symmetry would demand that the adjacent element have $\overline{u'w'}$ stresses acting in the -x direction on both faces. If the two elements are then considered together as one larger element (forgetting then about the interface between them) one sees that the $\overline{u'w'}$ stresses on the two xy faces are equal and opposite. The forces on the element no longer appear symmetrical. It is thus concluded that symmetry in the tangential direction can be satisfied only when the $\overline{u'w'}$ stresses are everywhere zero.

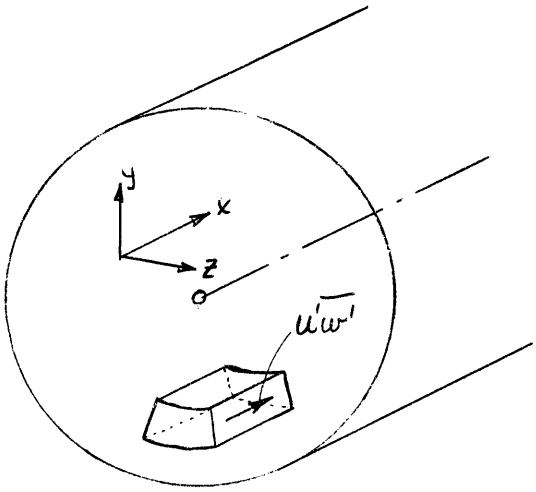

Similar arguments may be applied to a turbulent flow between infinite parallel plates to show that symmetry demands the $\overline{u'w'}$ and $\overline{v'w'}$ stresses be zero.

Turbulent Stresses In Rectangular Ducts

The boundary conditions for the turbulent stresses simply require that the stresses vanish at all solid boundaries. This is due to the fact that all velocities (both mean and fluctuating components) must be zero at the boundaries. In order to deal with a single quadrant in formulating the theoretical problem it is necessary to investigate the "boundary conditions" along the axes of symmetry $y = a$ and $z = b$.

First, consider the $\overline{v'w'}$ stresses. Imagine a fluid element centered on the axis of symmetry $y = a$ as shown in the accompanying sketch. The $\overline{v'w'}$ stress acts on the xy face in the y direction (also on the xz face in the z direction). The only way that the forces on the element appear symmetrical about the axis $y = a$ is if this stress $\overline{v'w'} = 0$. Similarly, it may be reasoned that this stress is zero on the axis of symmetry $z = b$. Thus, the boundary conditions for $\overline{v'w'}$ in a single quadrant are

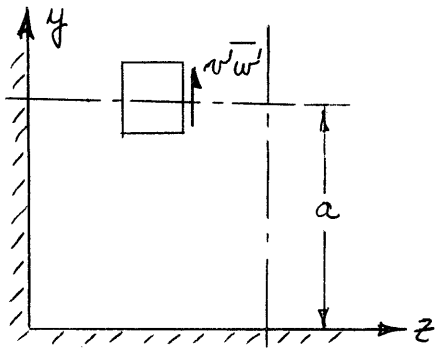

$$\overline{v'w'} = 0 \quad \text{along} \quad y = 0, \quad z = 0, \quad y = a, \quad z = b$$

Now consider the shear stresses $\overline{u'v'}$ and $\overline{u'w'}$. An elemental control volume centered about the axis $y = a$ is shown below. The $\overline{u'v'}$ stress (τ_{yx}) acts in the axial (x) direction on an xz face. Symmetry about the axis $y = a$ requires that the τ_{yx} stresses acting on the two xz faces (in xz plane) be equal (same direction). To determine the magnitude of this stress it is necessary to write the axial momentum equation for this element (equation 1a). When written in terms of stresses and specialized for fully developed flow, one obtains

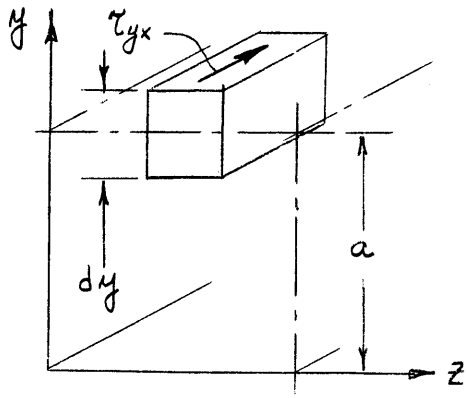

$$\rho\left(\bar{v}\frac{\partial \bar{u}}{\partial y} + \bar{w}\frac{\partial \bar{u}}{\partial z}\right) = -\frac{\partial p}{\partial x} + \frac{\partial}{\partial y}(\tau_{yx}) + \frac{\partial}{\partial z}(\tau_{zx})$$

According to the above argument that the τ_{yx} stress must be the same on both sides of the elemental control volume the derivative $\partial \tau_{yx} / \partial y$

may be expressed as $\partial \tau_{yx} / dy$. The momentum equation then becomes

$$\rho\left(\bar{v}\frac{\partial \bar{u}}{\partial y} + \bar{w}\frac{\partial \bar{u}}{\partial z}\right) = -\frac{\partial p}{\partial x} + \frac{\partial \tau_{yx}}{dy} + \frac{\partial}{\partial z}(\tau_{zx})$$

None of the terms in this equation are expected to be infinite. Therefore as dy is allowed to approach zero as a limit the shear stress τ_{yx} must also approach zero to prevent the term from becoming infinite. Hence, it is concluded that τ_{yx} or the turbulent shear stress $\overline{u'v'}$ must vanish along $y = a$. (The viscous shear stress is easily shown to be zero.)

The turbulent stress $\overline{u'v'}$ is not expected to vanish along the axis of symmetry $z = b$, in fact it is expected to vary in a manner similar to the $\overline{u'v'}$ stress along the radius of a circular pipe. Hence, though it may at first seem that the turbulent stresses should be symmetrical about the diagonal in the case of the square duct, the fact that $\overline{u'v'} = 0$ along $y = a$ but $\overline{u'v'} \neq 0$ along $z = b$ indicates that $\overline{u'v'}$ is not symmetrical about the diagonal.

Similar arguments can be made to show that $\overline{u'w'} = 0$ along $z = b$ and that $\overline{u'w'}$ is not expected to be symmetrical across the diagonal.

APPENDIX 6.1 SECONDARY FLOW GENERATED BY BOUNDARY SHEAR TURBULENCE

In Section 6 the concept of a wall similarity relation applied to the turbulence intensity components $\tilde{u}'$, $\tilde{v}'$, and $\tilde{w}'$ is discussed and the experimental evidence in support of this concept is reviewed (Figure 44). It is shown that within the region of wall similarity a driving force for a secondary flow exists whenever there is a transverse gradient of wall shear stress. To determine the effect of this driving force in producing a secondary flow the equations of motion were solved near the wall by neglecting the turbulent shear stress terms. The object of this appendix is to present this solution.

Consider the axial vorticity equation specialized for fully developed flow.

$$\bar{v}\frac{\partial \bar{\xi}}{\partial y} + \bar{w}\frac{\partial \bar{\xi}}{\partial z} = \nu \nabla^2 \bar{\xi} + \frac{\partial^2}{\partial y \partial z}\left(\overline{v'^2} - \overline{w'^2}\right) - \frac{\partial^2}{\partial y^2}\left(\overline{v'w'}\right) + \frac{\partial^2}{\partial z^2}\left(\overline{v'w'}\right) \qquad (A\text{-}12)$$

Near the wall (y=0) the convective terms are negligible and $\partial^2\bar{\xi}/\partial z^2 \ll \partial^2\bar{\xi}/\partial y^2$. (See page 46 for a further discussion of these assumptions.) Numerical evaluation of the various terms in equation (A-12) from the experimental measurements verified these assumptions. In order to determine the secondary flow produced by the intensity term $\partial^2/\partial y \partial z\left(\overline{v'^2} - \overline{w'^2}\right)$ the other turbulent stress terms are assumed negligible, i.e.

$$-\frac{\partial^2}{\partial y^2}\left(\overline{v'w'}\right) + \frac{\partial^2}{\partial z^2}\left(\overline{v'w'}\right) = 0$$

The vorticity equation then simplifies to

$$\nu \frac{\partial^2}{\partial y^2}\left(\frac{\partial w}{\partial y}\right) = \frac{\partial^2}{\partial y \partial z}\left(\overline{w'^2} - \overline{v'^2}\right) \qquad (A\text{-}13)$$

where $\bar{\xi} = \frac{\partial \bar{w}}{\partial y} - \frac{\partial \bar{v}}{\partial z}$ and $\frac{\partial \bar{v}}{\partial z} << \frac{\partial \bar{w}}{\partial y}$ near y = 0

Equation (A-13) can be integrated over y to obtain an expression for the secondary velocity w as a function of y. The solution procedes as follows. Integrating once from y = 0 to y = y

$$\nu \frac{\partial}{\partial y}\left(\frac{\partial \bar{w}}{\partial y}\right) = \frac{\partial}{\partial z}\left(\overline{w'^2} - \overline{v'^2}\right) + \nu\left[\frac{\partial}{\partial y}\left(\frac{\partial \bar{w}}{\partial y}\right)\right]_{y=0}$$

Integrating again over the same limits.

$$\nu \frac{\partial w}{\partial y} = \int_0^y \frac{\partial}{\partial z}\left(\overline{w'^2} - \overline{v'^2}\right) dy + \nu\left[\frac{\partial}{\partial y}\left(\frac{\partial \bar{w}}{\partial y}\right)\right]_{y=0} y + \nu \frac{\partial \bar{w}}{\partial y}\Big)_{y=0}$$

Final integration over y from y = 0 to y = y gives

$$\bar{w} = \frac{1}{\nu}\int_0^y \left[\int_0^y \frac{\partial}{\partial z}\left(\overline{w'^2} - \overline{v'^2}\right) dy\right] dy + \nu\left[\frac{\partial}{\partial y}\left(\frac{\partial w}{\partial y}\right)\right]_{y=0} \frac{y^2}{2} + \nu \frac{\partial \bar{w}}{\partial y}\Big)_{y=0} y \qquad \text{(A-14)}$$

Boundary conditions on $\partial \bar{w}/\partial y$ and $\partial^2 \bar{w}/\partial y^2$ are necessary to evaluate this relation. If there were no secondary flow $\bar{w}$ would be everywhere zero and $\partial \bar{w}/\partial y = \partial^2 \bar{w}/\partial y^2 = 0$ at the wall. To determine the effect of the $(\overline{w'^2} - \overline{v'^2})$ term in a shear gradient in producing a secondary flow, it seems reasonable to set $\bar{w}$ and its derivatives equal to zero at the wall and compute the resulting distribution of $\bar{w}$ vs y. Thus, equation (A-14) becomes

$$\bar{w} = \frac{1}{\nu}\int_0^y \left[\int_0^y \frac{\partial}{\partial z}\left(\overline{w'^2} - \overline{v'^2}\right) dy\right] dy \qquad \text{(A-15)}$$

The intensity term is evaluated numerically from the wall similarity relation shown by Figure 44. This term is expressed in terms of the wall similarity variables $\tilde{v}'/u^*$, $\tilde{w}'/u^*$ and y^* as follows

$$\frac{\partial}{\partial z}\left(\overline{w'^2}-\overline{v'^2}\right) = \frac{\partial}{\partial z}\left(w^{*2}u^{*2} - v^{*2}u^{*2}\right)$$

where $w^* = \frac{\sqrt{\overline{w'^2}}}{u^*}$; $v^* = \frac{\sqrt{\overline{v'^2}}}{u^*}$; $u^* = \sqrt{\frac{\tau_o g}{\rho}}$

Taking the z derivative

$$\frac{\partial}{\partial z}\left(\overline{w'^2}-\overline{v'^2}\right) = u^{*2}\,2w^*\frac{\partial w^*}{\partial y^*}\frac{\partial y^*}{\partial z} + w^{*2}\frac{\partial u^{*2}}{\partial z} - u^{*2}\,2v^*\frac{\partial v^*}{\partial y^*}\frac{\partial y^*}{\partial z} - v^{*2}\frac{\partial u^{*2}}{\partial z}$$

remembering that $y^* = y/\nu u^*$ and $u^{*2} = \tau_o g/\rho$

$$\frac{\partial}{\partial z}\left(\overline{w'^2}-\overline{v'^2}\right) = \frac{\partial}{\partial z}\left(\frac{\tau_o g}{\rho}\right)\left[w^*\left(y^*\frac{\partial w^*}{\partial y^*}+w^*\right) - v^*\left(y^*\frac{\partial v^*}{\partial y^*}+v^*\right)\right]$$

$$= \frac{\partial}{\partial z}\left(\frac{\tau_o g}{\rho}\right)\cdot F_1(y^*) \qquad (A\text{-}16)$$

The function $F_1(y^*)$ was evaluated from the solid lines shown on Figure 44. Substituting equation (A-16) into equation (A-15) and transforming the variable of integration from y to y^*

$$w = \frac{\nu}{\tau_o g/\rho}\frac{\partial}{\partial z}\left(\frac{\tau_o g}{\rho}\right)\int_o^{y^*}\left[\int_o^{y^*} F_1(y^*)\,dy^*\right]dy^*$$

or (A-17)

$$w = \frac{\nu}{\left(\tau_o g/\rho\right)}\frac{\partial}{\partial z}\left(\frac{\tau_o g}{\rho}\right)\cdot F_2(y^*)$$

Along any normal z = const the secondary velocity profile w vs y is proportional to the profile of $F_2(y^*)$. This function was evaluated in the manner indicated by equation (A-17) and is shown in Figure 11. It is zero at the wall and has zero slope and curvature at this point due to the boundary conditions imposed. However, this function rises sharply with increasing y^*.

It is interesting now to compare with measured values, the value of $\bar{w}$ at various distances from the wall as determined from equation (A-17). Consider a profile at z = .5 inch (square duct). From Figure 27 the transverse wall shear stress gradient is found to be

$$\frac{1}{\tau_0 g/\rho}\,\frac{\partial}{\partial z}\left(\frac{\tau_0 g}{\rho}\right) = 2.5\ 1/\mathrm{FT}$$

so that with $\nu = 1.67 \times 10^{-4}$ ft^2/sec

$$\frac{\nu}{(\tau_0 g/\rho)}\,\frac{\partial}{\partial z}\left(\frac{\tau_0 g}{\rho}\right) = 4.25 \times 10^{-4} \text{ ft/sec}$$

At a Reynolds number of 68,000, u_ℓ = 30 ft/sec and the average wall shear stress parameter $\tau_0 g/\rho = 1.85$ ft^2/sec^2. Thus at y = .075 inches $y^* = 50$ and

$$\bar{w} = 4.25 \times 10^{-4} \times 980 = .415 \text{ ft/sec}$$

making $$\frac{\bar{w}}{u_\ell} = \frac{.415}{30} = .0138$$

For comparison the experimental measurements indicate a maximum value of $\bar{w}/u_\ell = .016$ at y = .050 inches. Both measured and calculated velocities are in the same direction. Measurements also indicate that the slope $\partial w/\partial y$ is not zero at the wall but rather has a relatively large value. The fact that the above calculation of the $\bar{w}$ profile near the wall gives a value of $\bar{w}$ equal to the maximum observed value so close to the wall, in spite of having forced the gradient and curvature to be zero at the wall, indicates that the secondary flow driving force due

to boundary shear turbulence is indeed a significant factor in causing the secondary flow.

The plot of the function $F_2(y^*)$ versus y^* (Figure 11) may easily be used to determine the secondary velocity profile near the wall (based on the above analysis) for any other position (z) or Reynolds number. The position z = .5 inches was selected for the example above because it represents a rather modest shear stress gradient (see Figure 27). Nearer the corner the shear gradients become much larger. At lower Reynolds numbers slightly lower values of $\bar{w}/u_\tau$ are obtained at any position y, z. This is due principally to the fact that y^* is nearly proportional to Reynolds number whereas the curve of $\bar{w}$ vs y^* is concave upward (Figure 11). However, it must be remembered that at lower Reynolds numbers the region of influence of the boundary shear turbulence term extends further into the flow (y^* = 30 corresponds to greater value of y - see page 45) so that a greater overall effect would be expected.

APPENDIX 7.1 CALCULATION OF AXIAL VELOCITY PROFILES FROM MIXTURE LENGTH THEORY AND MEASURED SECONDARY FLOWS

Using mixture length theory for estimating the turbulent shear stresses $\overline{u'v'}$ and $\overline{u'w'}$ and using the measured secondary flows, it has been possible to compute axial velocity profiles that agree reasonably well with the measurements.

The axial momentum equation restricted to fully developed flow is

$$\bar{v}\frac{\partial \bar{u}}{\partial y} + \bar{w}\frac{\partial \bar{u}}{\partial z} = -\frac{1}{\rho}\frac{\partial p}{\partial x} + \nu\left[\frac{\partial^2 u}{\partial y^2} + \frac{\partial^2 u}{\partial z^2}\right] - \frac{\partial}{\partial y}(\overline{u'v'}) - \frac{\partial}{\partial z}(\overline{u'w'}) \quad (4a)$$

This equation may be solved for the axial velocity distribution ($\bar{u}$) if the turbulent stresses are related to the flow distribution and if the measured values of secondary velocities $\bar{v}$ and $\bar{w}$ are employed. Mixture length theory relates the turbulent stresses to the axial velocity distribution in the following way

$$-\overline{u'v'} = \ell_y^2 \left(\frac{\partial u}{\partial y}\right)^2 \quad (A\text{-}18)$$

$$-\overline{u'w'} = \ell_z^2 \left(\frac{\partial u}{\partial z}\right)^2$$

where ℓ denotes the mixture length.

Prandtl assumed that in a turbulent shear flow close to a solid boundary the mixture length was proportional to the distance from the wall. Thus,

$$\ell = k y \quad (A\text{-}19)$$

From pipe flow measurements he determined $k = 0.4$.

Kármán reasoned that the mixture length should depend on the local flow properties and proposed the following relation for ℓ

$$\ell = K \frac{\partial \bar{u}/\partial y}{\partial^2 \bar{u}/\partial y^2} \quad ; \quad K = 0.36 \tag{A-20}$$

Revising the momentum equation by combining the viscous and turbulent stresses

$$\frac{\partial}{\partial y}\left(\mu \frac{\partial \bar{u}}{\partial y} - \rho \overline{u'v'}\right) + \frac{\partial}{\partial z}\left(\mu \frac{\partial \bar{u}}{\partial z} - \rho \overline{u'w'}\right) = \frac{\partial p}{\partial x} + \rho\left(v \frac{\partial u}{\partial y} + w \frac{\partial u}{\partial z}\right)$$

Substituting the mixture length expressions (equation A-18)

$$\frac{\partial}{\partial y}\left[\mu \frac{\partial \bar{u}}{\partial y} + \rho \ell_y^2 \left(\frac{\partial \bar{u}}{\partial y}\right)^2\right] + \frac{\partial}{\partial z}\left[\mu \frac{\partial \bar{u}}{\partial z} + \rho \ell_z^2 \left(\frac{\partial \bar{u}}{\partial z}\right)^2\right] = \frac{\partial p}{\partial x} + \rho\left(\bar{v} \frac{\partial \bar{u}}{\partial y} + \bar{w} \frac{\partial \bar{u}}{\partial z}\right)$$

In the viscous sublayer the turbulent stresses may be neglected and the convective terms $\bar{v}\,\partial \bar{u}/\partial y$ and $w\,\partial \bar{u}/\partial z$ are negligible. Also the viscous stress term $\mu\,\partial^2 u/\partial z^2$ is negligible; hence the momentum equation simplifies to

$$\mu \frac{\partial^2 u}{\partial y^2} = \frac{\partial p}{\partial x}$$

The solution of this equation results in the very nearly linear velocity profile through the viscous region. It is expressed by

$$\tau_o = \mu \frac{\partial u}{\partial y} \quad ; \quad 0 < y^* < 11.65 \tag{A-21}$$

In the turbulent region ($y^* > 11.65$) the viscous shear stresses are neglected compared with the turbulent stresses. Then the momentum equation simplifies to

$$\frac{\partial}{\partial y}\left[\ell_y^2\left(\frac{\partial u}{\partial y}\right)^2\right] = \frac{1}{\rho}\frac{\partial p}{\partial x} + \left(\bar{v}\frac{\partial \bar{u}}{\partial y} + \bar{w}\frac{\partial \bar{u}}{\partial z}\right) - \frac{\partial}{\partial z}\left[\ell_z^2\left(\frac{\partial u}{\partial z}\right)^2\right]$$

Integration over y from $y = 0$ to $y = y$ yields the following expression for the velocity gradient

$$\frac{\partial \bar{u}}{\partial y} = \left[\frac{\frac{1}{\rho}\frac{\partial p}{\partial x}\,y + \frac{\tau_o}{\rho} + \int_o^y \bar{v}\frac{\partial \bar{u}}{\partial y}\,dy + \int_o^y \bar{w}\frac{\partial \bar{u}}{\partial z}\,dy - \int_o^y \frac{\partial}{\partial z}\left[\ell_z^2\left(\frac{\partial u}{\partial z}\right)^2\right]dy}{\ell_y^2}\right]^{1/2}$$

The term τ_o appearing above represents the constant of integration from evaluating the left hand integral (shear stress) at the wall. The term involving the pressure gradient $\partial p/\partial x$ may be expressed in terms of the wall shear stress by considering a control volume around the boundaries of the duct

$$-\frac{\partial p}{\partial x}\,4ab = \bar{\tau}_o\,(a+b)\,4$$

For the square duct this gives

$$-\frac{\partial p}{\partial x} = \frac{2\bar{\tau}_o}{a}$$

The equation for the velocity gradient then becomes

$$\frac{\partial \bar{u}}{\partial y} = \left[\frac{\frac{\tau_o g}{\rho} - 2\frac{\bar{\tau}_o g}{\rho}\cdot\frac{y}{a} + \int_o^y \bar{v}\frac{\partial \bar{u}}{\partial y}\,dy + \int_o^y \bar{w}\frac{\partial \bar{u}}{\partial z}\,dy - \int_o^y \frac{\partial}{\partial z}\left[\ell_z^2\left(\frac{\partial \bar{u}}{\partial z}\right)^2\right]dy}{\ell_y^2}\right]^{1/2} \quad \text{(A-22)}$$

Note that τ_o denotes the local wall shear stress whereas $\bar{\tau}_o$

denotes the average wall shear stress.

Equation (A-22) was solved for $\partial\bar{u}/\partial y$ at various points along a profile (s = constant) by a stepwise numerical calculation procedure. Dividing the profile up into a number of discrete steps in y the gradient $\partial\bar{u}/\partial y$ is calculated at each value of y from equation (A-22) beginning at the wall (y = 0) and marching outward. The terms on the right hand side involve only the history of the profile from the wall out and therefore can be evaluated by numerical integration of the computed results. The term $\int_0^y \bar{v}\,\partial\bar{u}/\partial y\,dy$ was evaluated from the computed values of $\partial\bar{u}/\partial y$ along the profile. The other terms involving $\partial\bar{u}/\partial z$ were evaluated for this calculation from the measured values but could in principle be determined from the calculated results by an iterative procedure. After determining the gradient $\partial\bar{u}/\partial y$ along the profile by this procedure the velocity distribution $\bar{u}$ vs y was obtained simply by numerical integration.

The numerical integrations involved in this calculation, both for determining $\partial\bar{u}/\partial y$ and $\bar{u}$ vs y, were performed by using the average gradient over the distance interval. For example to integrate $\bar{u}$ from y_1 to y_2 the mean gradient $\partial\bar{u}/\partial y$ over the interval $y_1 < y < y_2$ is determined by

$$\left(\frac{\partial u}{\partial y}\right)_{\text{avg } 1\text{-}2} = \frac{1}{2}\left[\left(\frac{\partial u}{\partial y}\right)_1 + \left(\frac{\partial u}{\partial y}\right)_2\right]$$

and

$$\bar{u}_2 = \bar{u}_1 + \left(\frac{\partial u}{\partial y}\right)_{\text{avg } 1\text{-}2} (y_2 - y_1)$$

Inspection of equations (A-22), (A-19) and (A-20) shows that the calculation procedure described above is straightforward if Prandtl's mixture length expression is used but involves tedious iteration when employing Kármán's mixture length. The calculations reported here were made by using Prandtl's mixture length as a first approximation and then making corrections where necessary to conform to Kármán's mixture length. The two mixture lengths were found to be identical over much of the velocity profile with important differences occurring only near the central portion of the flow. This fact simplified the calculations greatly. Better agreement with measured profiles was obtained using Kármán's mixture length.

Calculations for axial velocity profiles were carried out for the square duct only along $z/a = .4$ and $z/a = 1.0$, at a Reynolds number of 34,000. The resulting profiles are shown in Figure 45 and compared with the experimental measurements. The overall agreement is seen to be remarkably good. Although the slopes of the calculated curves are not everywhere equal to those of the measured profiles, the magnitudes of the calculated and measured velocities compare favorably throughout. The fact that the slopes are not in agreement is understandable remembering that the turbulent stress terms evaluated from the experimental measurements were found to differ considerably in certain portions of the flow from those evaluated from mixture length theory. (See discussion in Section 5, page 38.)

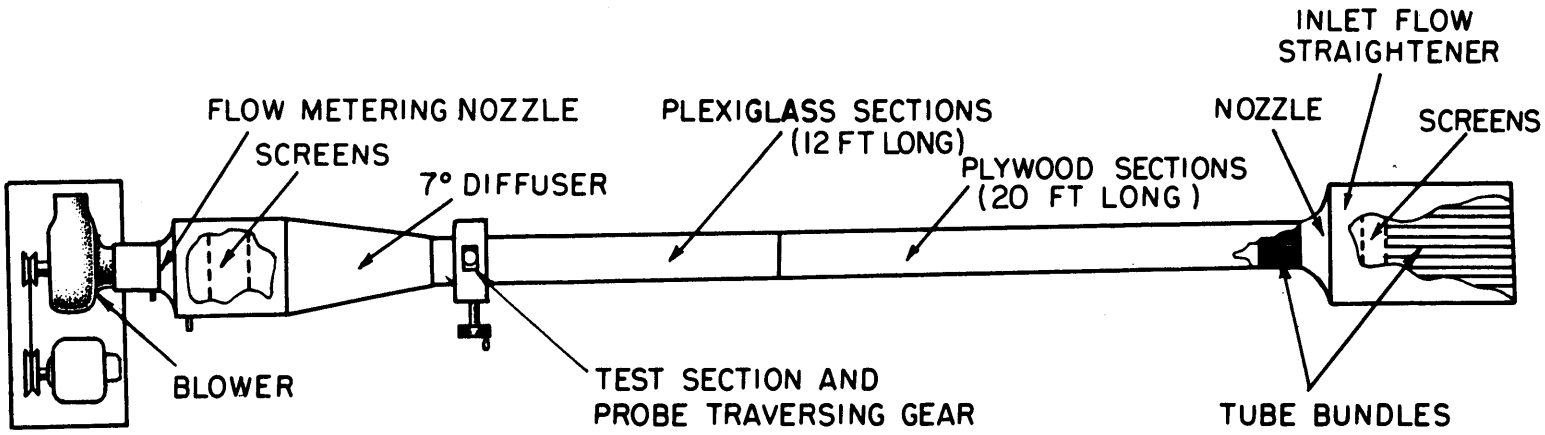

a) PLAN VIEW OF APPARATUS

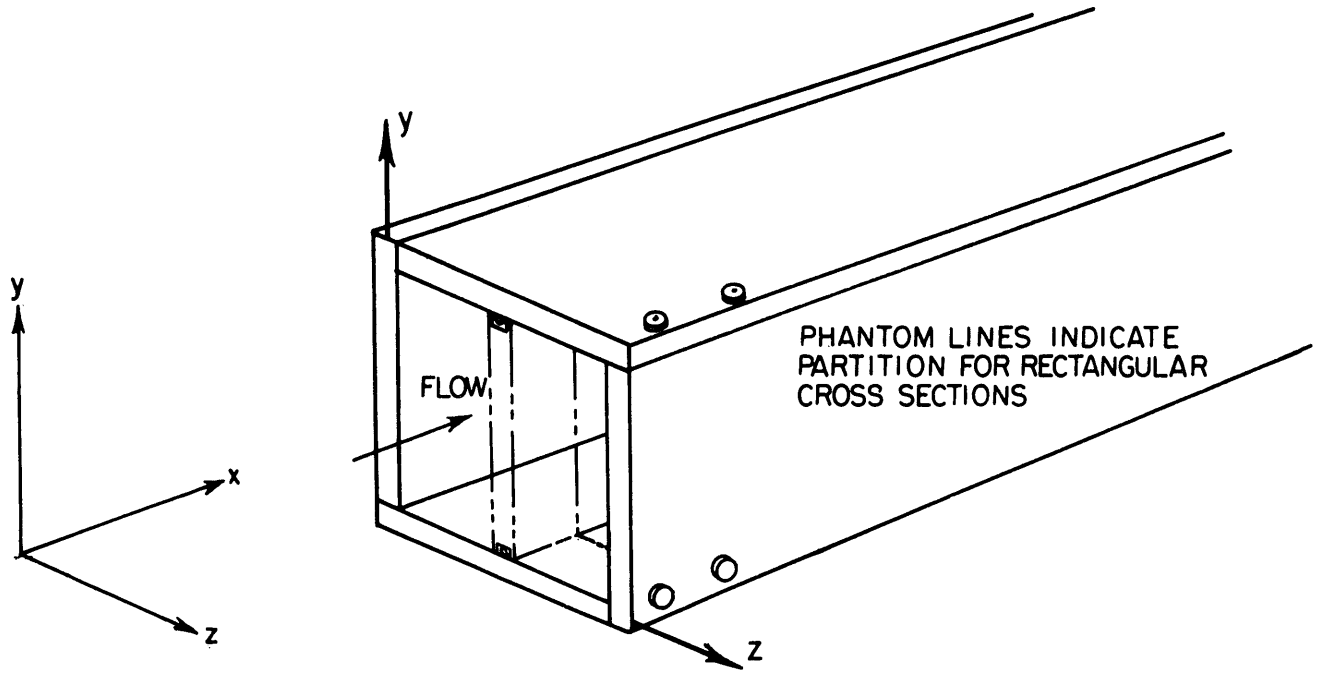

b) DUCT CONSTRUCTION

FIG 1 DIAGRAM OF EXPERIMENTAL APPARATUS

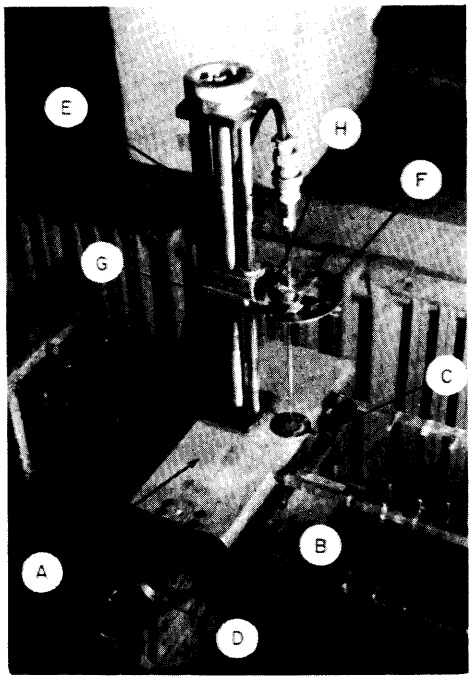

A) SLIDING PLATE

B) HORIZONTAL TRAVERSING SCREW

C) POINTER AND SCALE

D) GRADUATED MICROMETER DRUM

E) VERTICAL TRAVERSING SCREW

F) PROTRACTOR DISC

G) TRAVELING BLOCK

H) SPRING YOKE

a) TEST SECTION - PROBE TRAVERSING GEAR

INCLINED MANOMETER

RUBICON SPOTLIGHT GALVANOMETER

FLOW CORP. HWB HOT WIRE BRIDGE CIRCUIT AND AMPLIFIER

BRIDGE CIRCUIT FOR FLOW DIRECTION PROBE

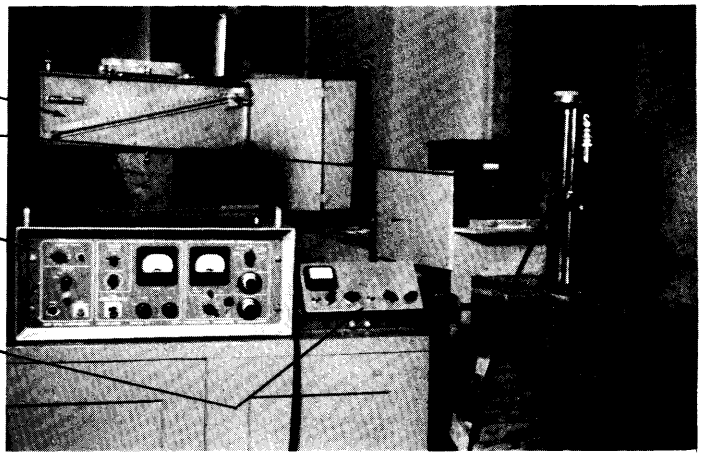

b) INSTRUMENTATION

FIG. 2 PHOTOGRAPHS OF TEST SECTION AND INSTRUMENTATION

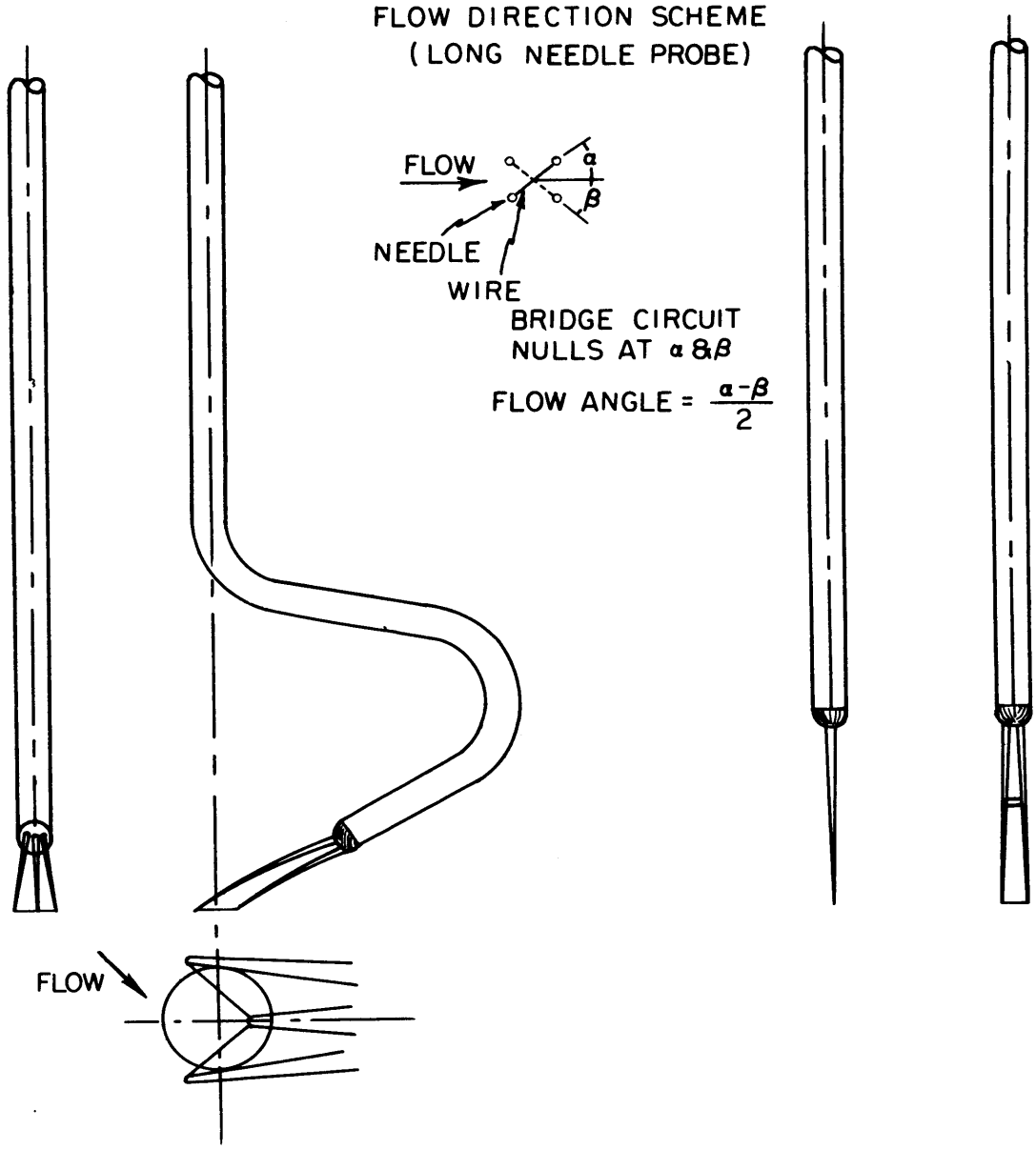

"V" WIRE (GOOSENECK) PROBE
0.0005 IN DIA TUNGSTEN
FILAMENTS

STANDARD LONG
NEEDLE PROBE
0.0003 IN DIA TUNGSTEN
FILLAMENT

APPROXIMATELY TO SCALE

FIG 3 HOT WIRE PROBES

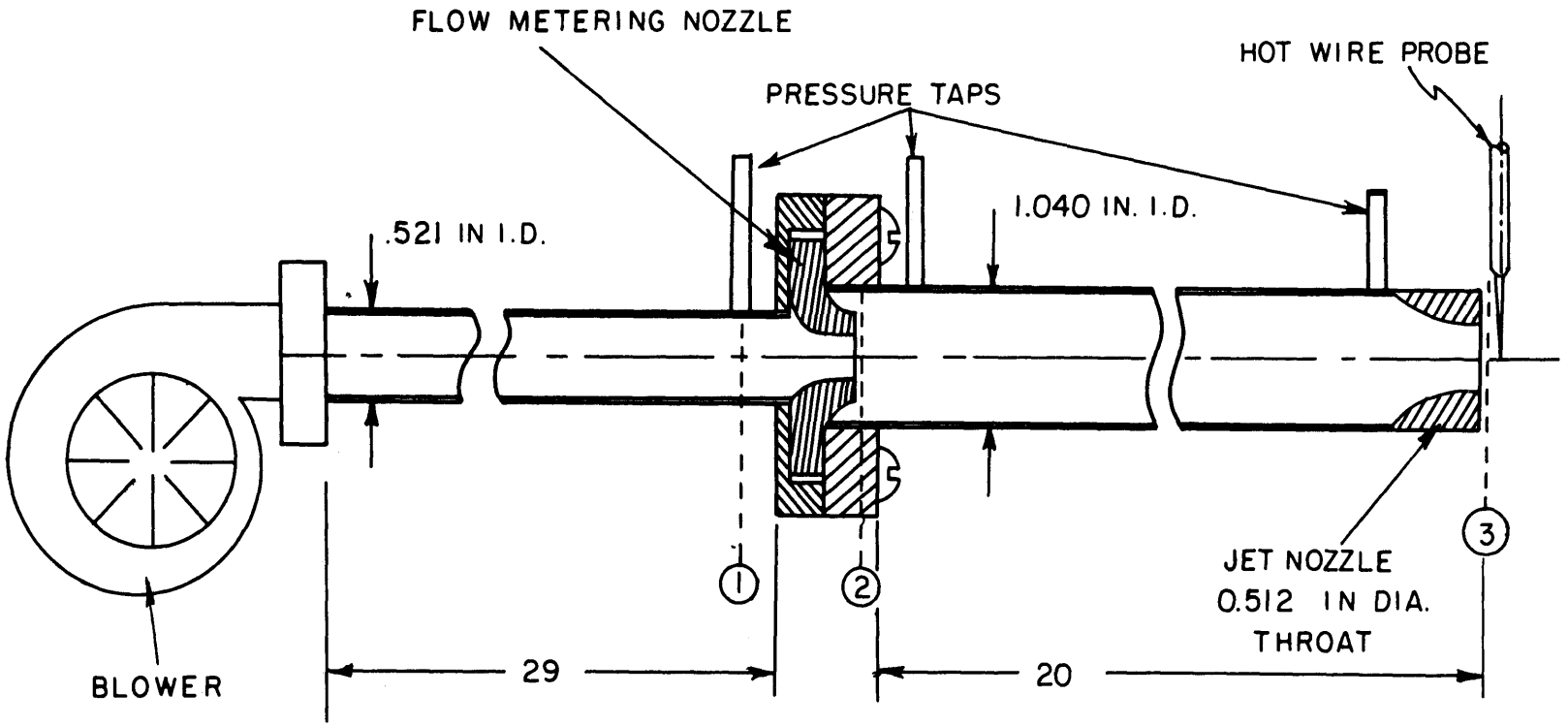

FIG 4 HOT WIRE CALIBRATION APPARATUS

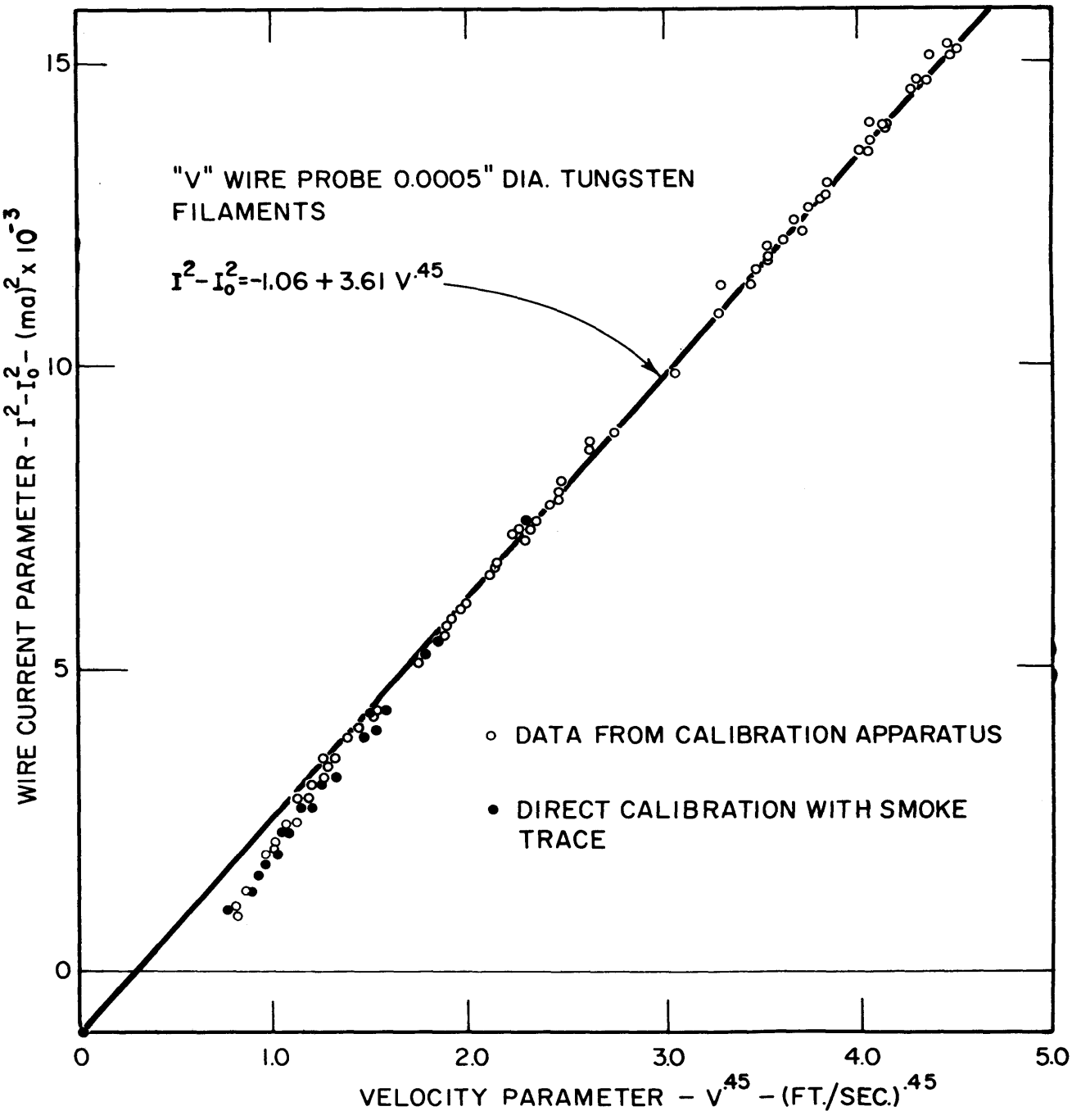

FIGURE 5 TYPICAL HOT WIRE CALIBRATION FOR GOOSENECK PROBE. ACCORDING TO COLLIS' RELATION

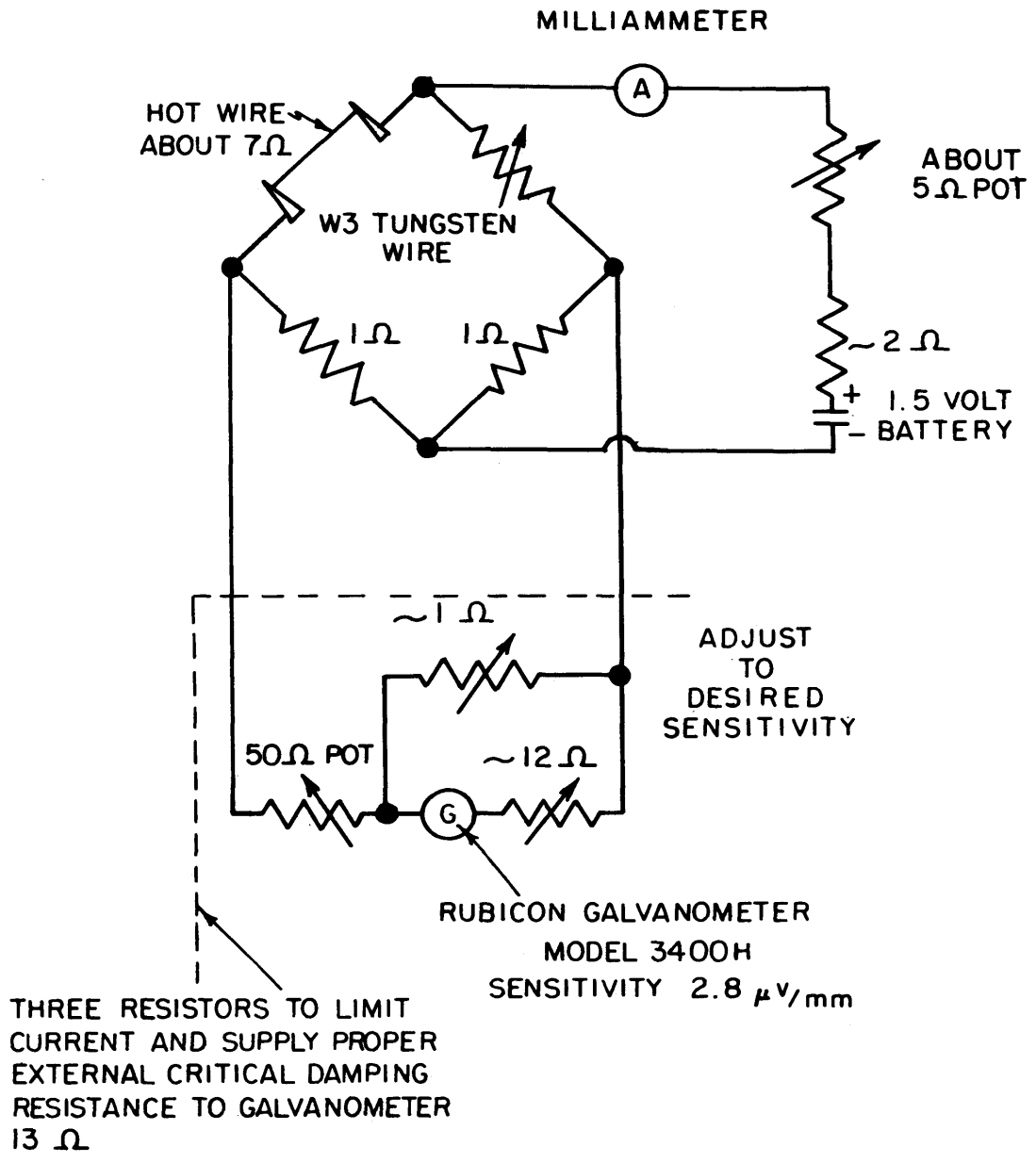

FIG 6 CIRCUIT FOR HOT WIRE FLOW DIRECTION MEASUREMENTS

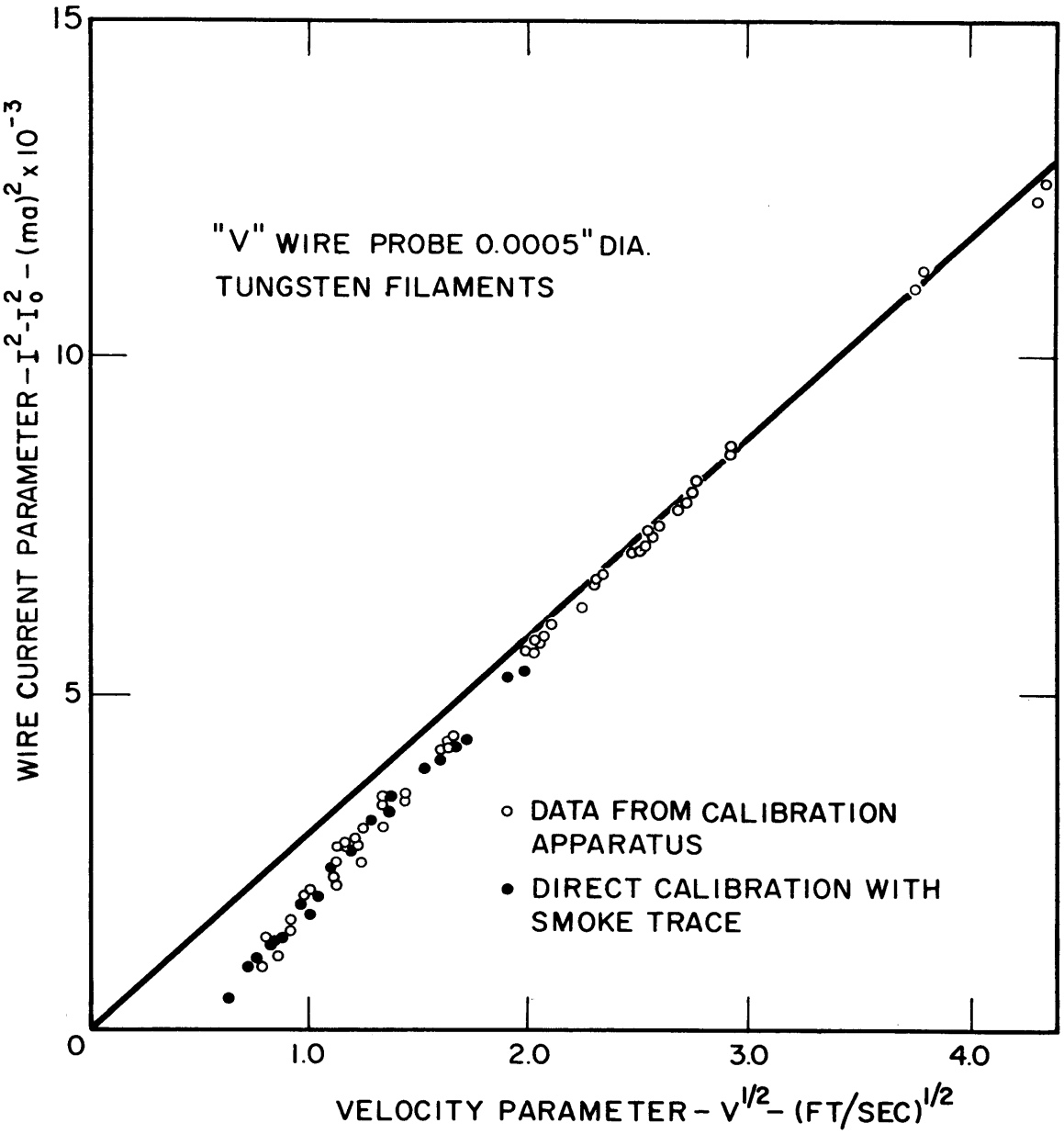

FIGURE 7 HOT WIRE CALIBRATION DATA PLOTTED ACCORDING TO "KING'S LAW"

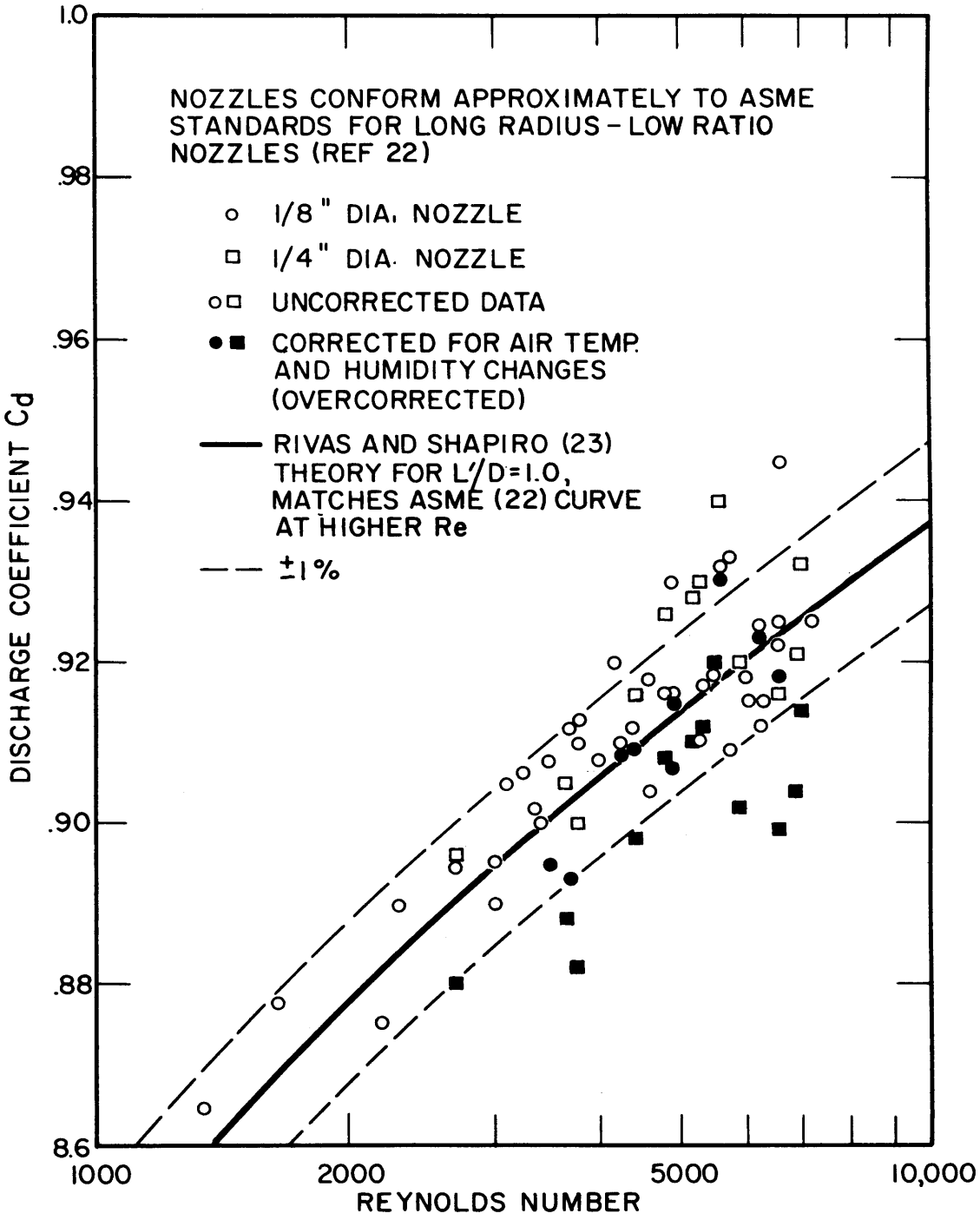

FIGURE 8 CALIBRATION OF FLOW METERING NOZZLES FOR HOT WIRE CALIBRATION APPARATUS

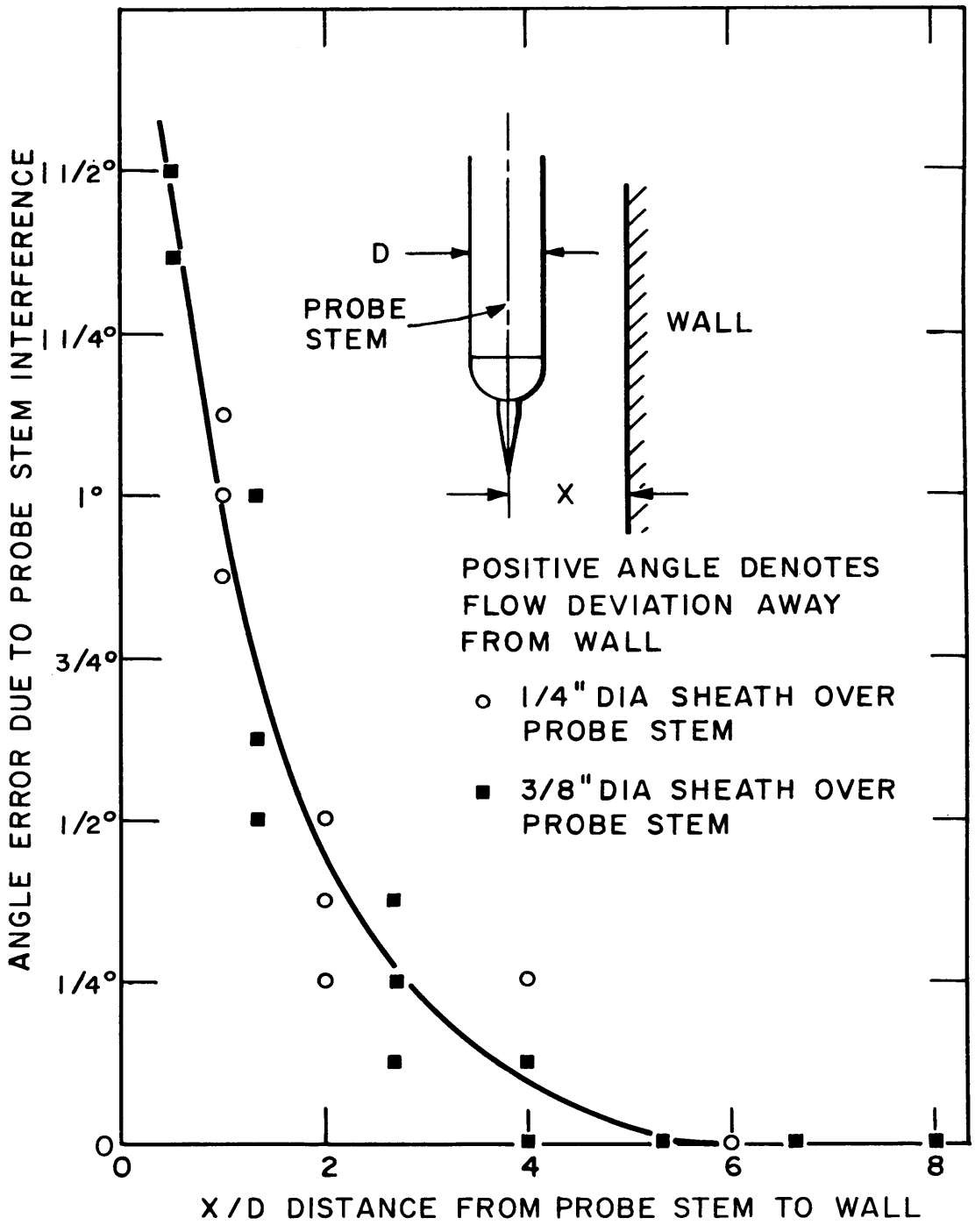

FIGURE 9 FLOW DEVIATION DUE TO PROBE STEM BLOCKAGE EFFECT NEAR WALL

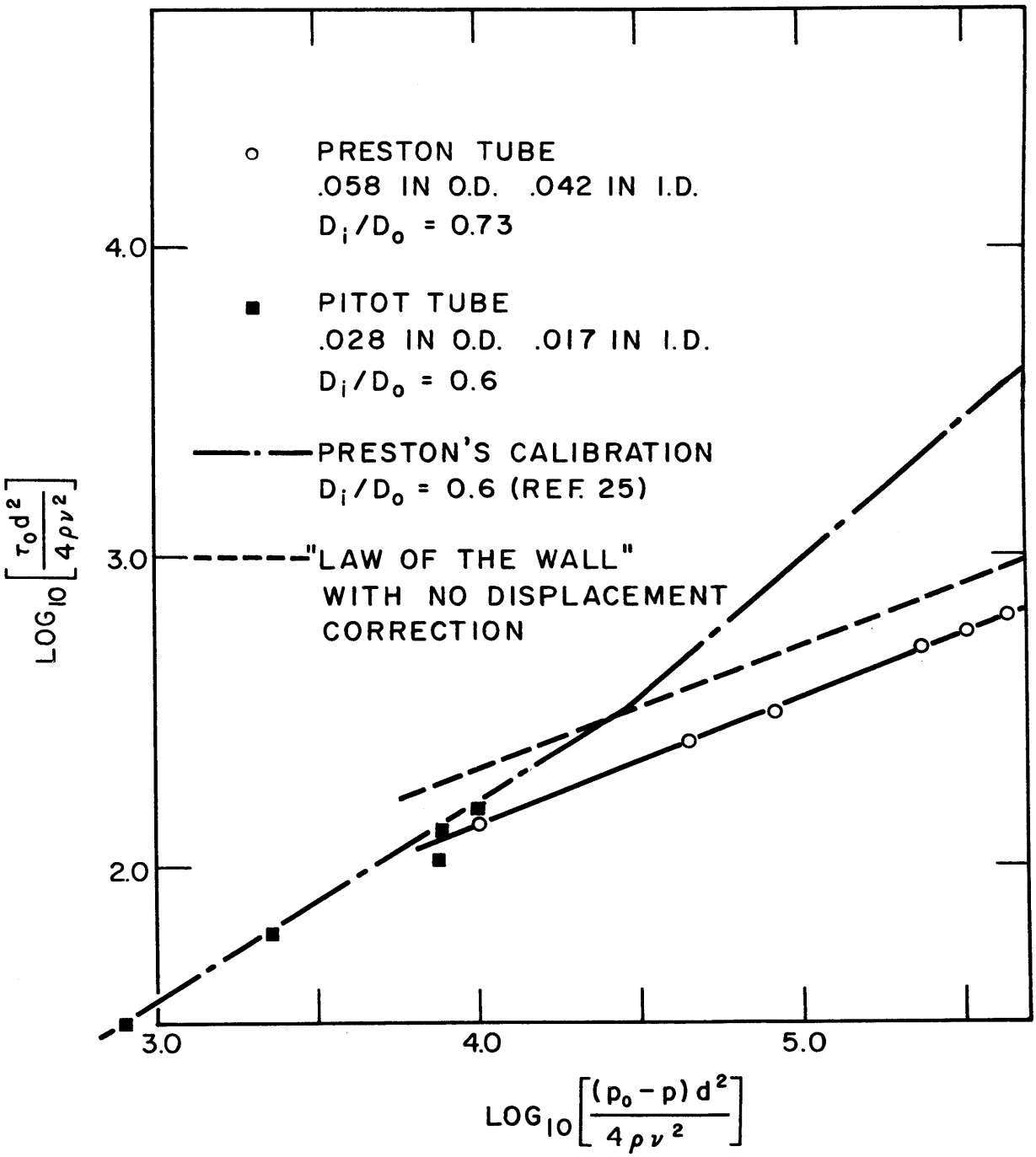

FIGURE 10 CALIBRATION OF PRESTON TUBES FOR MEASUREMENT OF WALL SHEAR STRESS

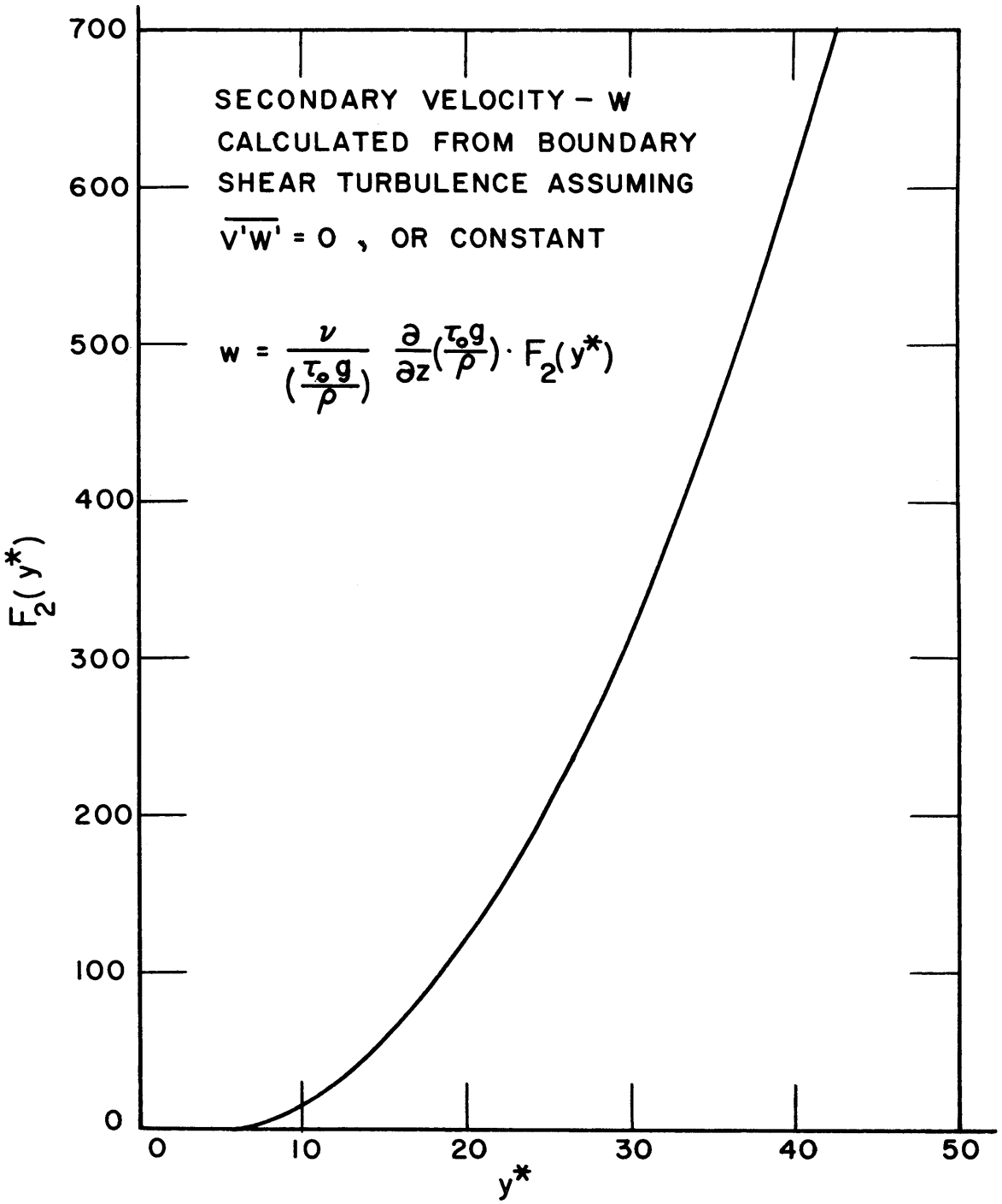

FIG 11 SECONDARY VELOCITY COMPUTED FROM BOUNDARY SHEAR TURBULENCE

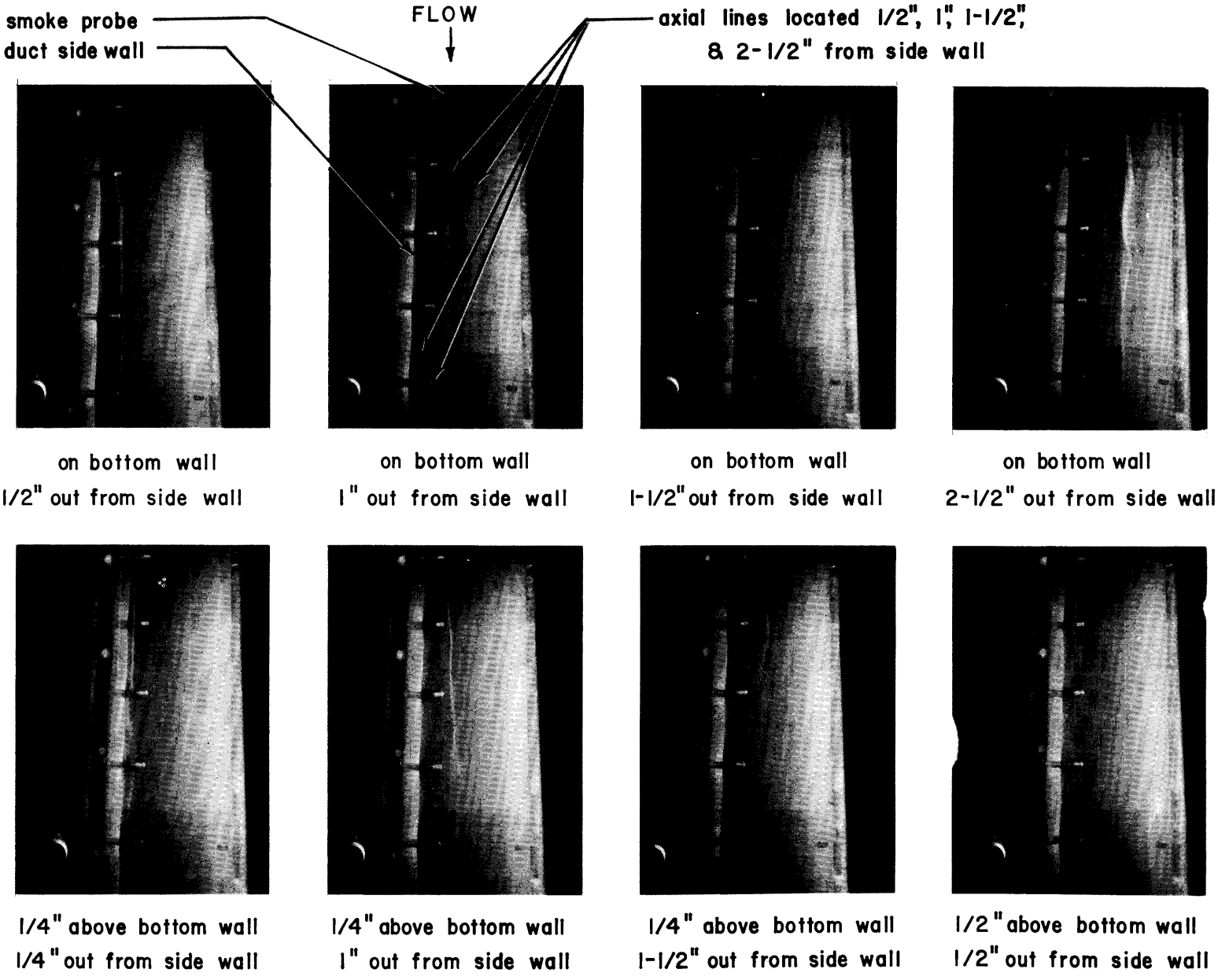

FIG. 12 SMOKE TRACES SHOWING SECONDARY FLOW IN 5 INCH SQUARE DUCT .

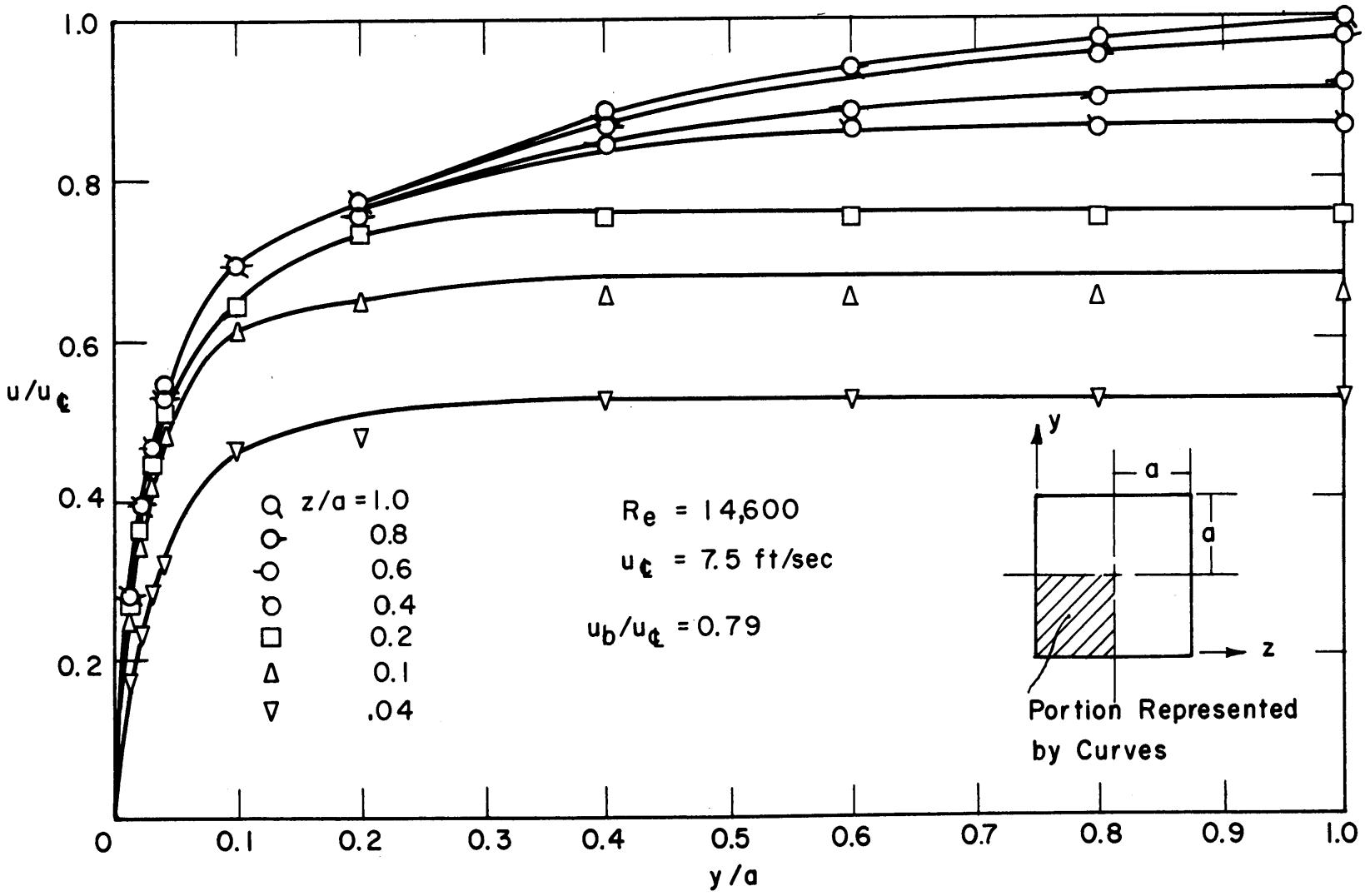

FIG 13 AXIAL VELOCITY DISTRIBUTION BASED ON HOT WIRE DATA - SQUARE DUCT - $R_e = 14,600$

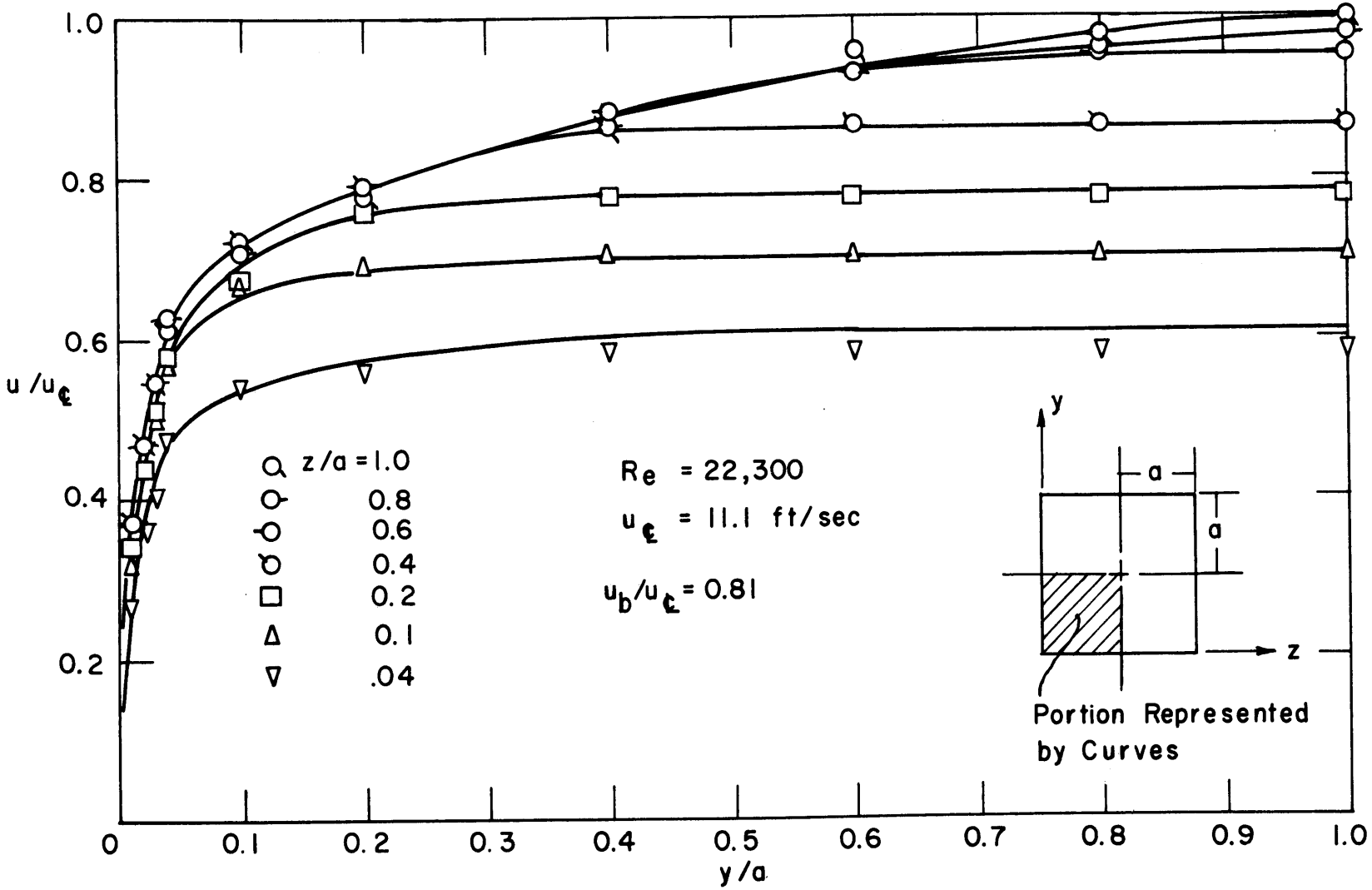

FIG 14 AXIAL VELOCITY DISTRIBUTION BASED ON HOT WIRE DATA - SQUARE DUCT - $R_e = 22,300$

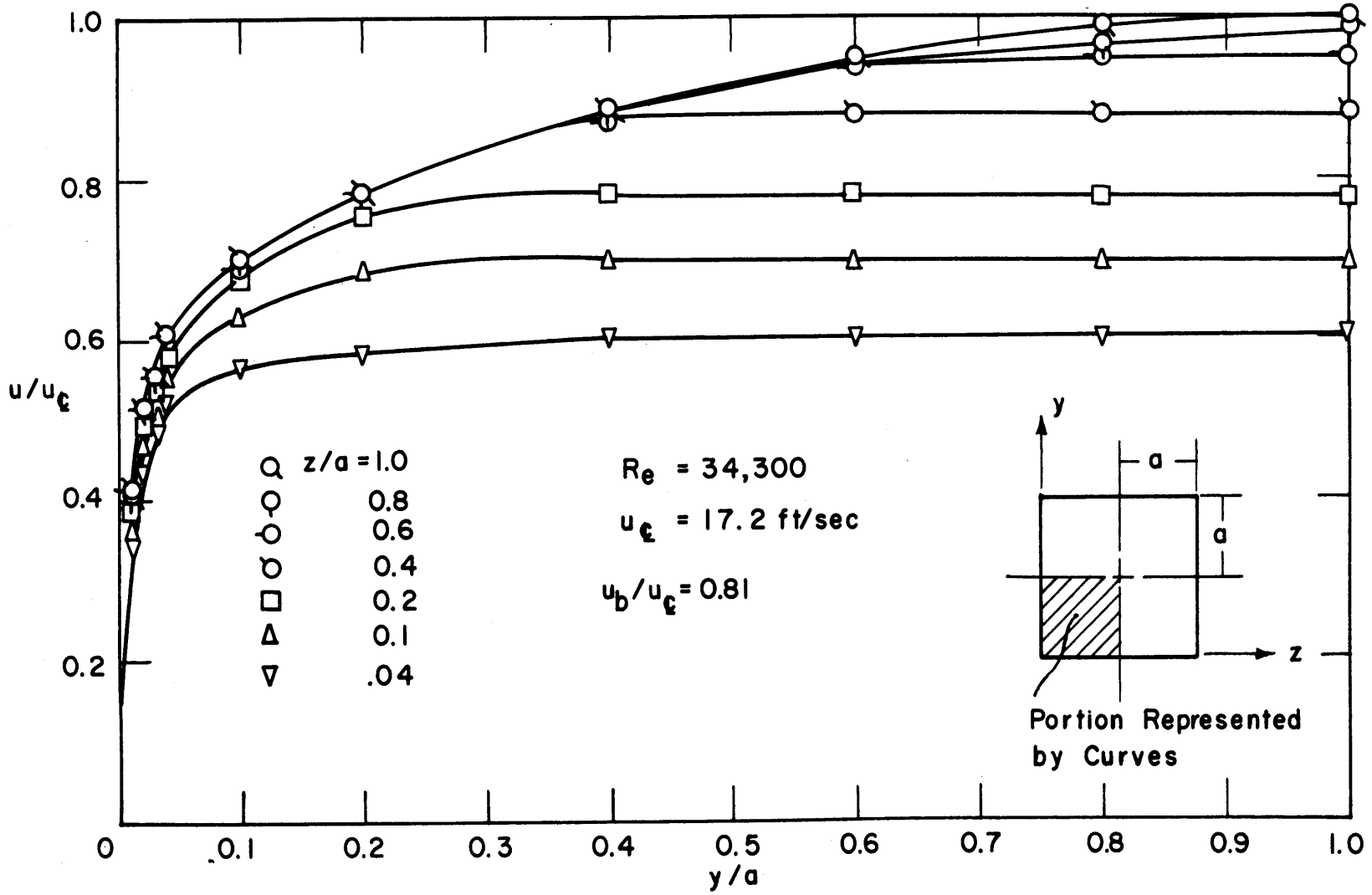

FIG 15 AXIAL VELOCITY DISTRIBUTION BASED ON HOT WIRE DATA - SQUARE DUCT - R_e = 34,600

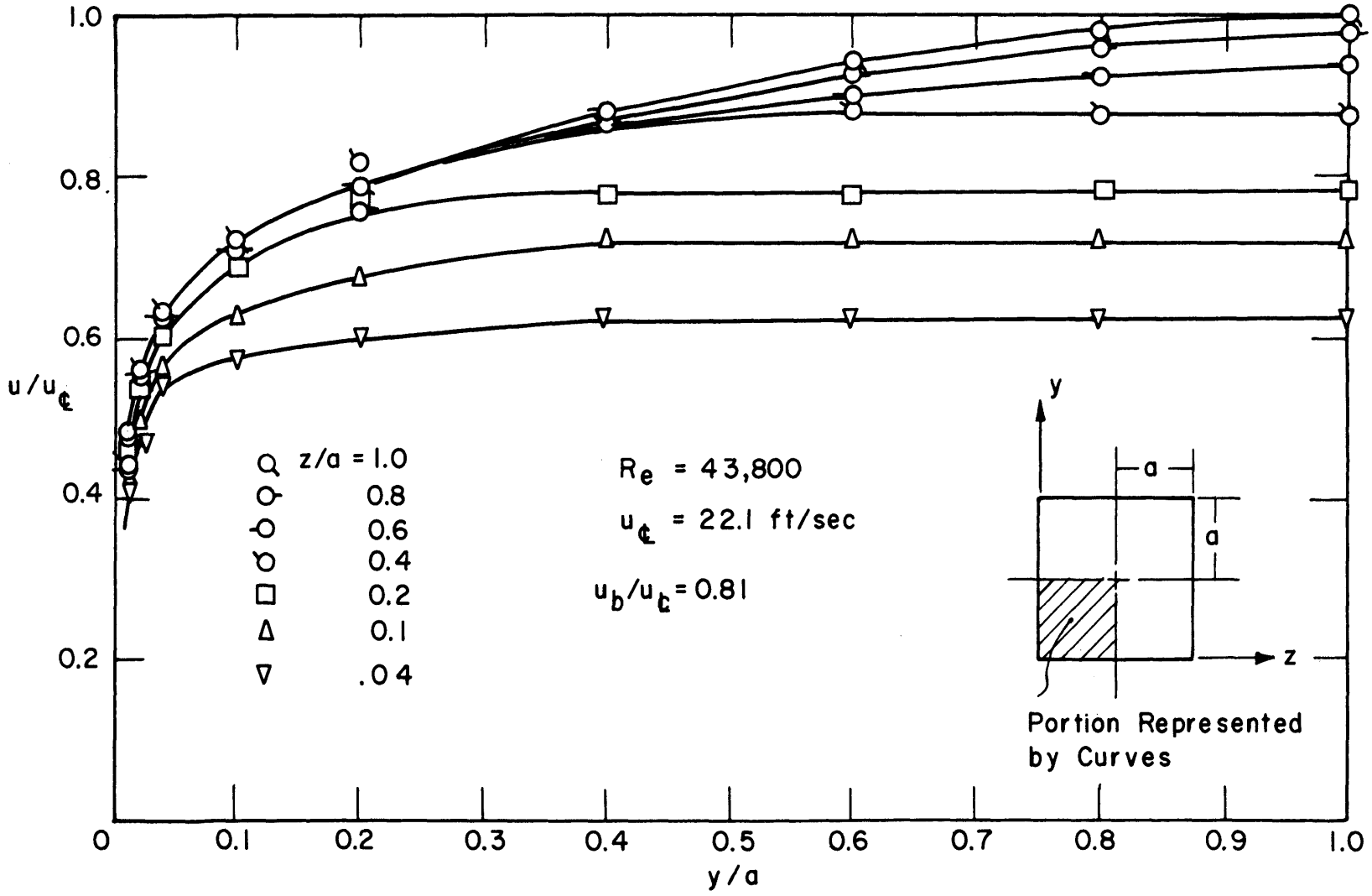

FIG 16 AXIAL VELOCITY DISTRIBUTION BASED ON HOT WIRE DATA - SQUARE DUCT - R_e = 43,800

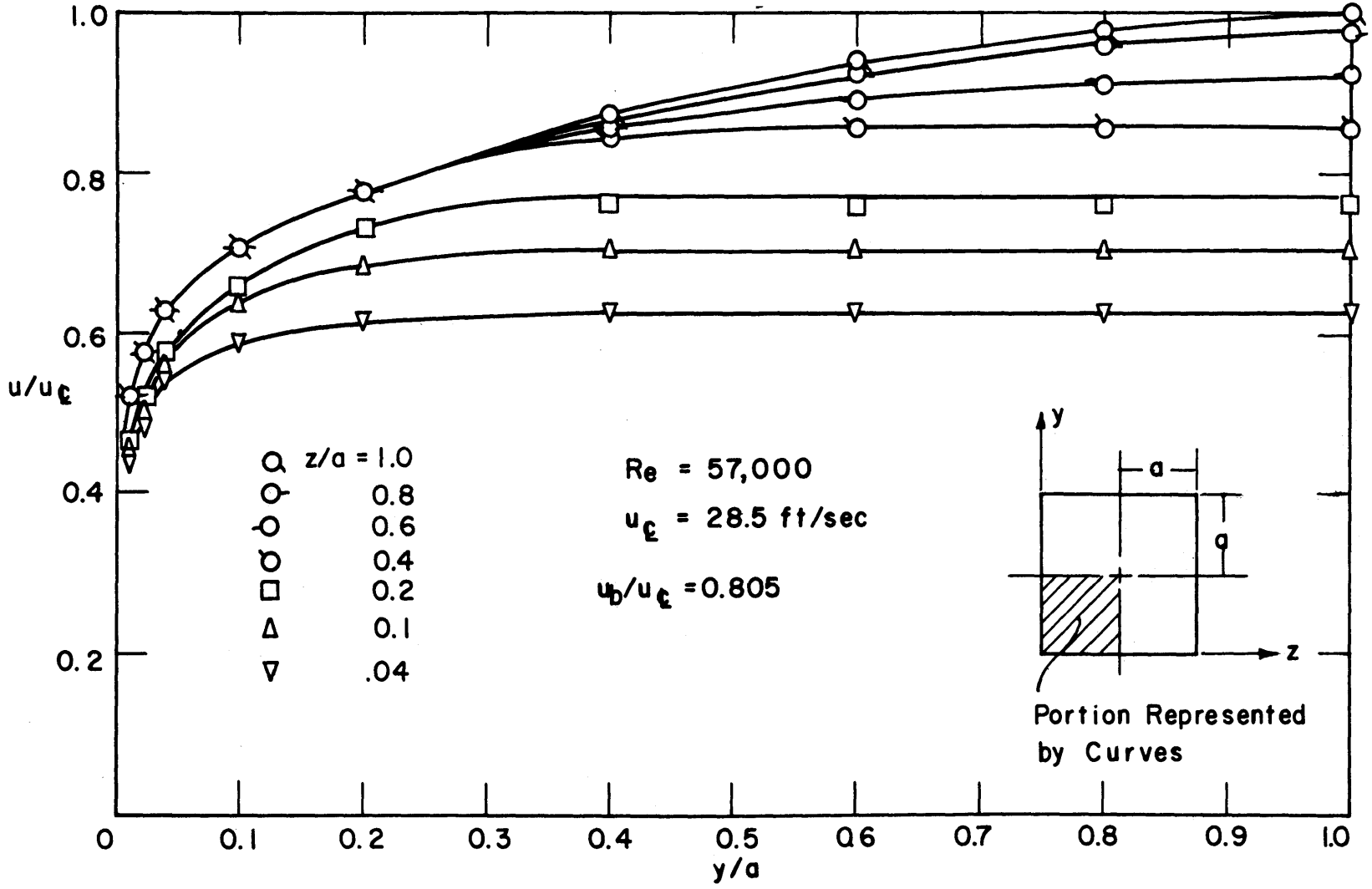

FIG 17 AXIAL VELOCITY DISTRIBUTION BASED ON HOT WIRE DATA - SQUARE DUCT - R_e = 57,000

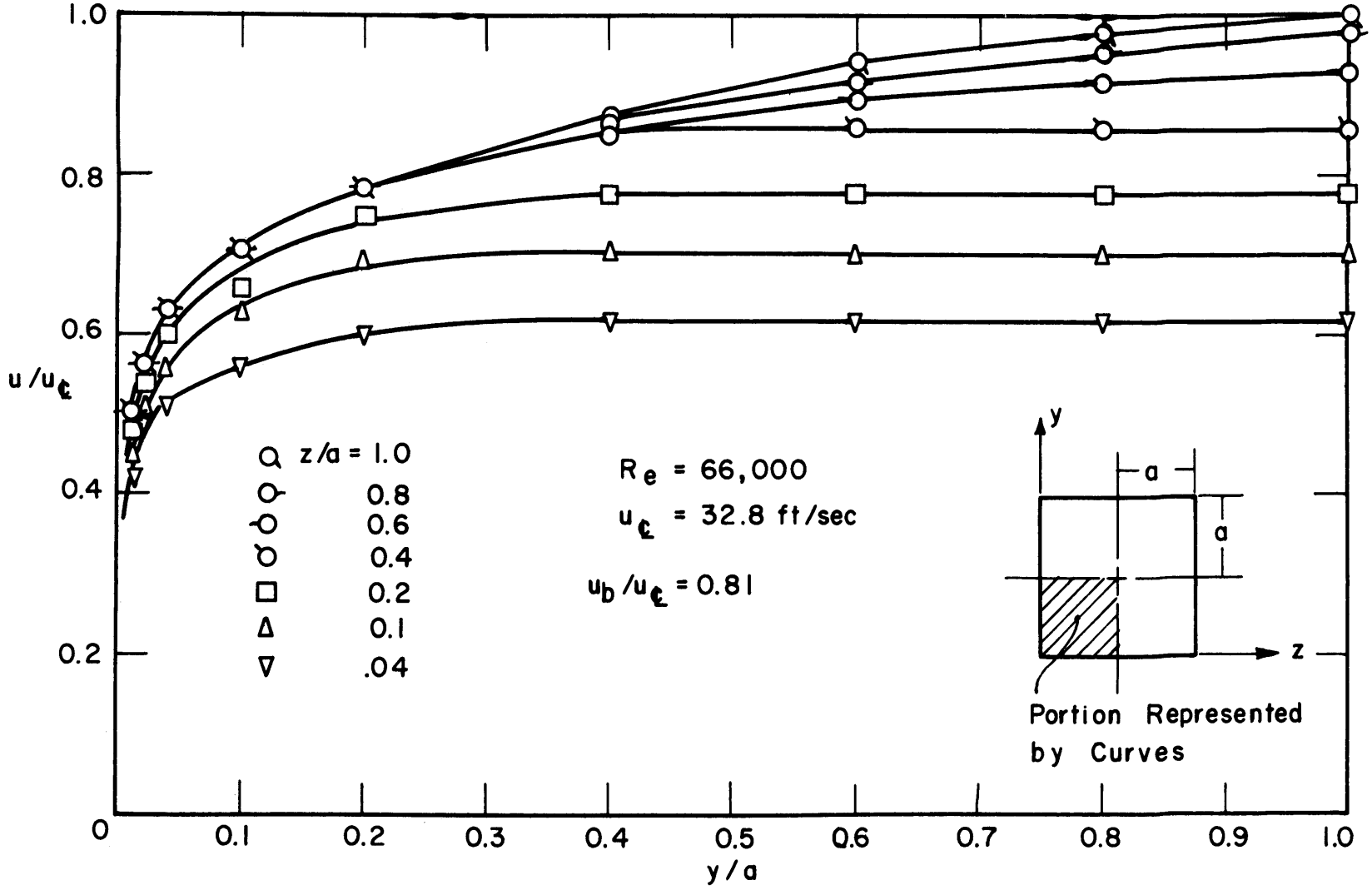

FIG 18 AXIAL VELOCITY DISTRIBUTION BASED ON HOT WIRE DATA - SQUARE DUCT - $R_e = 66{,}000$

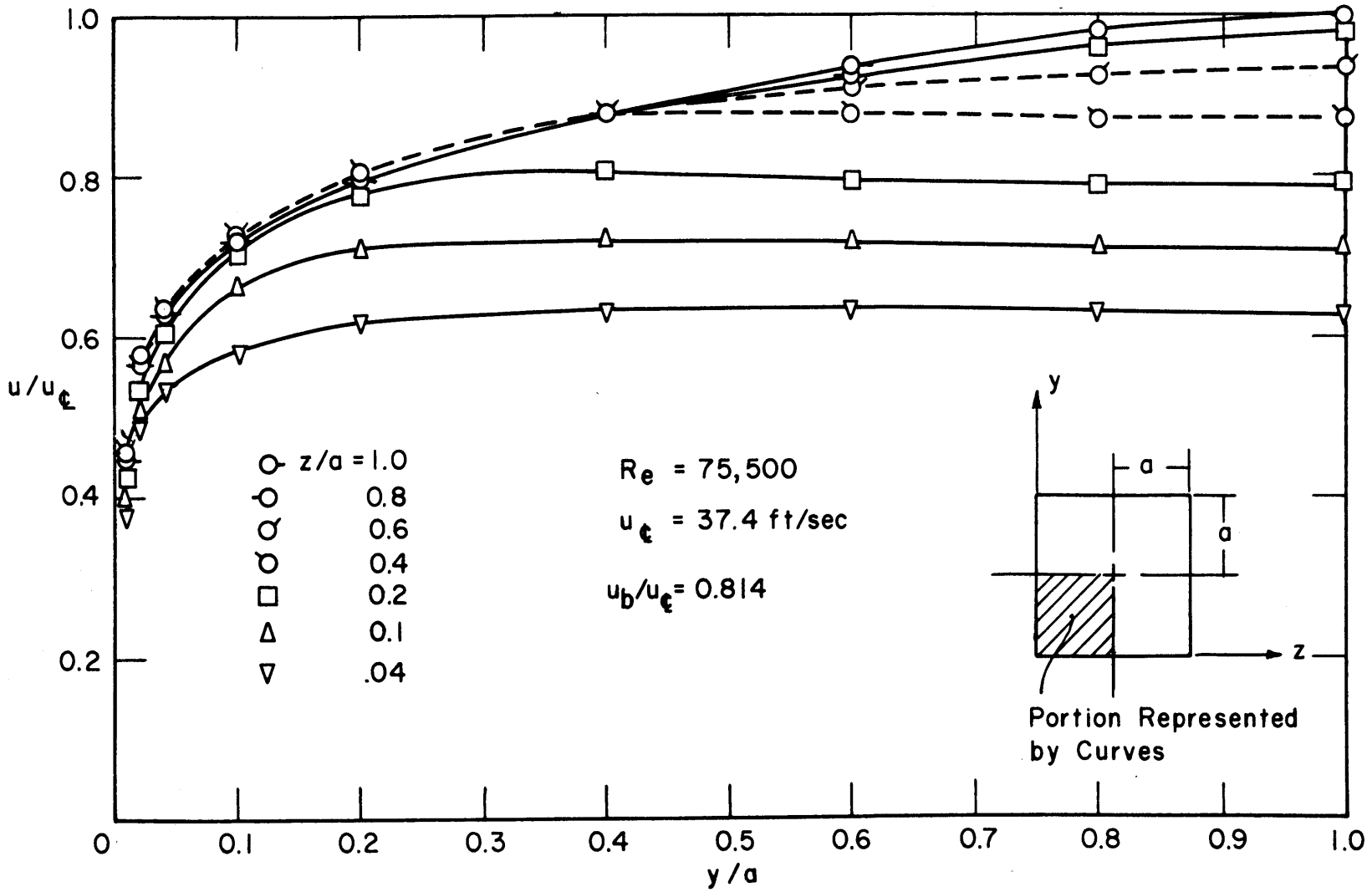

FIG 19 AXIAL VELOCITY DISTRIBUTION BASED ON PITOT TUBE DATA - SQUARE DUCT - $R_e = 75,500$

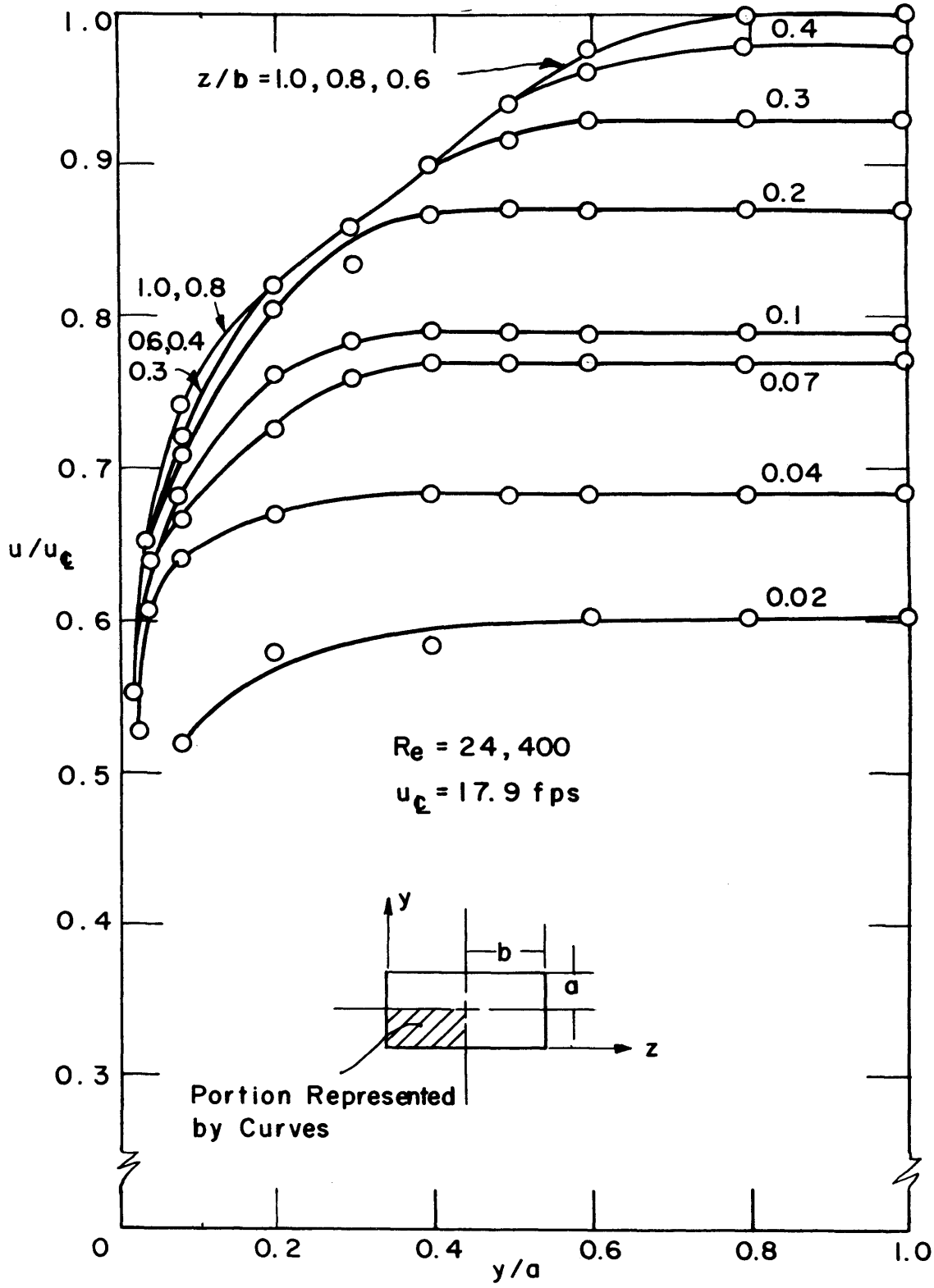

FIG. 20 AXIAL VELOCITY DISTRIBUTION BASED ON HOT WIRE DATA - 2 1/2x5 INCH DUCT - R_e = 24,400

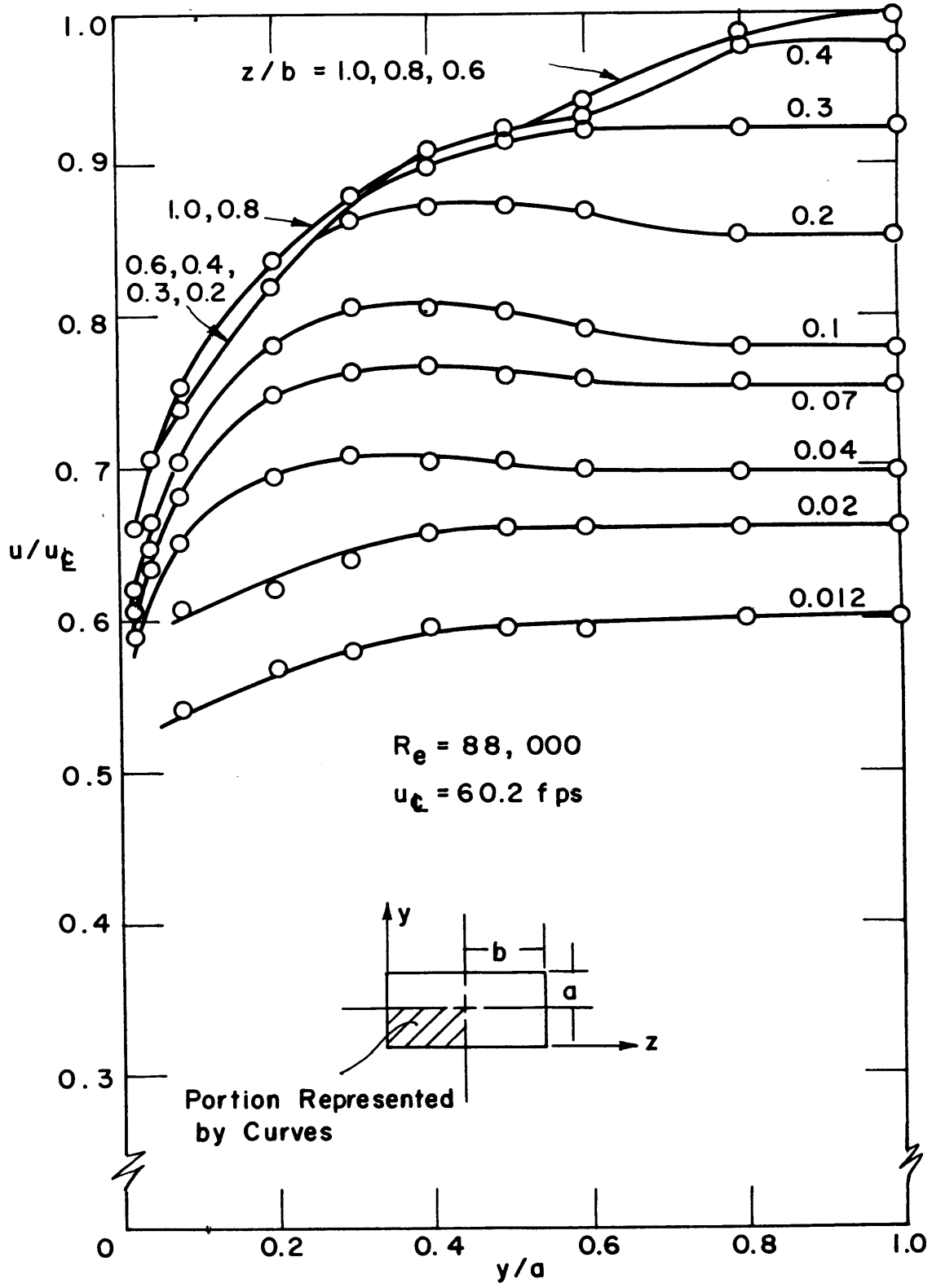

FIG. 21 AXIAL VELOCITY DISTRIBUTION BASED ON HOT WIRE DATA – 2 1/2 X 5 INCH DUCT – R_e = 88,000

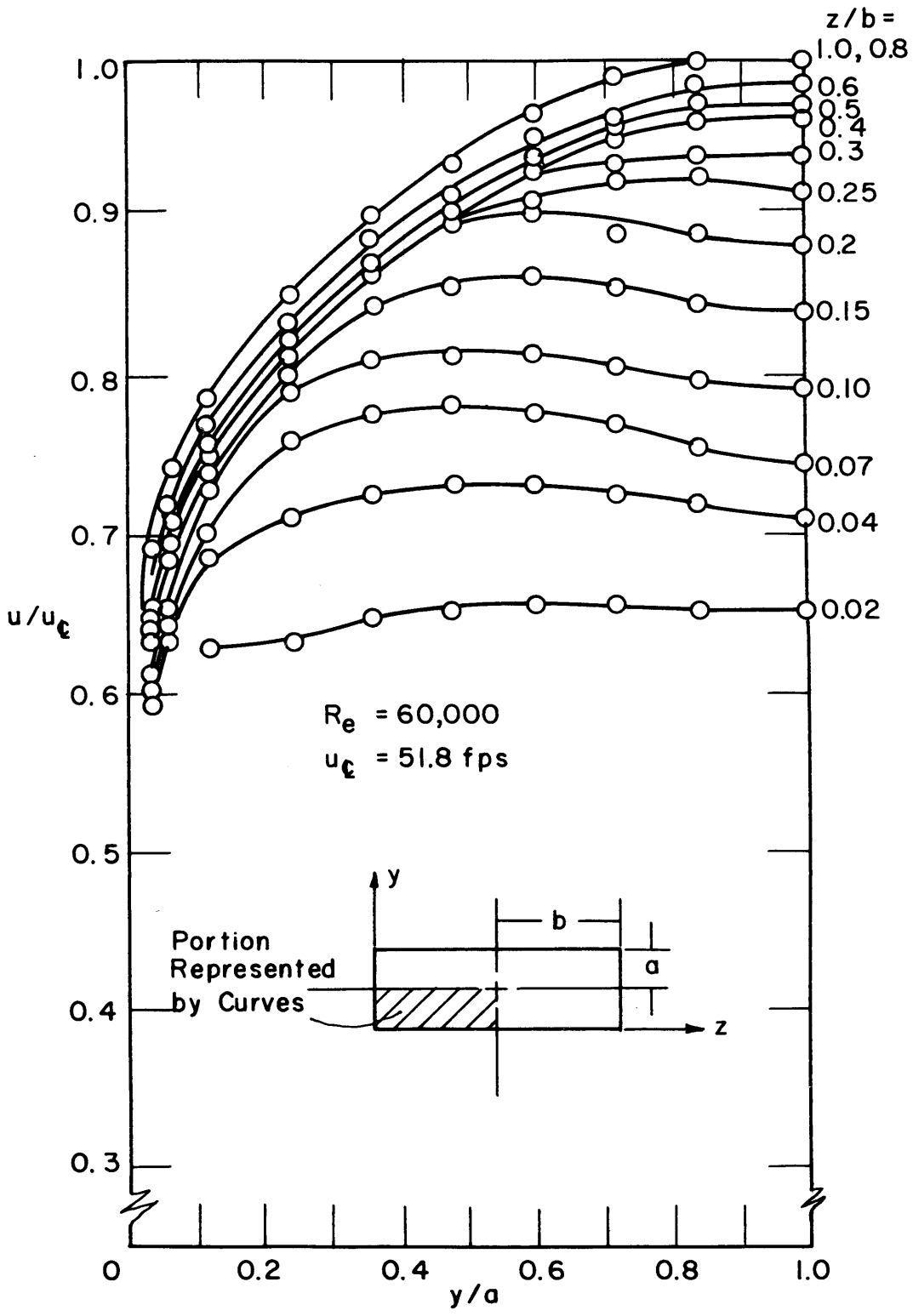

FIG. 22 AXIAL VELOCITY DISTRIBUTION BASED ON HOT WIRE DATA – 1 2/3 X 5 INCH DUCT – R_e = 60,000

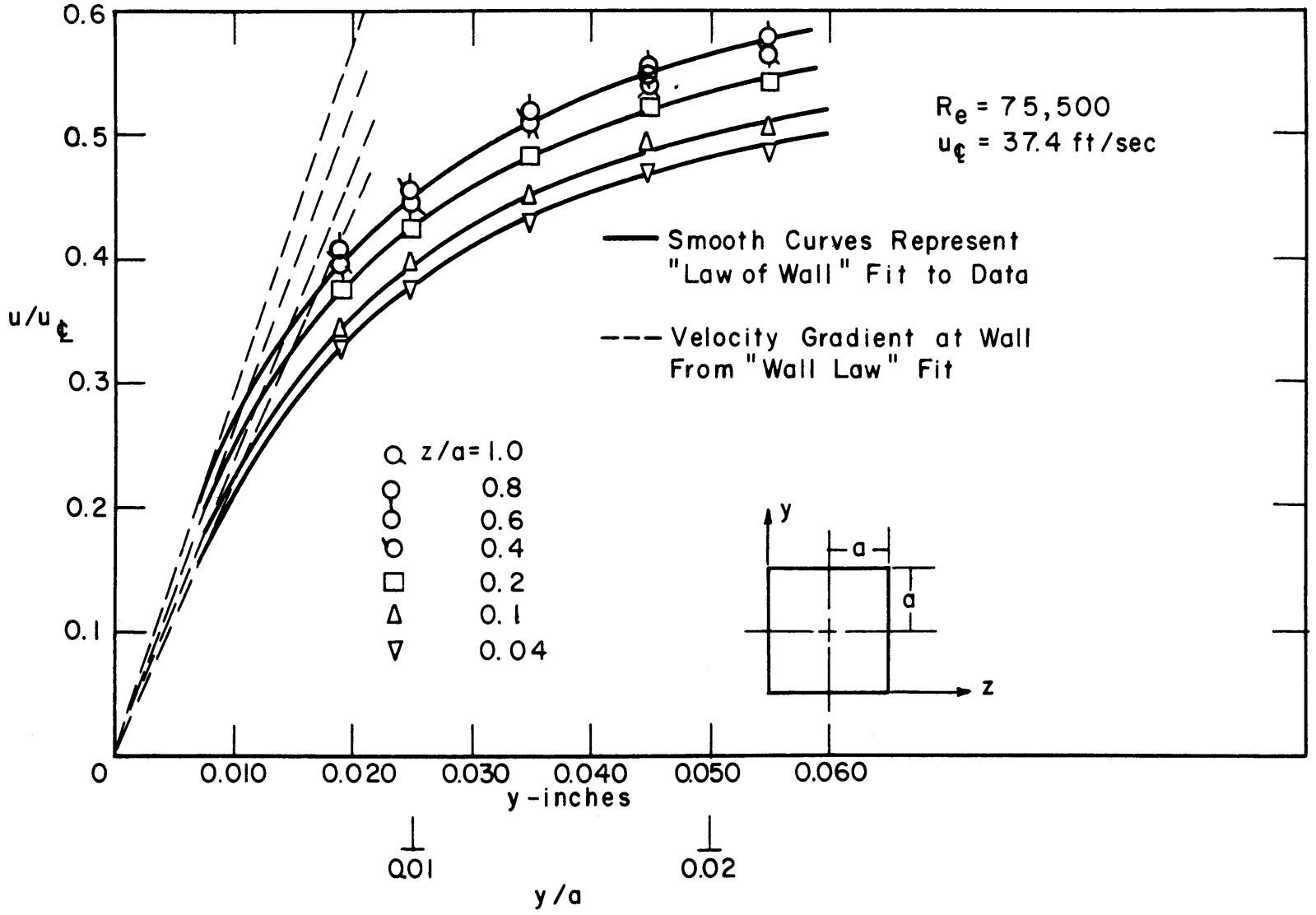

FIG 23 VELOCITY PROFILES NEAR WALL - PITOT TUBE DATA FROM SQUARE DUCT - R_e=75,500

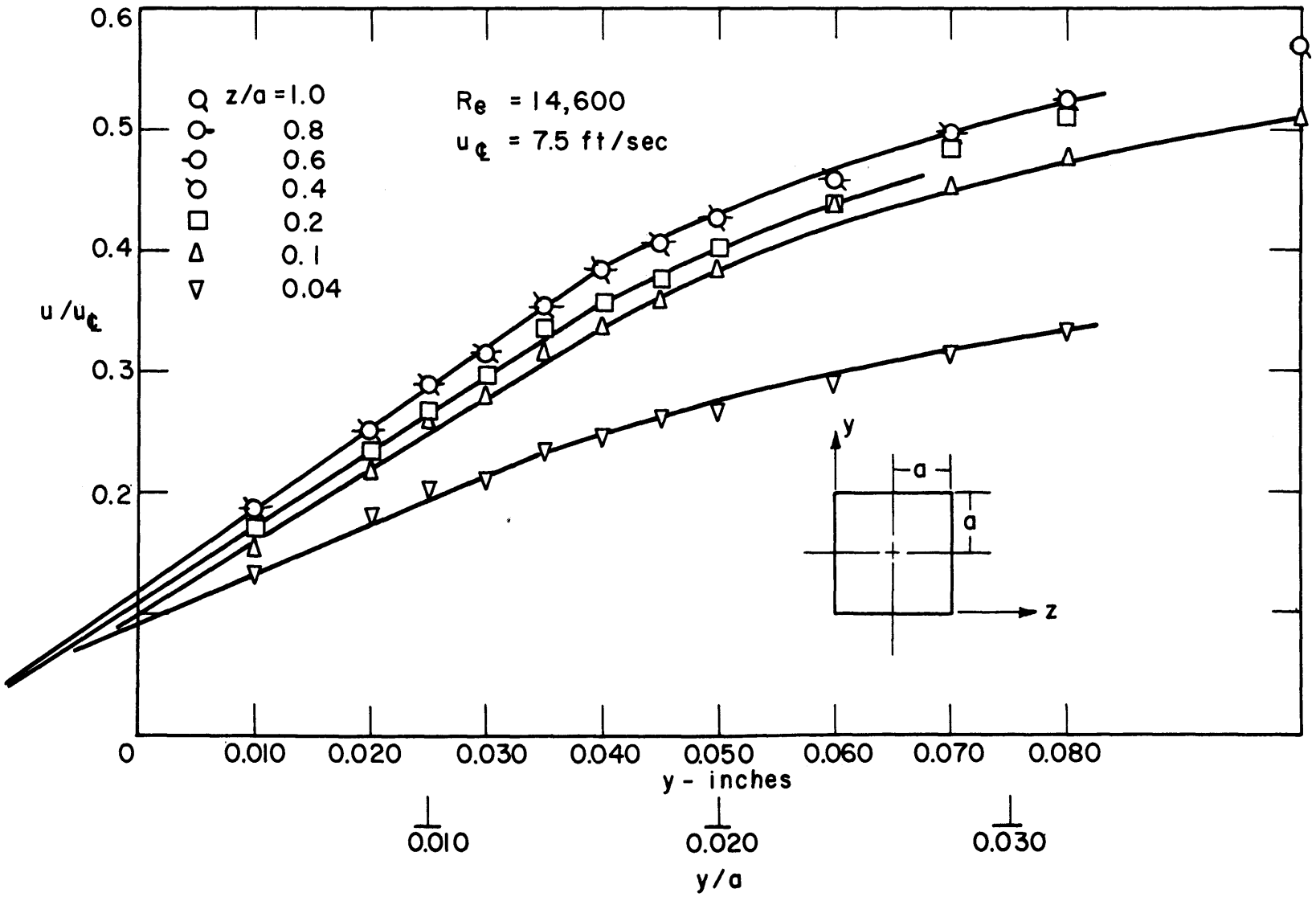

FIG 24 VELOCITY PROFILES NEAR WALL - HOT WIRE DATA FROM SQUARE DUCT - R_e = 14,600

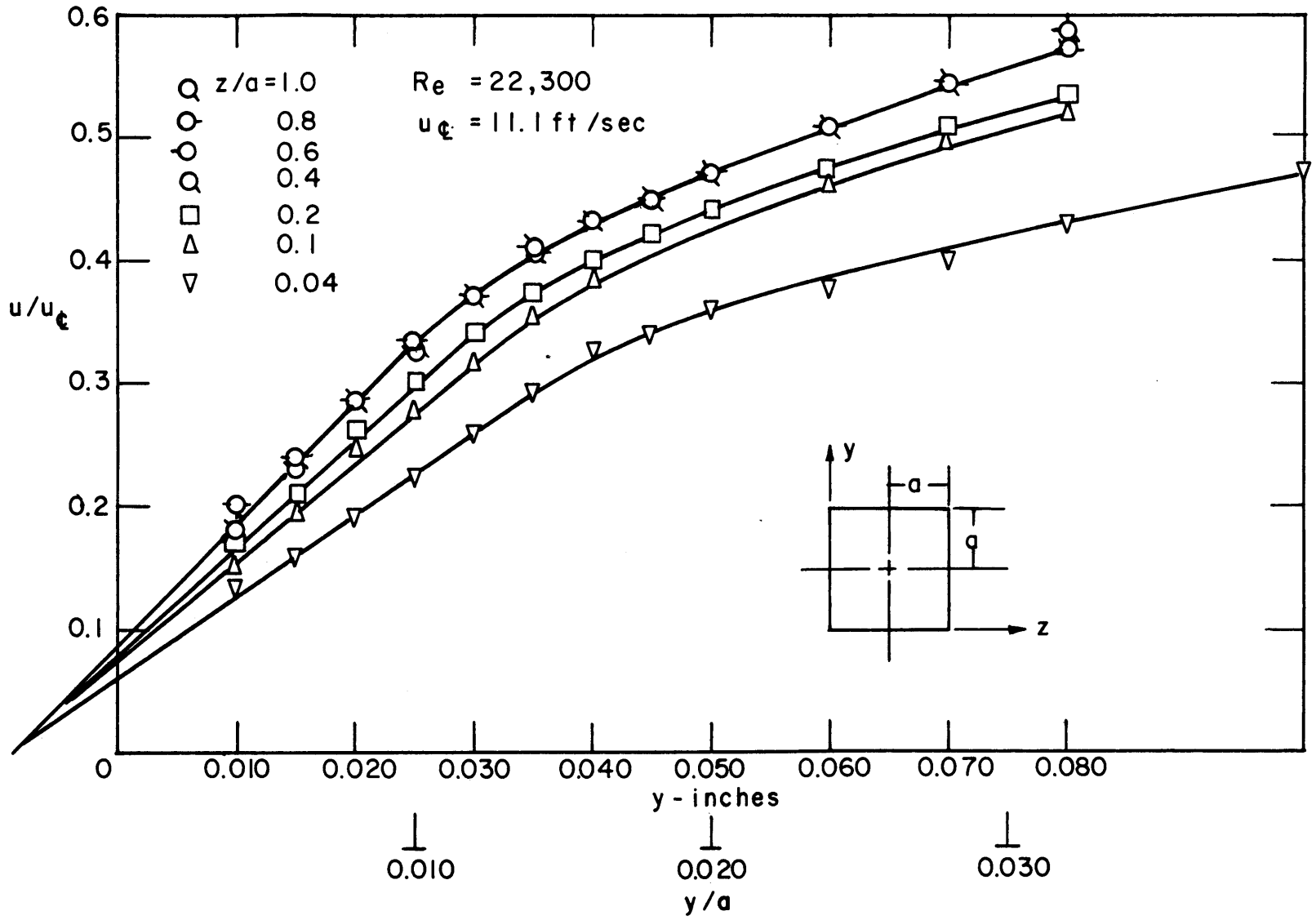

FIG 25 VELOCITY PROFILES NEAR WALL- HOT WIRE DATA FROM SQUARE DUCT- $R_e = 22,300$

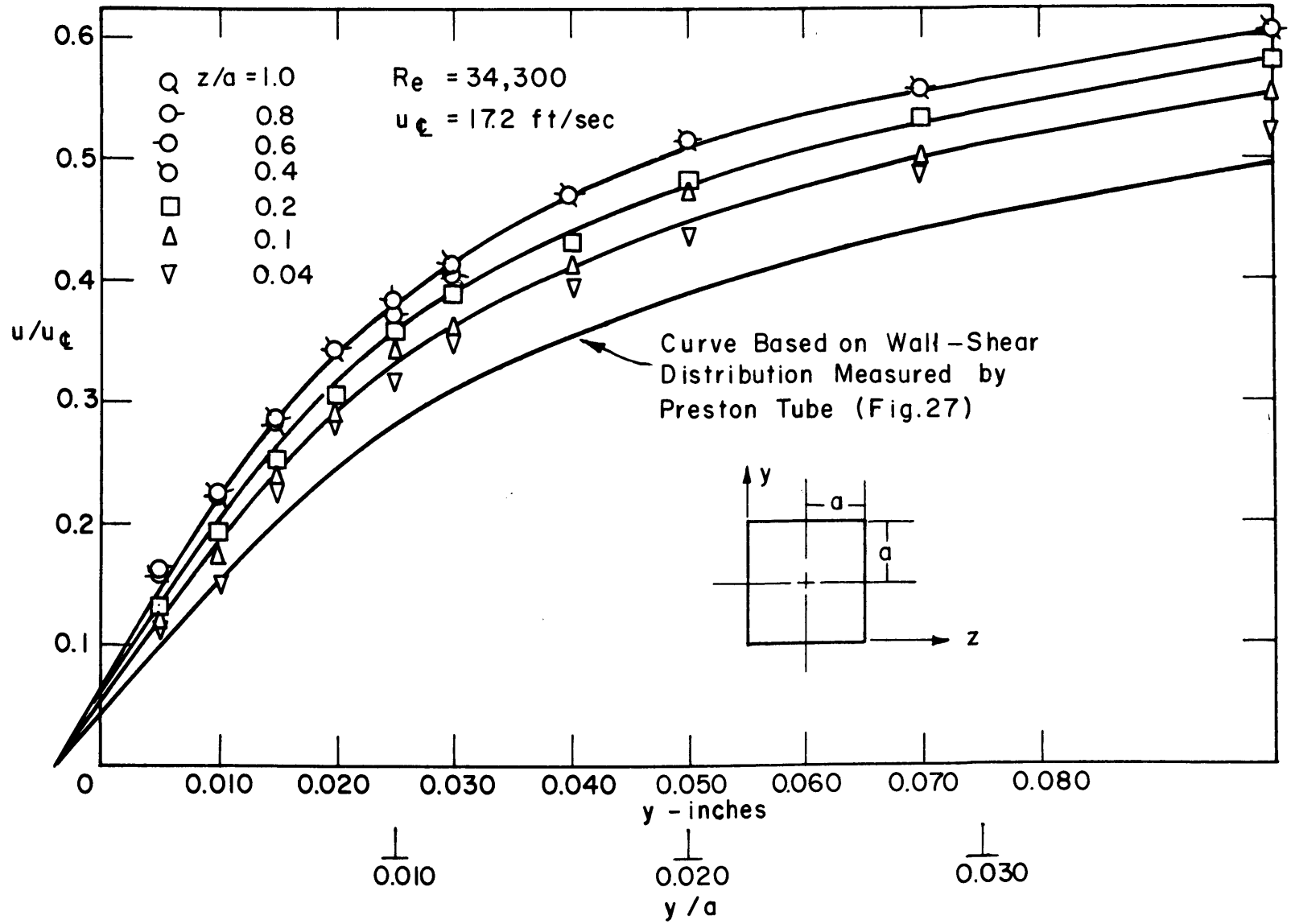

FIG 26 VELOCITY PROFILES NEAR WALL- HOT WIRE DATA FROM SQUARE DUCT - $R_e = 34,300$

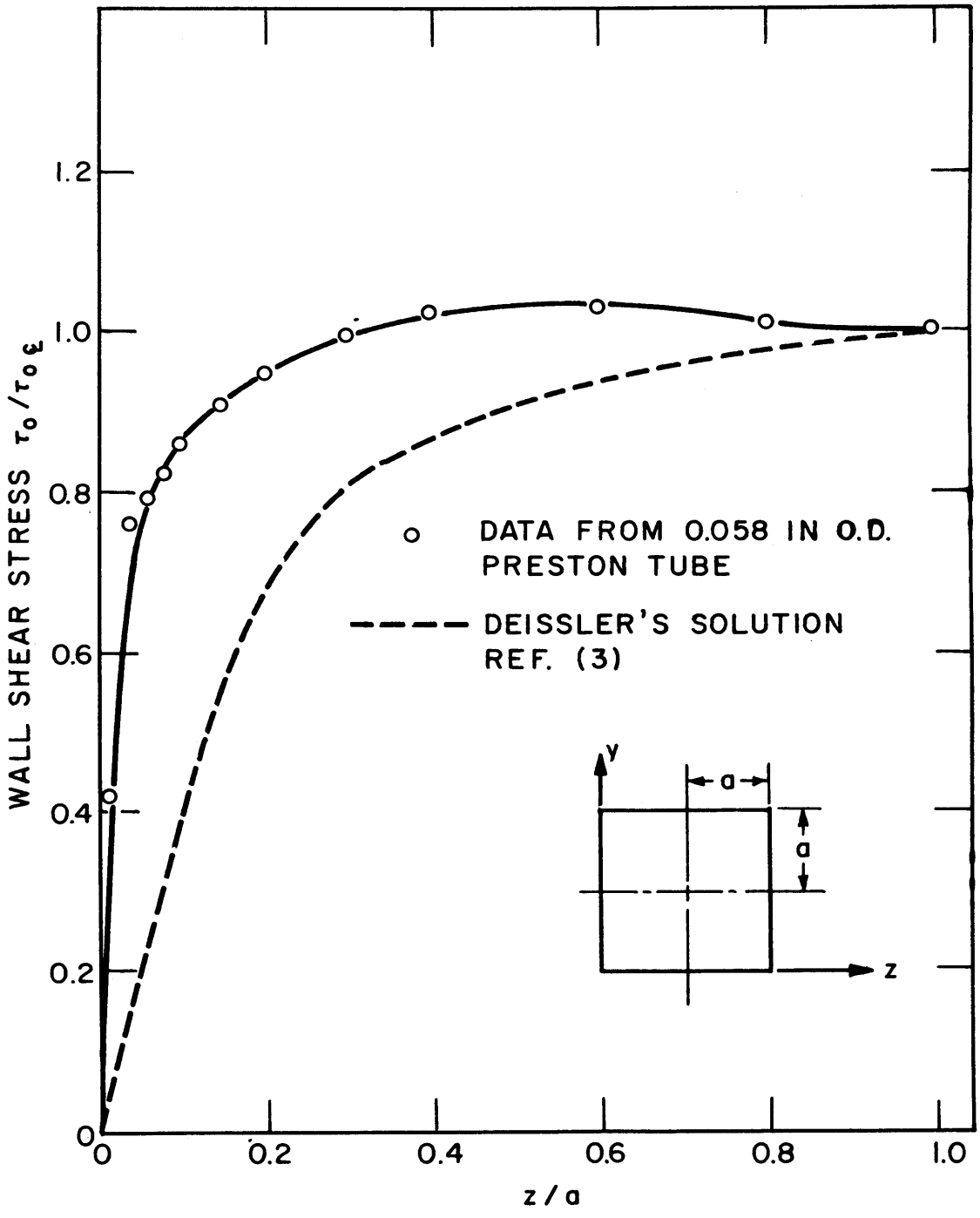

FIGURE 27 WALL SHEAR STRESS DISTRIBUTION— SQUARE DUCT

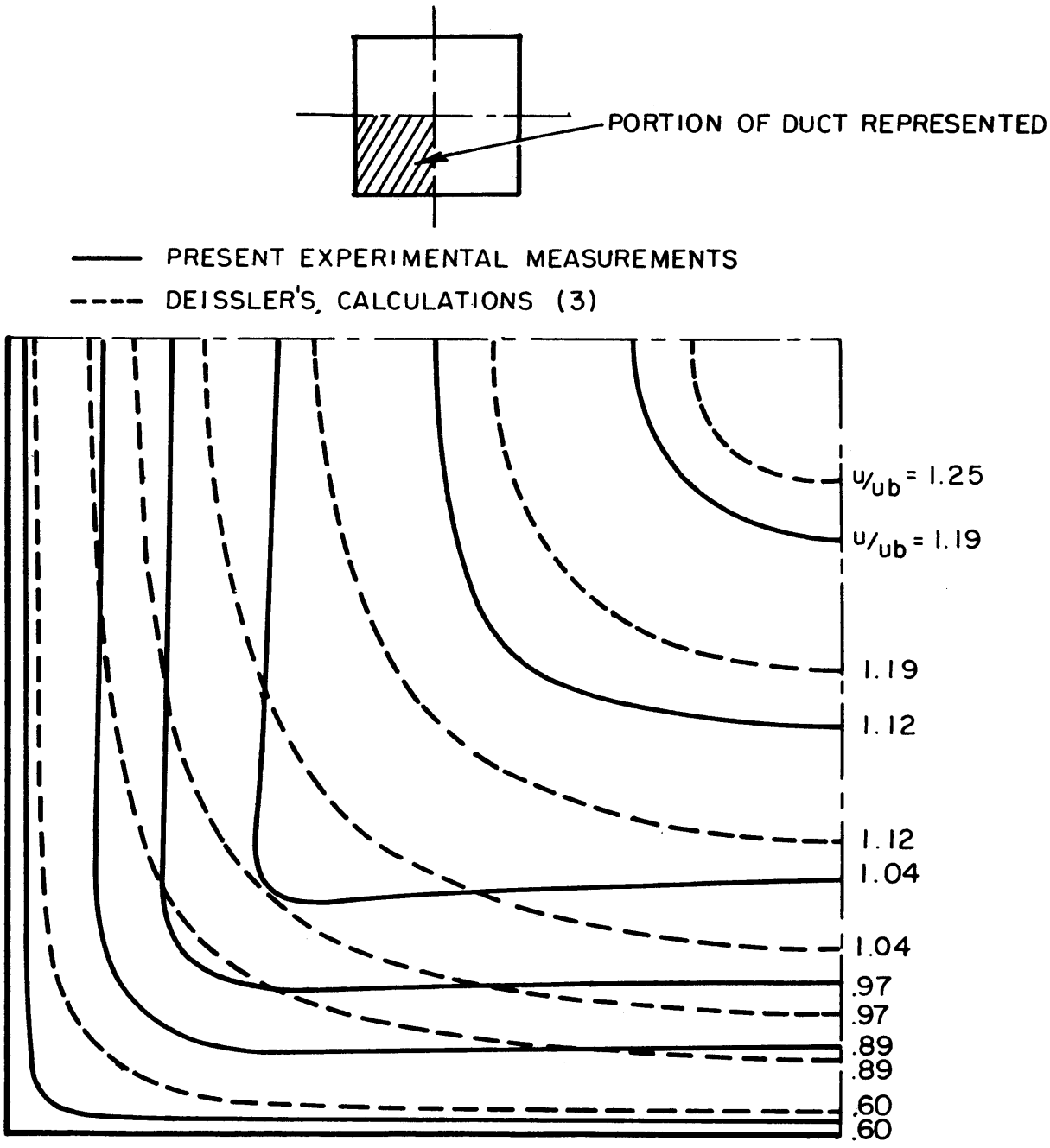

FIG. 28 CONTOURS OF CONSTANT AXIAL VELOCITY – SQUARE DUCT – $R_e = 75{,}500$

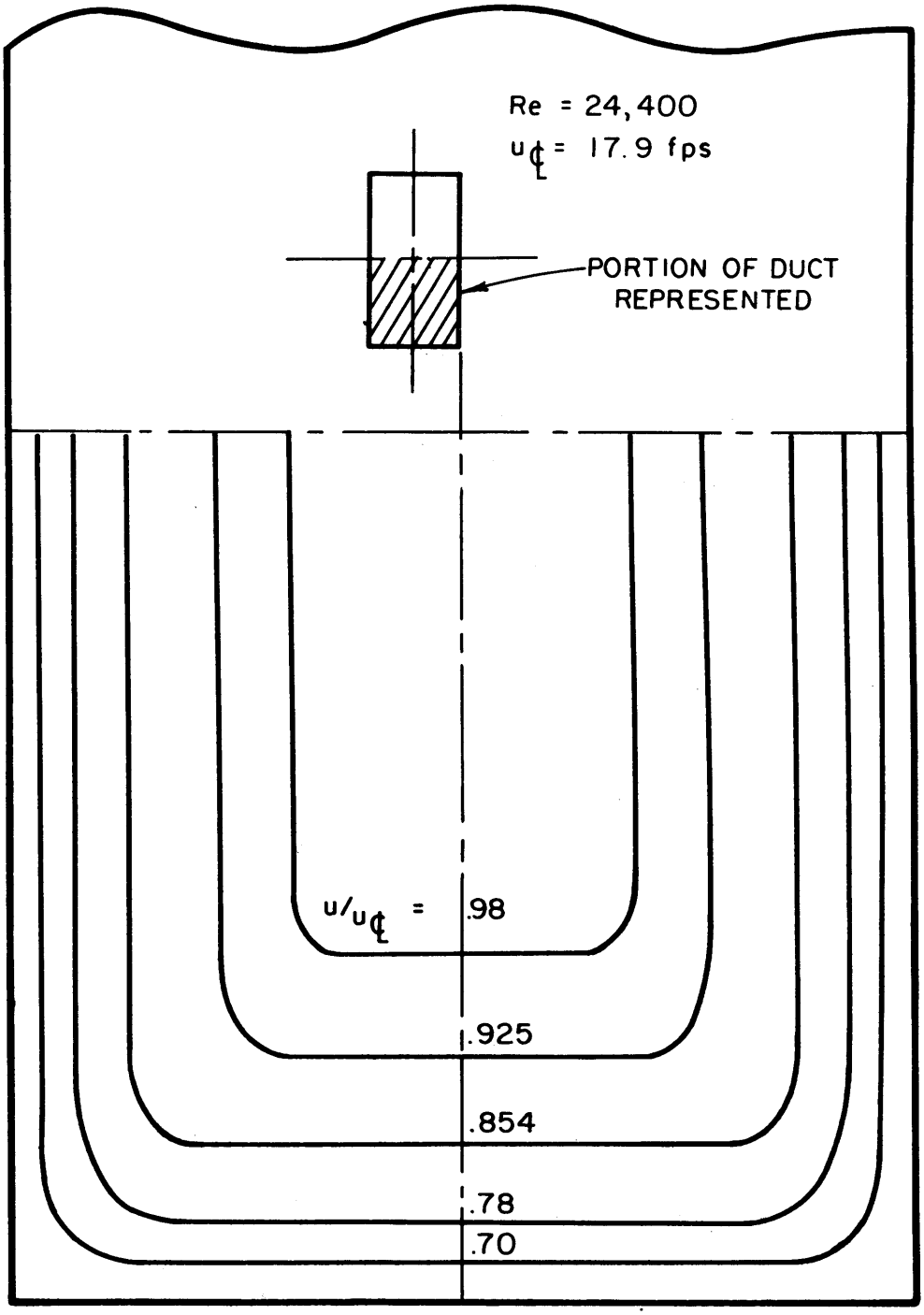

FIG. 29 CONTOURS OF CONSTANT AXIAL VELOCITY – 2 1/2 X 5 INCH DUCT – R_e = 24,400

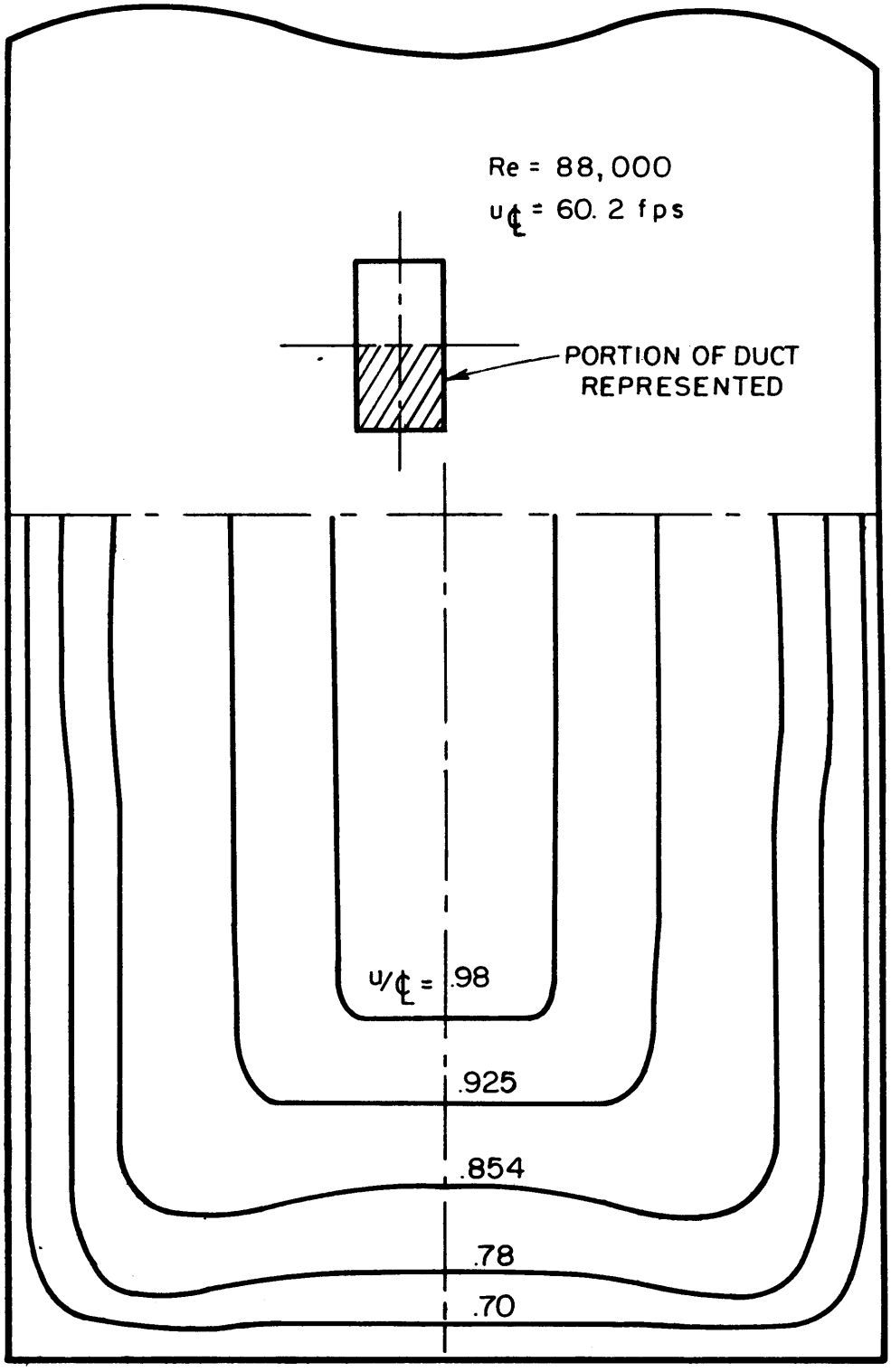

FIG. 30 CONTOURS OF CONSTANT AXIAL VELOCITY - 2 1/2 X 5 INCH DUCT - R_e = 88,000

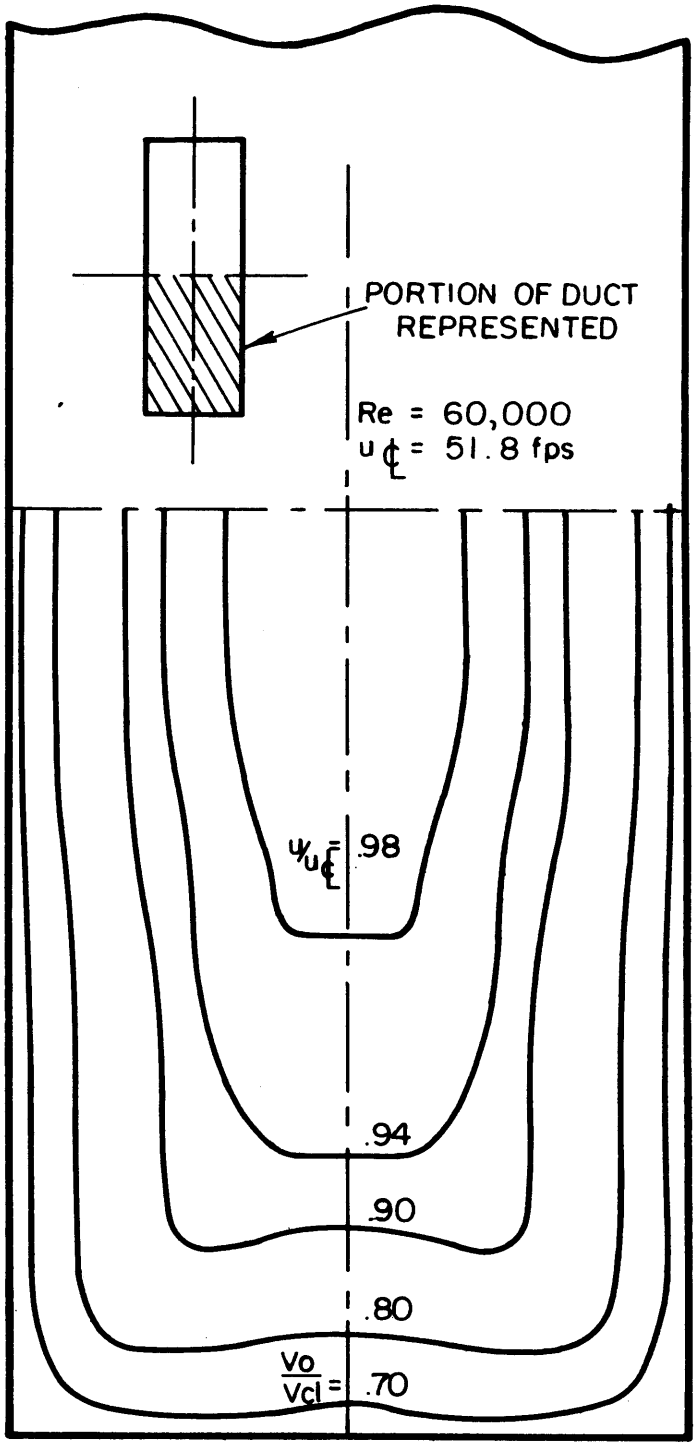

FIG. 31 CONTOURS OF CONSTANT AXIAL VELOCITY – 1 2/3 X 5 INCH DUCT – R_e = 60,000

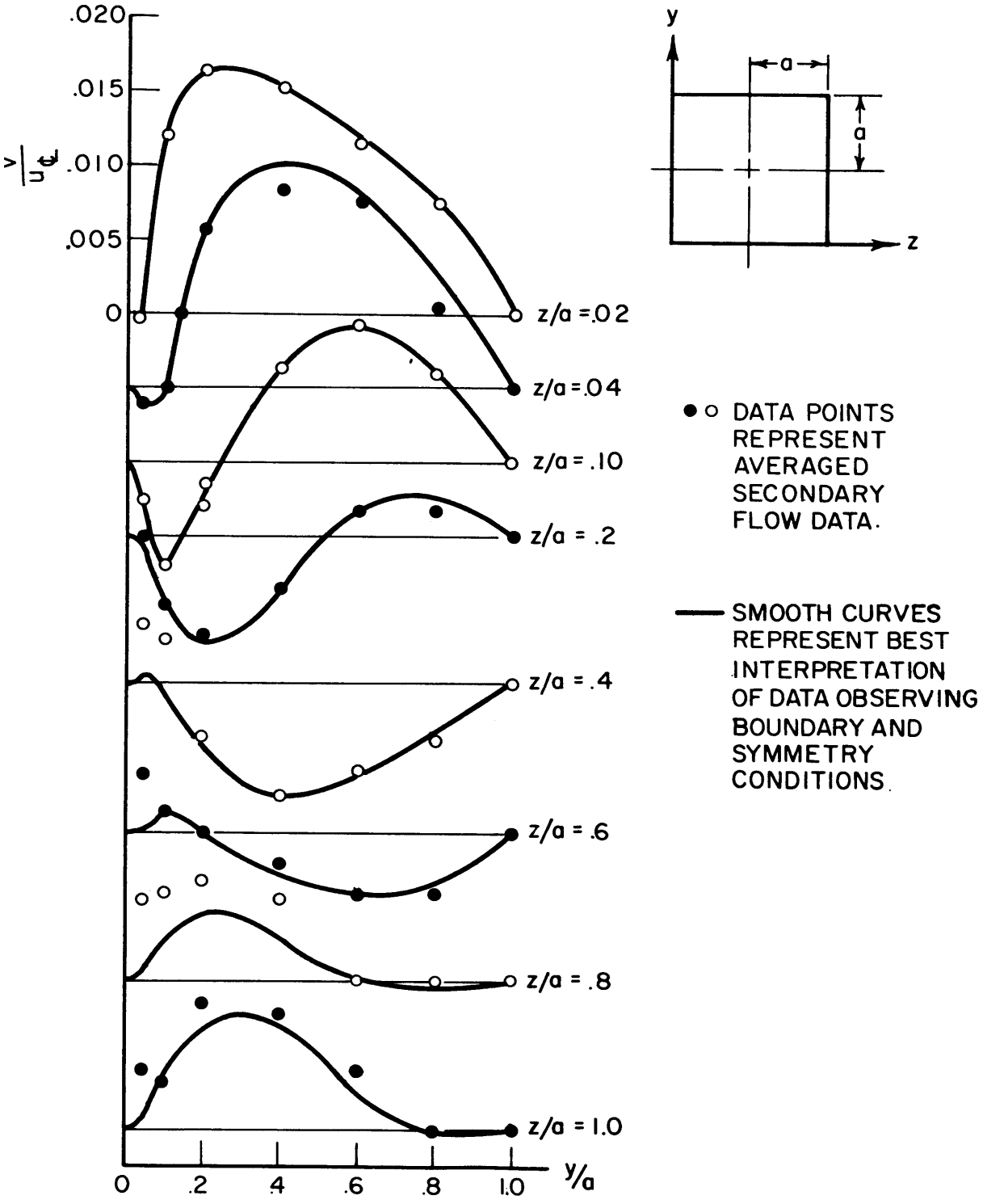

FIGURE 32 SECONDARY VELOCITY PROFILES, SQUARE DUCT, v vs. y OR w vs. z

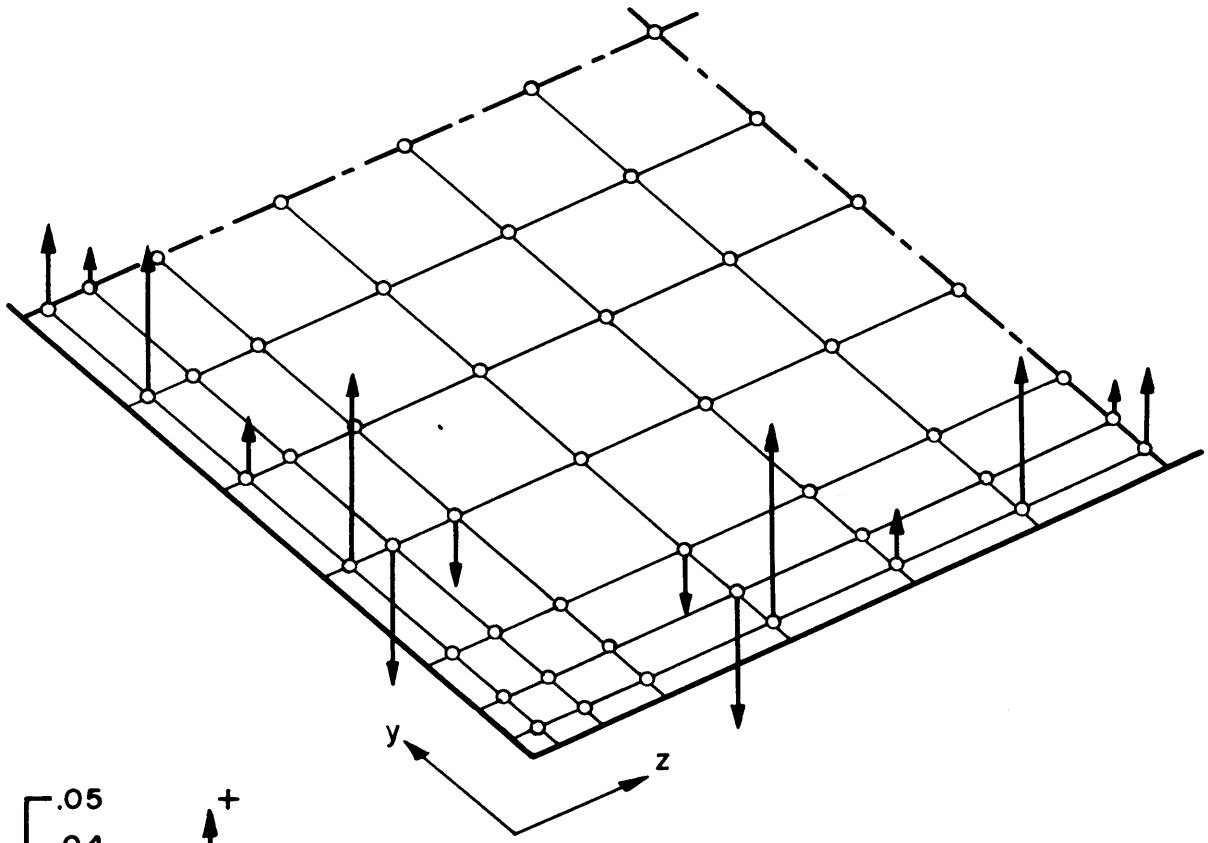

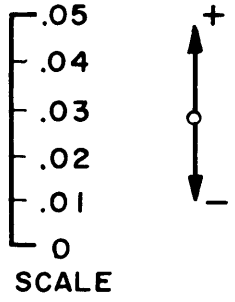

VECTORS REPRESENT DIMENSIONLESS DIVERGENCE

$$\left[\frac{\partial v}{\partial y} + \frac{\partial w}{\partial z}\right]\frac{a}{u_{\ell}}$$

DETERMINED FROM SMOOTH CURVES PASSED THROUGH SECONDARY FLOW DATA POINTS.

FIGURE 33 DIVERGENCE BASED ON SECONDARY VELOCITY MEASUREMENT – SQUARE DUCT

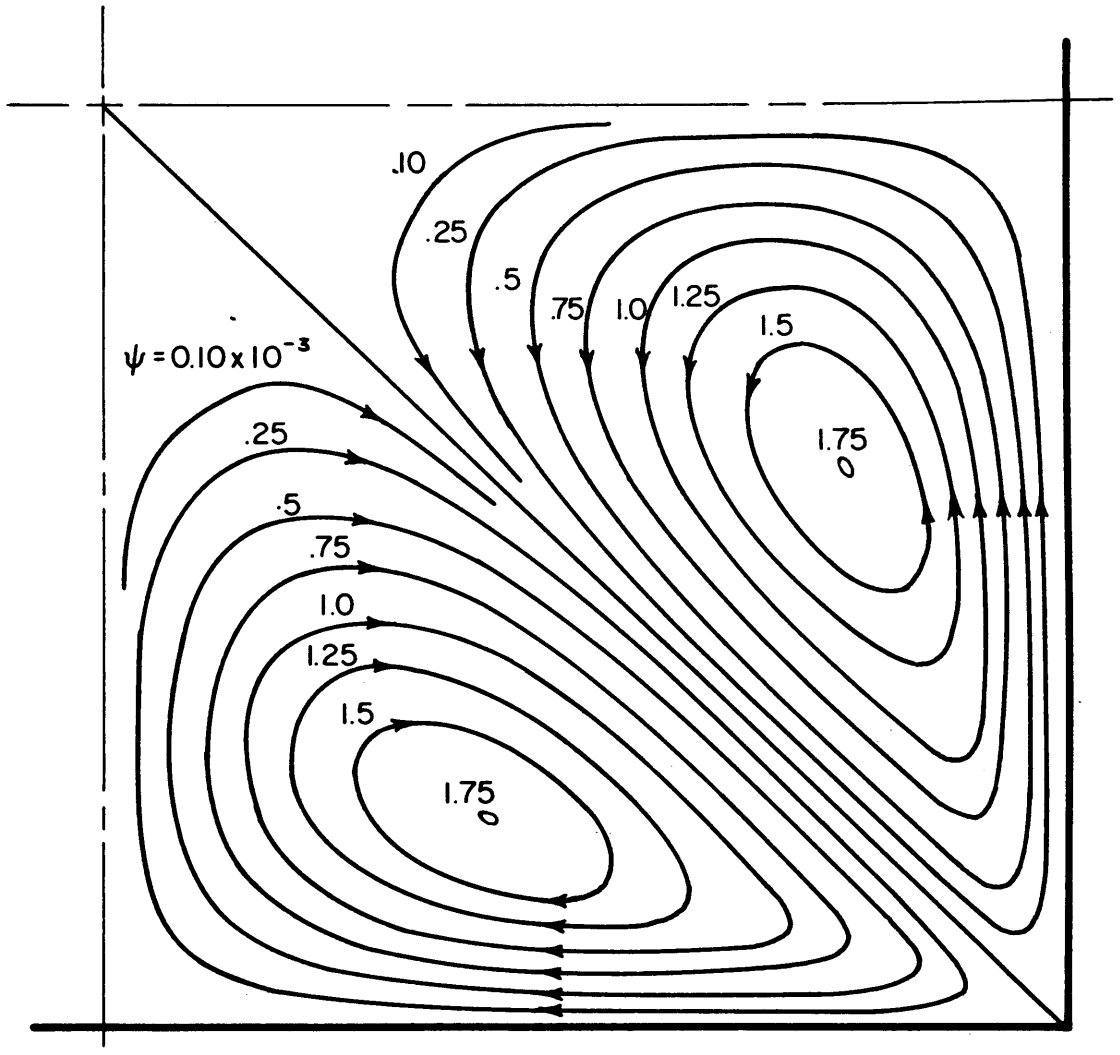

Lines of Constant Stream Function ψ

$$\frac{\partial \psi}{\partial (z/b)} = \frac{v}{u_{\text{℄}}}$$

FIGURE 34 SECONDARY FLOW STREAM LINES, SQUARE DUCT

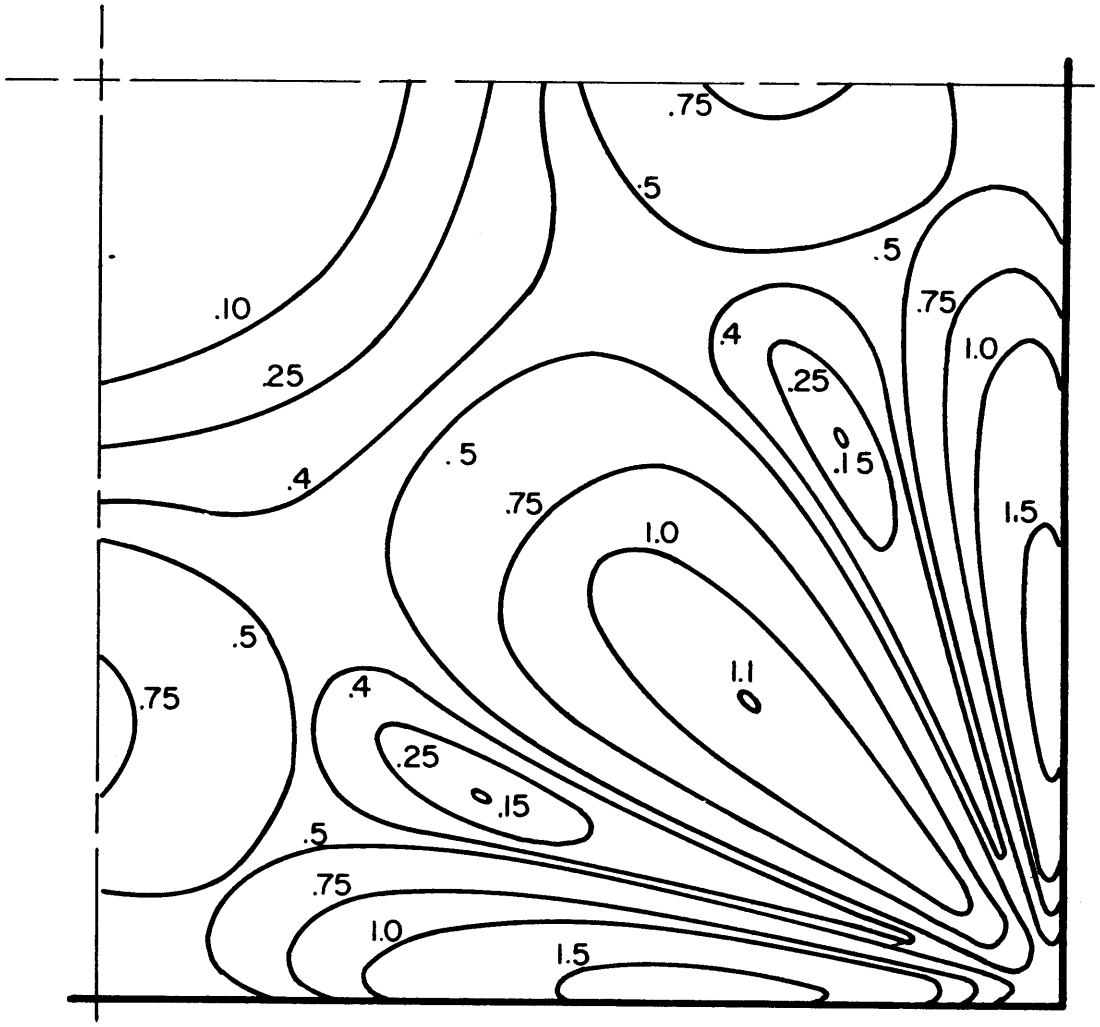

NUMBERS ON CURVES DENOTE $\frac{V_{sec}}{u_{\ell}}$ IN PERCENT

FIGURE 35 CONTOURS OF CONSTANT SECONDARY VELOCITY, SQUARE DUCT.

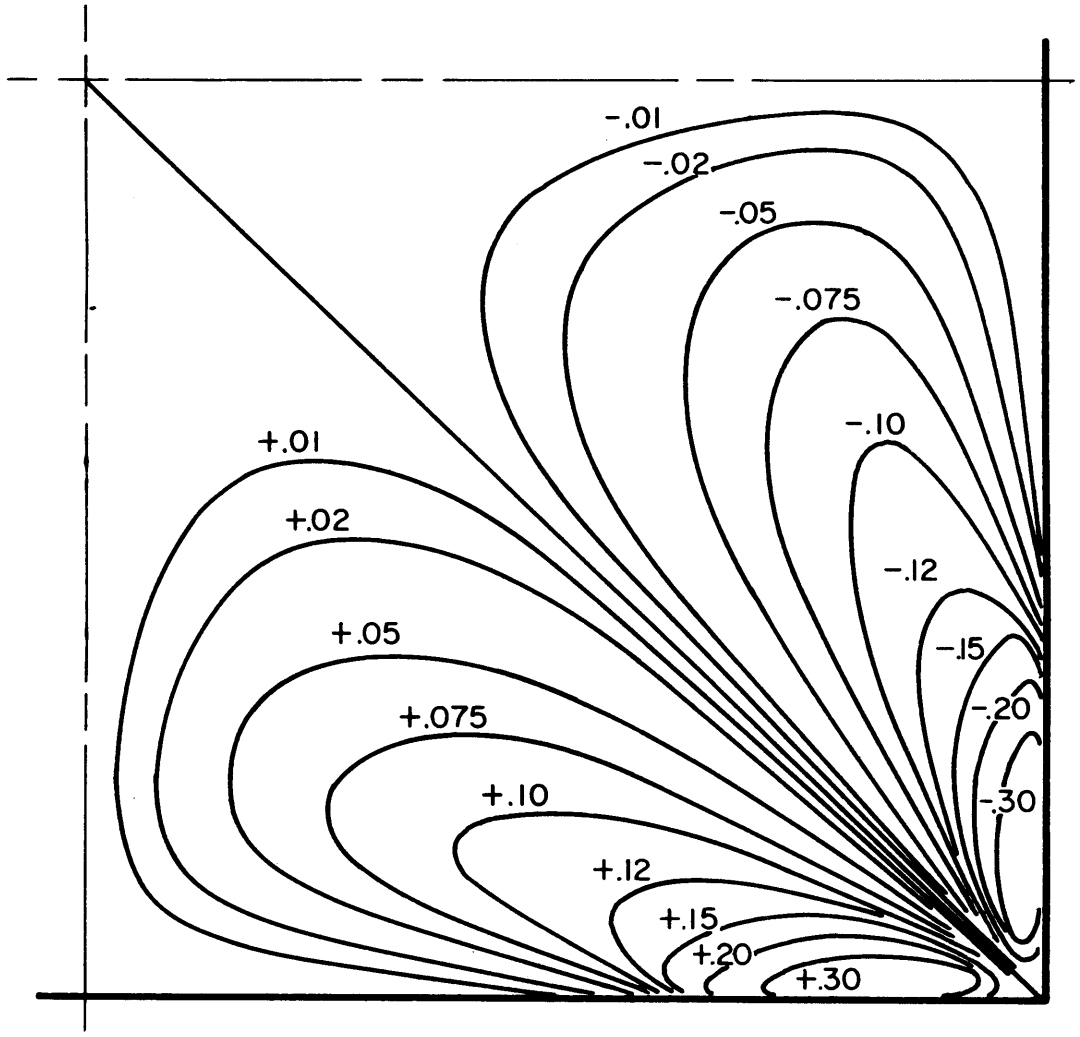

NUMBERS ON CURVES REPRESENT $\xi^* = \left(\frac{\partial w}{\partial y} - \frac{\partial v}{\partial z}\right)\frac{a}{u_{\mathbb{C}}}$

FIGURE 36 CONTOURS OF CONSTANT AXIAL VORTICITY, SQUARE DUCT.

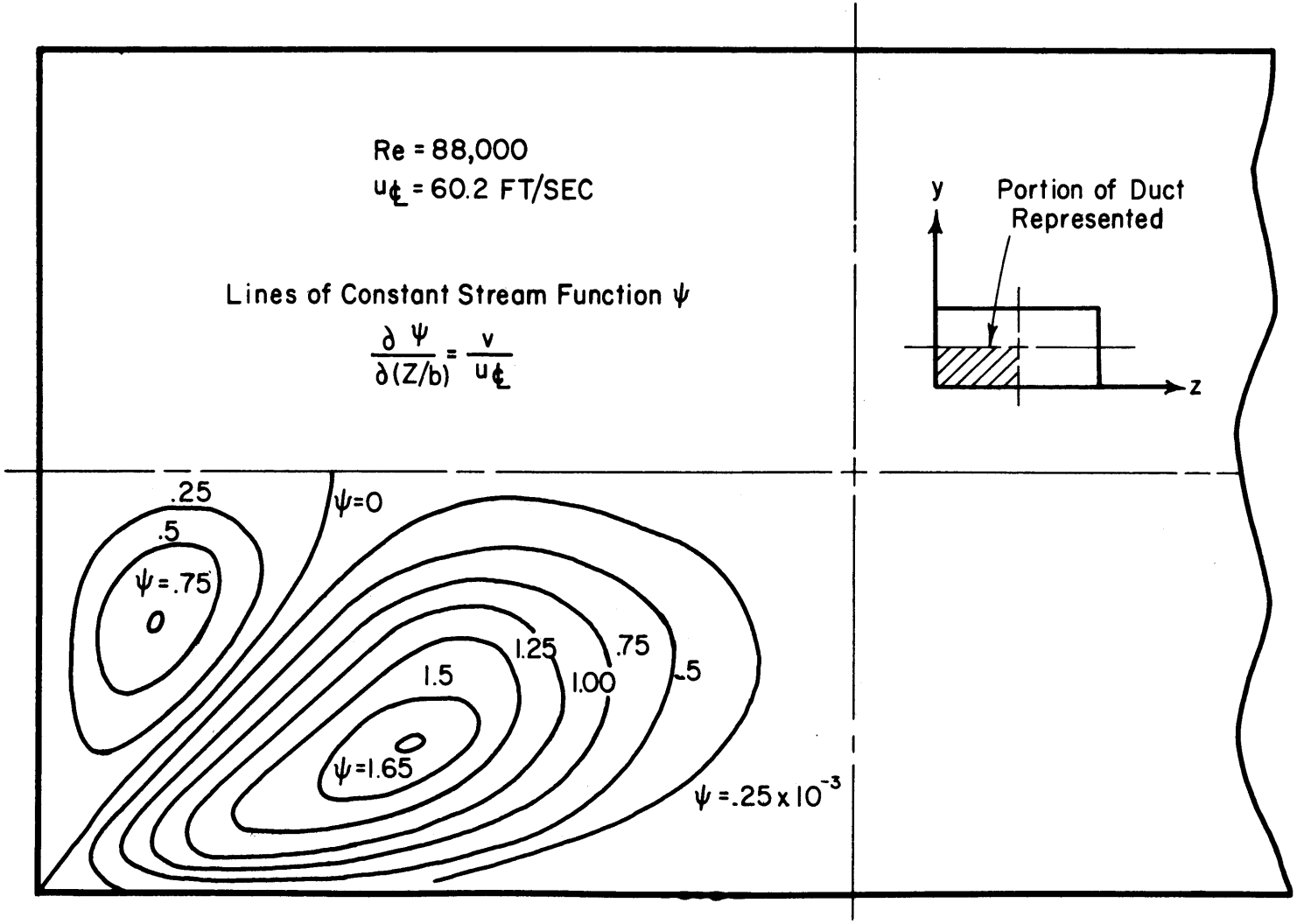

FIGURE 37 SECONDARY FLOW STREAM LINES, 2 1/2 x 5 IN DUCT

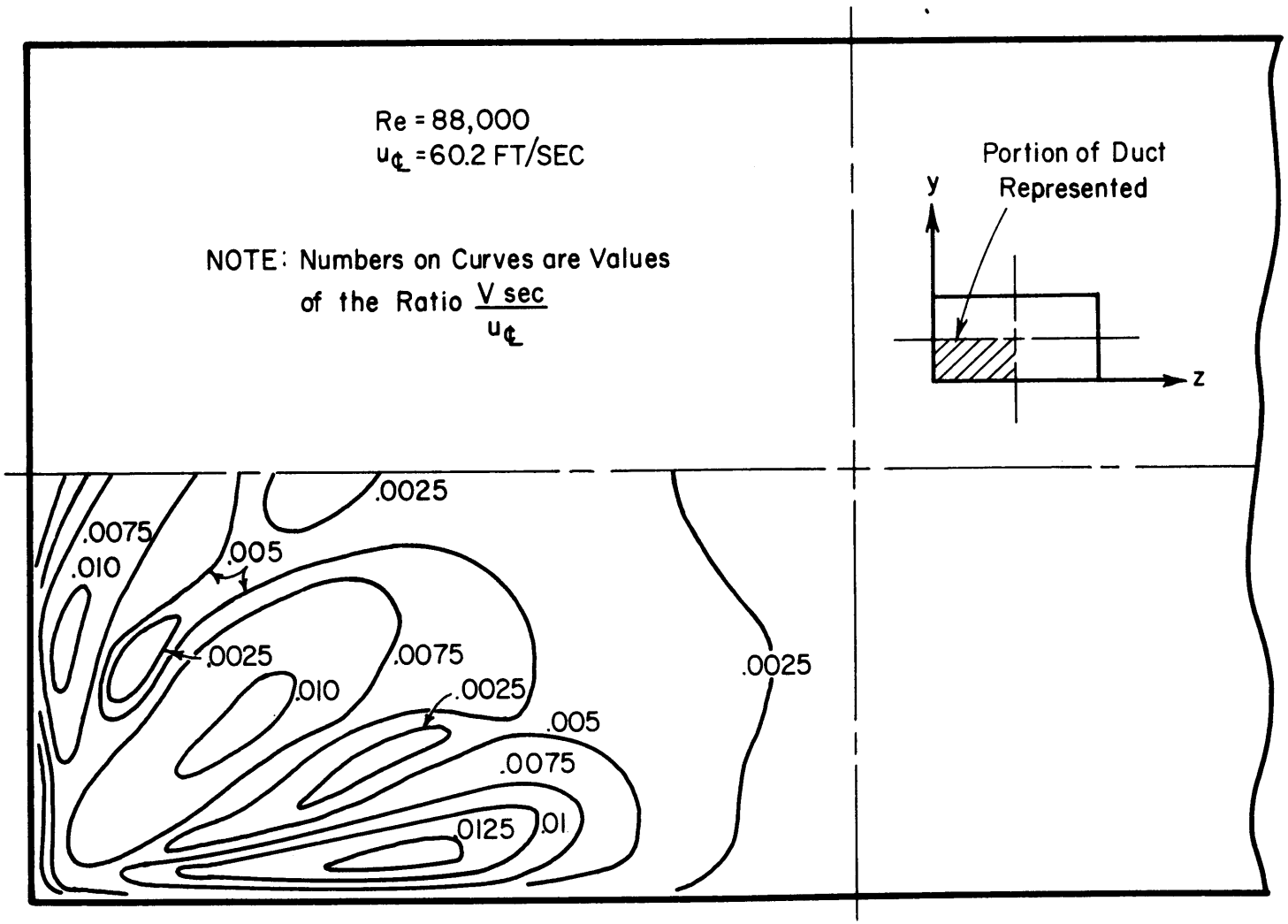

FIGURE 38 CONTOURS OF CONSTANT SECONDARY VELOCITY, 2 1/2 x 5 IN. DUCT

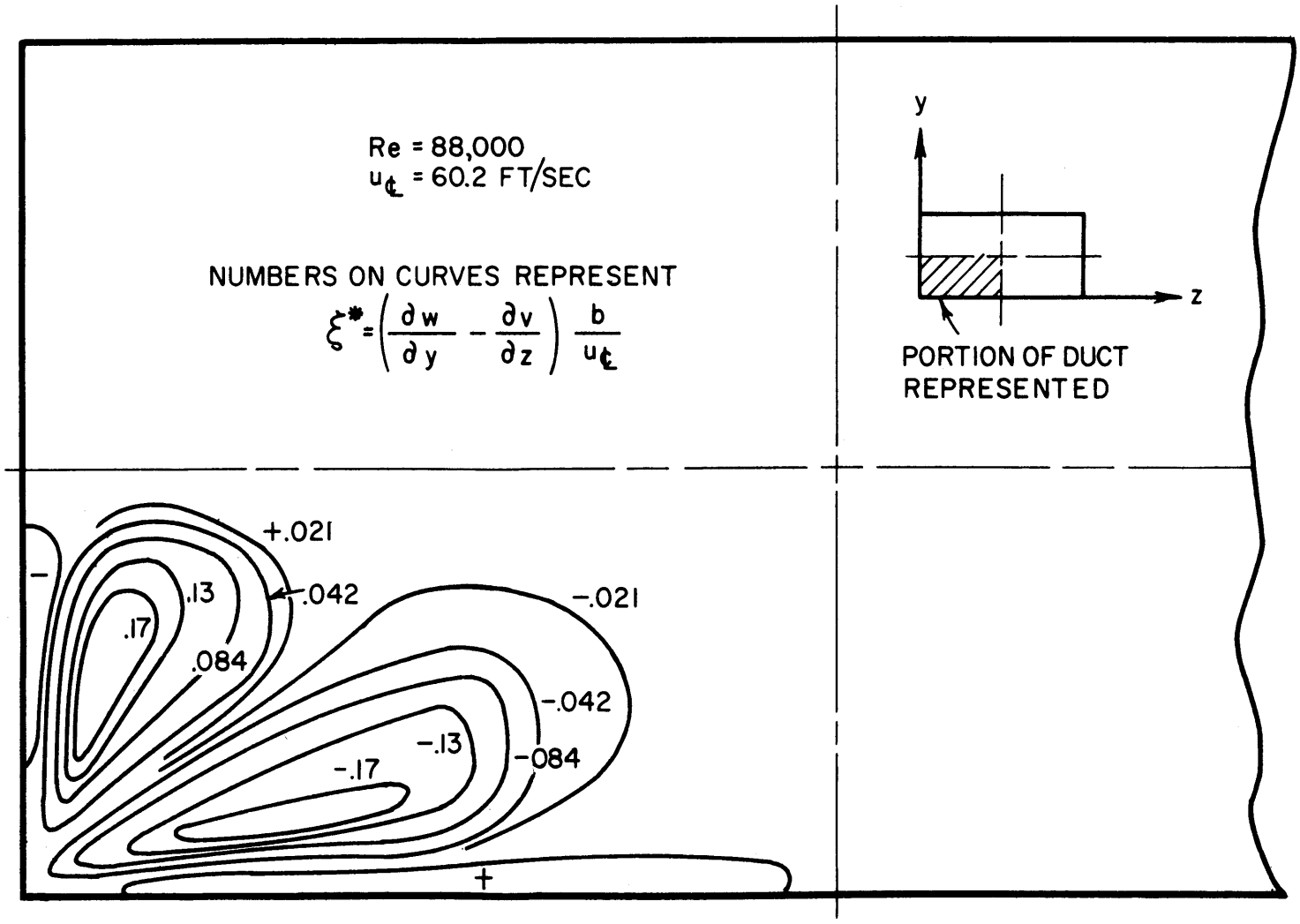

FIGURE 39 CONTOURS OF CONSTANT AXIAL VORTICITY, 2 1/2 x 5" DUCT

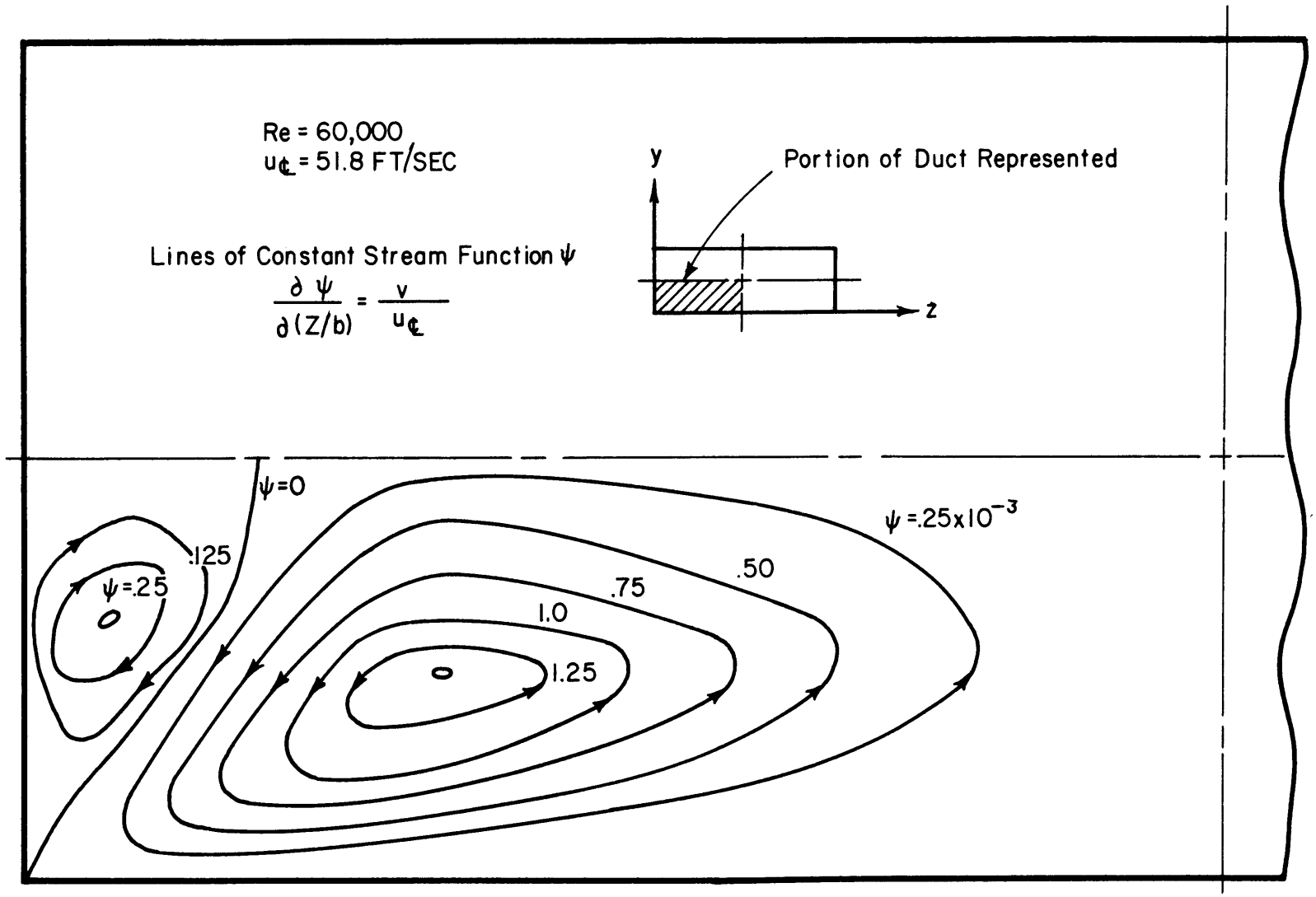

FIGURE 40 SECONDARY FLOW STREAM LINES, 12/3 x 5 IN. DUCT

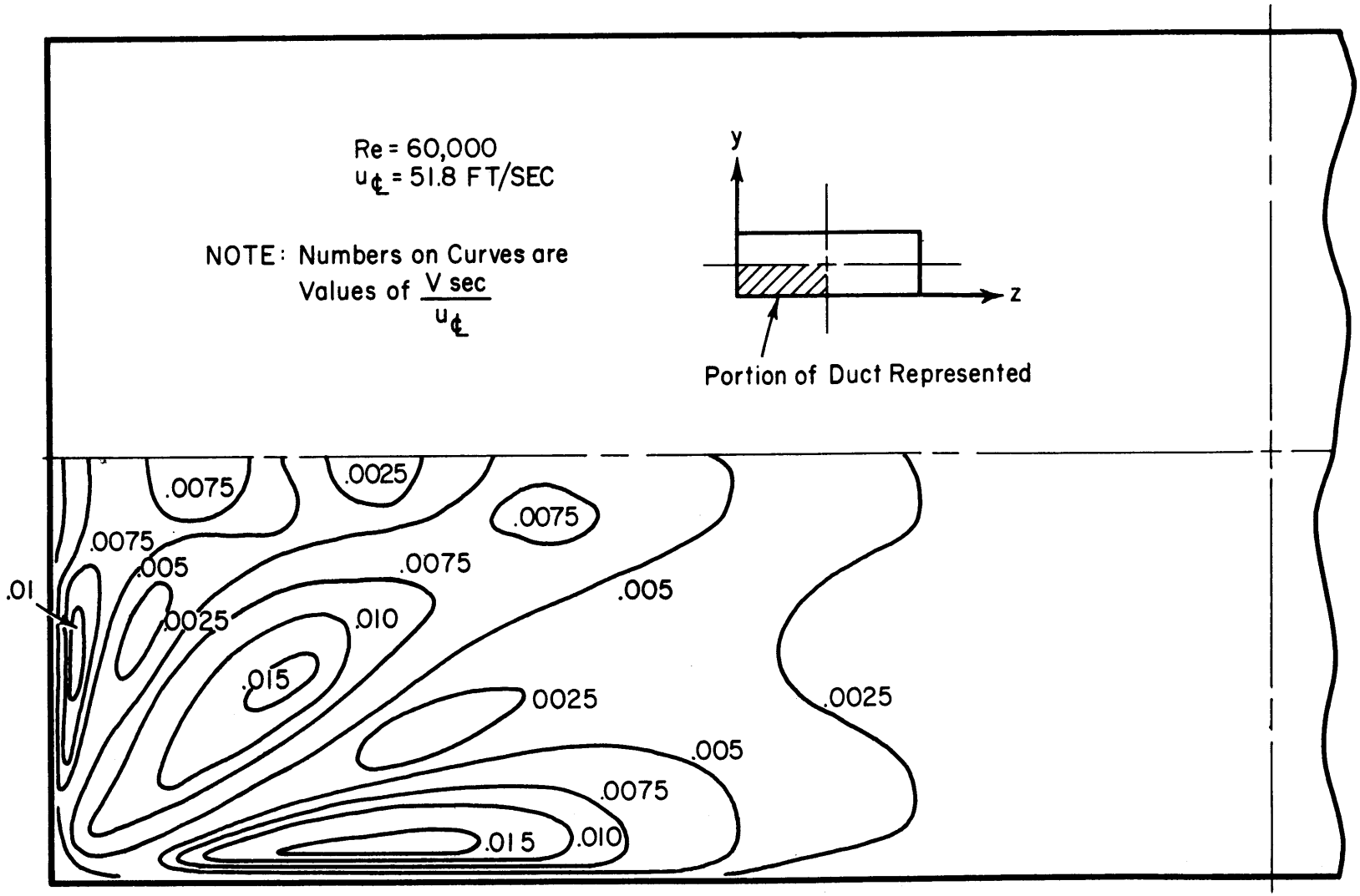

FIGURE 41 CONTOURS OF CONSTANT SECONDARY VELOCITY, 1 2/3 x 5 IN. DUCT

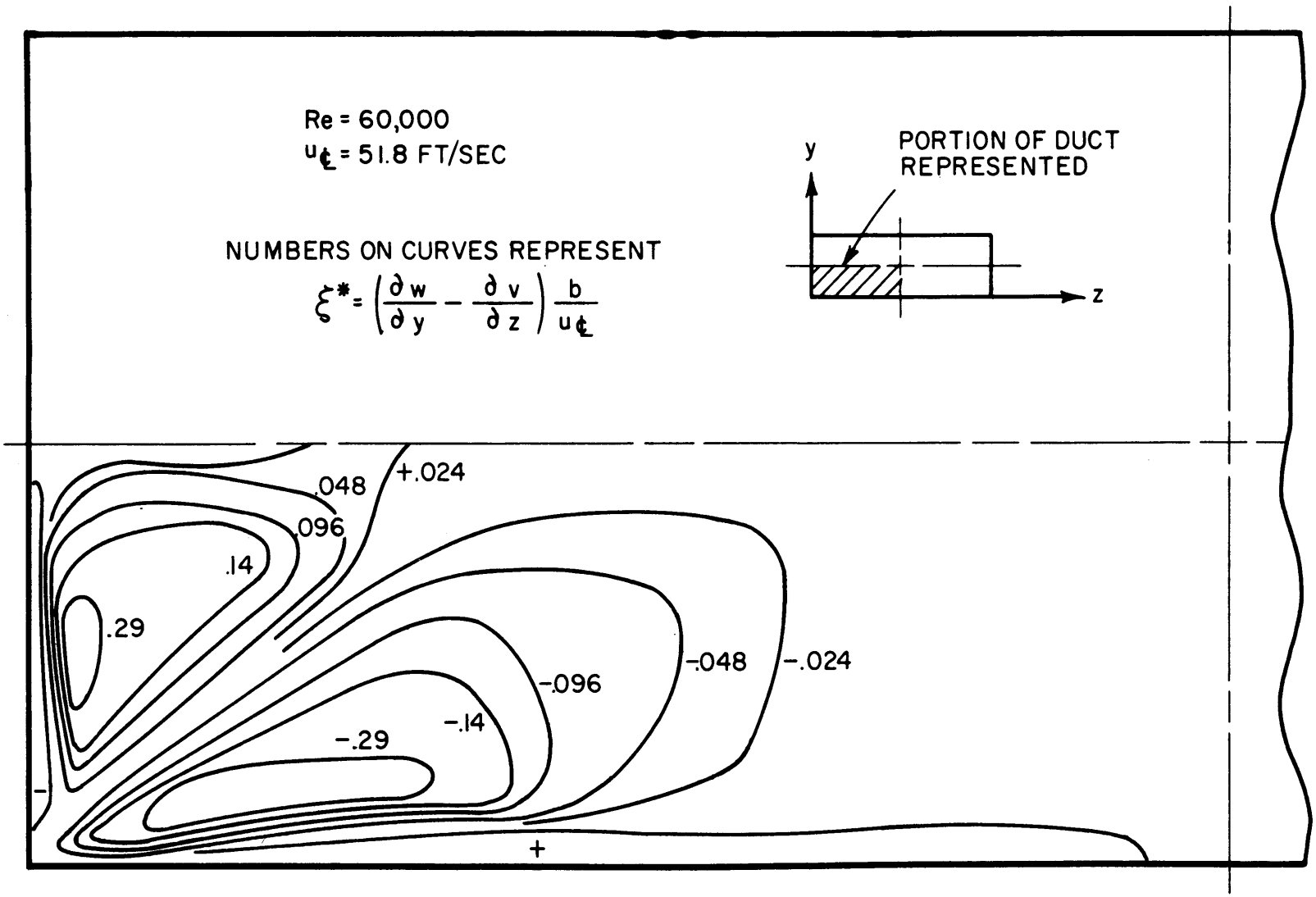

FIGURE 42 CONTOURS OF CONSTANT AXIAL VORTICITY, 1 2/3 x 5" DUCT

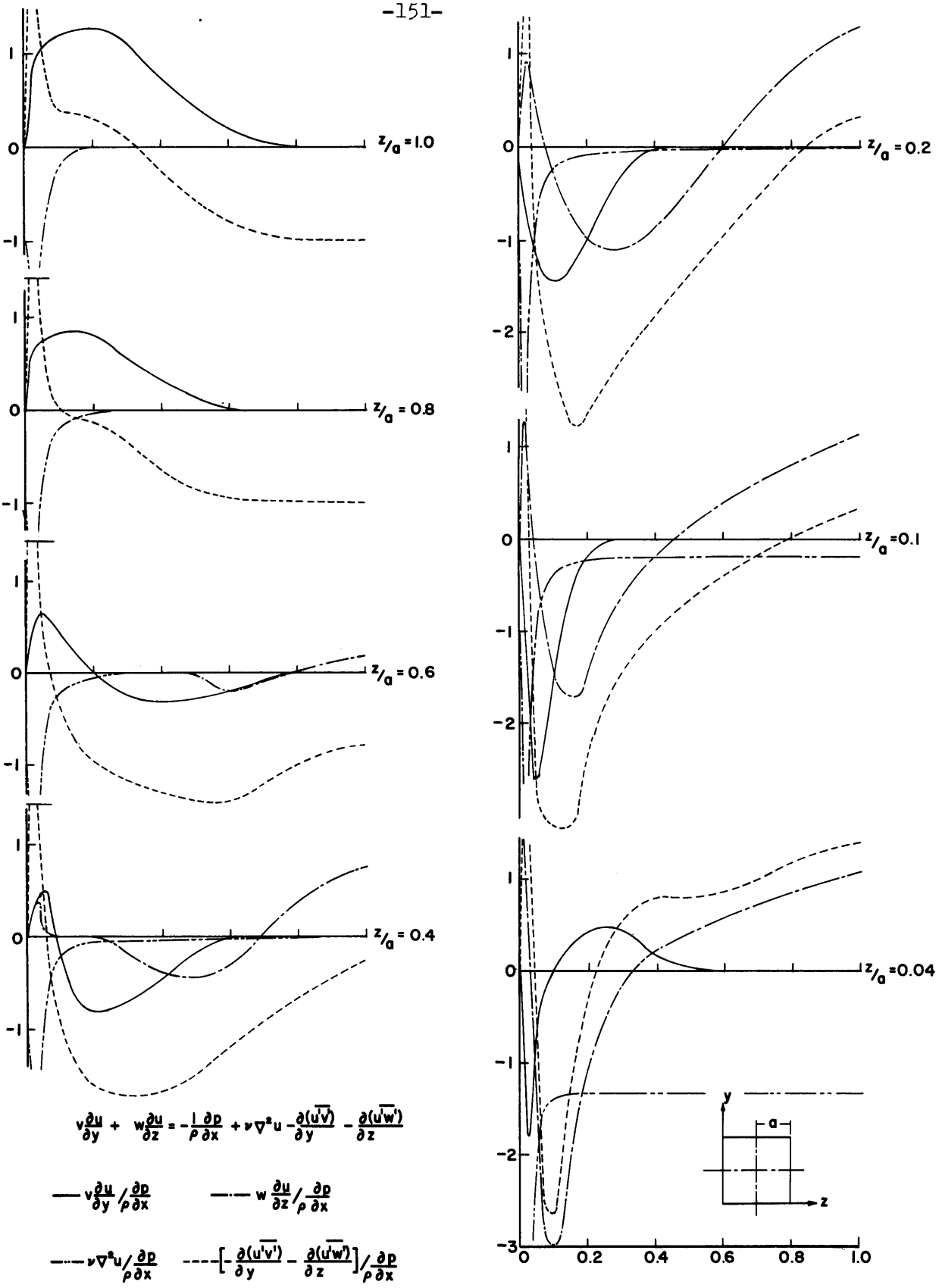

FIG 43 COMPARISON OF TERMS IN AXIAL MOMENTUM EQUATION— 5 INCH SQUARE DUCT

PIPE FLOW - LAUFER (24) { ○ Re = 50,000 τ_o = .00053 PSF
□ Re = 500,000 τ_o = .035 PSF

BOUNDARY LAYER - KLEBANOFF (14) △ τ_o = .0081 PSF

DIVERGENT CHANNEL - RUETENIK (15) ▽ τ_o = .0008 - .05 PSF

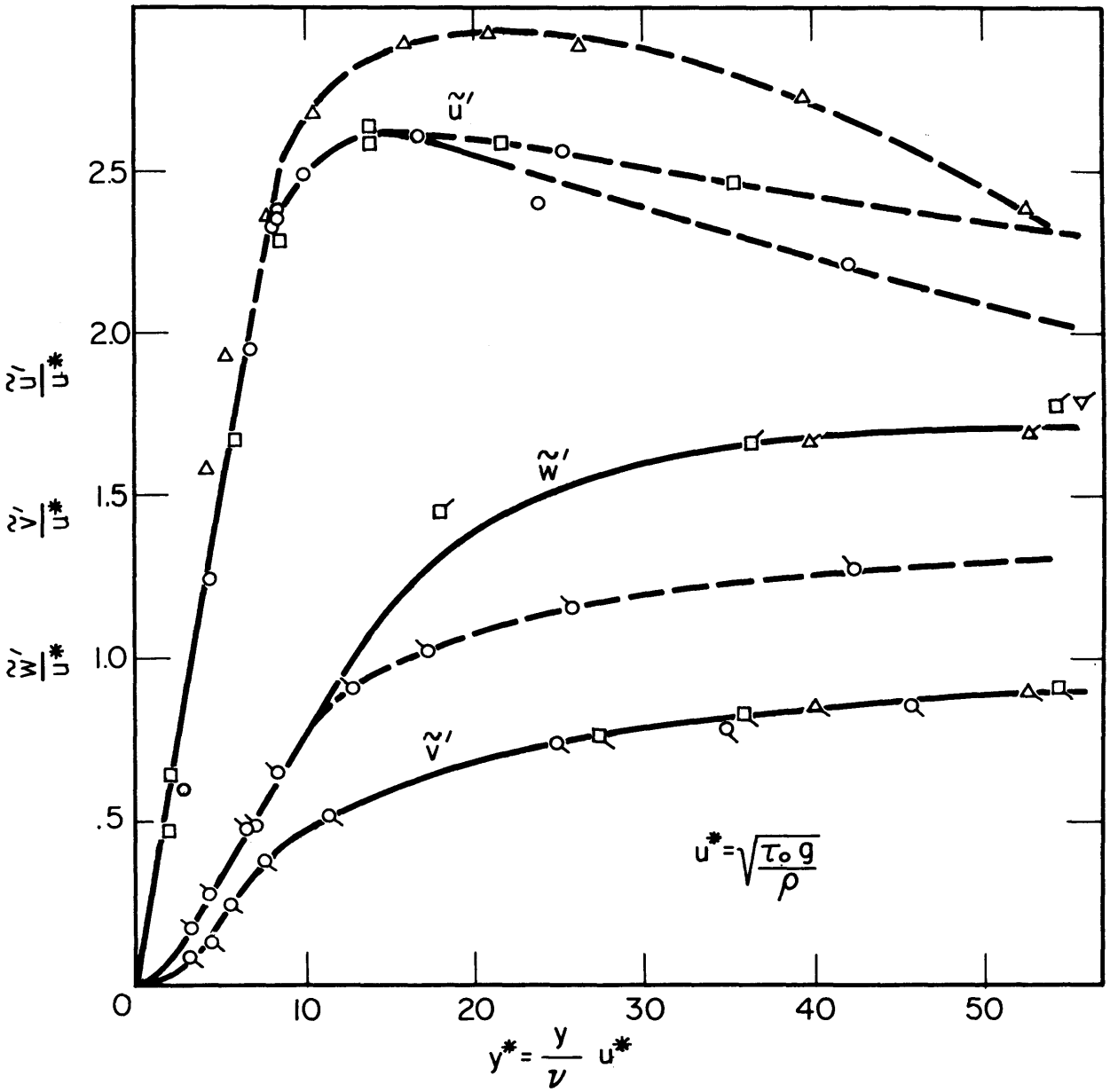

FIGURE 44 WALL SIMILARITY RELATION FOR TURBULENCE INTENSITY COMPONENTS

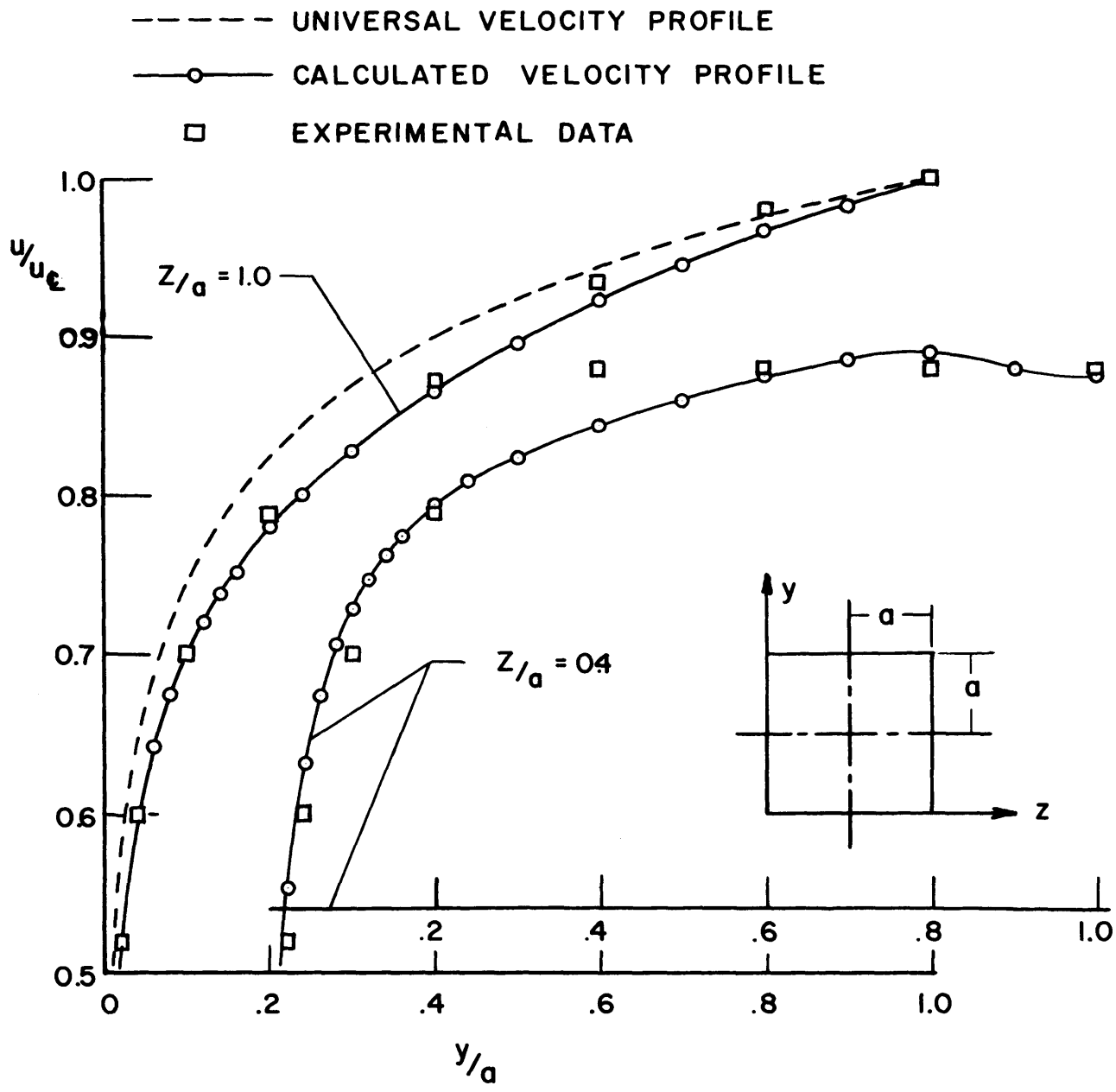

FIG 45 COMPARISON OF CALCULATED AND MEASURED AXIAL VELOCITY PROFILES.

BIBLIOGRAPHY

(1) Levy, S.; Fuller, R.A.; and Niemi, R.O.; "Heat Transfer To Water In Thin Rectangular Channels", Trans ASME, Journal of Heat Transfer, May 1959, p. 129.

(2) Irvine, T.F., Jr., "The Influence Of Radiation On Convection In Noncircular Ducts", ASME paper No. 58-A-155, presented annual meeting, Dec., 1958.

(3) Deissler, R.G., and Taylor, M.F., "Analysis of Turbulent Flow and Heat Transfer In Noncircular Passages", NACA-TN 4384, Sept., 1958.

(4) Delleur, J.W., and McManus, D.S., "Secondary Flow In Straight Open Channels", Proceedings 6th Midwest Conference on Fluid Mechanics, Austin, Texas, Sept., 1959, p. 81.

(5) Nikuradse, J., "Untersuchungen über die Geschwindikeitsverteitung in turbulenten strömungen", Thesis Göttingen (1926), VDI-Forschungsheft 281, Berlin (1926).

(6) Nikuradse, J., "Turbulente strömung in nicht kreisförmigen Rohren", Ing.-Arch., 1, 306 (1930).

(7) Prandtl, L., Proc. 2nd International Congress of Applied Mechanics (1926) p.71, et seq (Zurich, 1927) (Also translated as NACA TM-435).

(8) Moissis, R., "Secondary Flow In Rectangular Ducts", S.M.Thesis in Mech. Engr, M.I.T. June, 1957.

(9) Maslen, S.H., "Transverse Velocities In Fully Developed Flows", Quarterly of Applied Mathematics, Vol 16, 1958, p. 173.

(10) Howarth, L., "Concerning Secondary Flow In Straight Pipes", Proc., Cambridge Phil. Soc., 34, 1938.

(11) Einstein, H.A., and Li, Huon, "Secondary Currents In Straight Channels", Trans. Amer., Geophysical Union, Vol 39, No.6, 1958.

(12) Townsend, A.A., The Structure of Turbulent Shear Flow, Cambridge Monographs on Mechanics and Applied Mathematics, Cambridge Univ Press, London, 1956, p 259.

(13) Hinze, J.O., Turbulence, McGraw-Hill Book Co. Inc., New York, 1959, p 523.

(14) Klebanoff, P.S., "Characteristics Of Turbulence In A Boundary Layer With Zero Pressure Gradient", NACA TN-3178, Wash. 1954.

(15) Ruetenik, J.Ray, "Investigation Of Equilibrium Flow In A Slightly Divergent Channel", Report I-19-Contract Nonr 248(33) Johns Hopkins Univ - Institute for Cooperative Research, Baltimore, Md., Aug. 1954.

(16) Kihara, D.H., "Velocity Distribution Of Turbulent Flow In A Square Duct", S.B.Thesis, M.I.T., June 1957.

(17) Rouse, H., Advanced Mechanics of Fluids, John Wiley and Sons,Inc., New York, 1959.

(18) Nickerson, R.J., "Effects of Free Stream Oscillation On The Laminar Boundary Layers On A Flat Plate", ScD Thesis, Mech.Engr Dept, M.I.T., June 1957.

(19) Eckert, E.R.G., and Irvine, T.F.,Jr., "Incompressible Friction Factor, Transition And Hydrodynamic Entrance Length Studies Of Ducts With Triangular And Rectangular Cross-Sections", WADC - Technical Report No. 56-401, April 1957.

(20) Gilbert, G.B., "Secondary Flows In Straight Rectangular Ducts," S.M.Thesis in Mech. Engr., M.I.T., July 1960.

(21) Collis, D.C., "Forced Convection Of Heat From Cylinders At Low Reynolds Numbers", Jour. Aero. Sci., July 1956, p.697.

(22) "Flow Measurement" - ASME Power Test Codes - Supplement on Instruments and Apparatus, ASME, New York, 1949, p 38.

(23) Rivas, M.A.,Jr., and Shapiro, A.H., "On The Theory Of Discharge Coefficients For Rounded-Entrance Flowmeters And Venturis", Trans. ASME, Vol 78, April 1956, p 489.

(24) Laufer, John, "The Structure Of Turbulence In Fully Developed Pipe Flow", NACA report 1174, 1954.

(25) Preston, J.H., "The Determination Of Turbulent Skin Friction By Means Of Pitot Tubes", J. RAeS., Vol 58, p 109, Feb. 1954.

(26) Young, A.D., and Maas, J.N., "The Behavior Of A Pitot-Tube In A Transverse PressureGradient", A.R.C., R & M 1770.

(27) Richardson, E. G., "The Correction Of Hot-Wire Readings In A Boundary Layer For Proximity To The Solid Boundary", Jour. Aero. Sci., Readers Forum, Vol 23, No. 10, Oct. 1956.

(28) Goldstein, S., Modern Developments In Fluid Dynamics, Oxford Univ Press, 1938.

Biographical Note

The author was born in Marion, Ohio, on November 15, 1931. After graduation in 1949 from Whitmer High School in Toledo, Ohio, he entered the cooperative Engineering program at General Motors Institute, Flint, Michigan. In August, 1953, he was graduated from General Motors Institute with the four year diploma. During this time his cooperative work periods were spent with the Chevrolet-Toledo Division (1949-1951) and the Research Laboratories Division of General Motors Corporation (1951-1953). In August, 1954, after completing at the Research Laboratories Division the requirements for the Fifth Year Continuation Program, he was awarded the degree Bachelor of Mechanical Engineering from General Motors Institute.

The author entered the Graduate School of M.I.T. in September, 1954, and received the degree of Master of Science in Mechanical Engineering in September, 1955, and the degree of Mechanical Engineer in June, 1956. He was the recipient of Graduate Fellowships awarded by General Motors Corporation and The Fluor Foundation.

The following three years were spent teaching and conducting research leading to the ScD degree in the Mechanical Engineering Department at M.I.T. During these three years the author held a Teaching Assistantship (1956-1957) an Instructorship (1957-1958) and an Assistant Professorship (1958-1959) in the Mechanical Engineering Department.

He has been employed part time since 1957 and full time since September, 1959, by Microtech Research Company, a consulting engineering firm located near M.I.T.

The author is married and has four children.